OBSERVATOIRE EUROPÉEN AUSTRAL UNIVERSITÉ PARIS VII - DENIS DIDEROT
OBSERVATOIRE DE PARIS-MEUDON - DESPA

# THESE

présentée pour obtenir le diplôme de
DOCTEUR DE L'UNIVERSITÉ PARIS VII - DENIS DIDEROT
SPÉCIALITÉ: ASTROPHYSIQUE ET TECHNIQUES SPATIALES

par

PIERRE KERVELLA

# INTERFÉROMÉTRIE OPTIQUE AVEC LE VLT APPLICATION AUX ETOILES CÉPHÉIDES

## VOLUME II: DOCUMENTS

Soutenue le 14 Novembre 2001 devant le Jury composé de:

M. Daniel ROUAN, Président
M. Pierre LÉNA, Co-Directeur de thèse
M. Andreas GLINDEMANN, Co-Directeur de thèse
M. Denis MOURARD, Rapporteur
M. Stephen RIDGWAY, Rapporteur
M. Vincent COUDÉ DU FORESTO, Examinateur

*Photo de couverture: Observatoire de Paranal, depuis le "NTT Peak" (mars 2001).*

# Table des Matières

# 1. Introduction

Ce volume regroupe trois documents en langue anglaise écrits lors de mon travail de thèse, et qui ont été référencés dans le volume principal. Ils présentent une approche plus détaillée et plus technique de l'instrument. De manière à ne pas alourdir le document principal du mémoire de thèse, ils sont reproduits séparément dans ce second volume.

Les deux premiers documents (Sections 2 et 3) présentent le fonctionnement de l'instrument VINCI. Le premier, *"VINCI Software User Requirements"* (Section 2), donne les spécifications utilisées pour la programmation du logiciel de contrôle de VINCI. Il s'agit du document de référence pour comprendre le fonctionnement pratique de l'instrument, ainsi que ses possibilités d'évolution.

Le second document, *"LISA Test Report"* (Section 3), porte sur les résultats des tests effectués sur la caméra infrarouge de VINCI lors de son intégration à Garching. Il présente les caractéristiques techniques de la caméra, son principe de fonctionnement ainsi que ses performances.

Le dernier document concerne la précision de l'instrument VINCI. Déterminer la précision de mesure d'un instrument interférométrique est un exercice particulièrement délicat. Je présente dans la Section 4 une estimation de la contribution des différentes sources de bruit sur les mesures VINCI, ainsi que la précision résultante sur la visibilité. Ce document ayant été rédigé *avant* les premières observations de VINCI, le lecteur est invité à consulter le Volume I pour les résultats obtenus en conditions réelles.

# 2. LdV Software User Requirements

EUROPEAN SOUTHERN OBSERVATORY

Organisation Européenne pour des Recherches Astronomiques dans l'Hémisphère Austral
Europäische Organisation für astronomische Forschung in der südlichen Hemisphäre

# VERY LARGE TELESCOPE

## LEONARDO da VINCI

## Software User Requirements

Doc. No.: VLT-SPE-ESO-15810-1852

Issue: 1.11

Date: 16 September, 1999

Prepared: P. Kervella
. . . . . .
Name Date Signature

Approved: A. Glindemann
. . . . . .
Name Date Signature

Released: M. Tarenghi
. . . . . .
Name Date Signature

CHANGE RECORD

| Issue | Date | Section/Page affected | Reason/Initiation/Remarks |
|---|---|---|---|
| 1.0 | 6 July, 1999 | All | First release (v6.0 draft) |
| 1.1 | 2 August, 1999 | ▪ List of numbered reqs (2.19)<br>▪ GUI display parameters (2.18)<br>▪ Templates overview (2.17) | Includes corrections after the LdV FDR |
| 1.11 | 16 September, 1999 | ▪ Maintenance and engineering modes precised (2.7, 2.18)<br>▪ Some numbered reqs added (2.19) | Includes comments from J.-P. Dupin and A. Longinotti. |
| | | | |

## TABLE OF CONTENTS

# 1 INTRODUCTION

The VLT Interferometer Near-Infrared Commissioning Instrument, LEONARDO da VINCI (LdV) is composed of three subsystems with separate functions :

- two beams combiner (**VINCI**)
- alignment toolkit (**ALIU**)
- artificial star light source (**LEONARDO**)

ALIU and LEONARDO are intended to be facilities of the VLTI infrastructure for the other instruments and for alignment. VINCI will be used first to debug the VLTI and obtain the first fringes, and then as a fiducial point for fringe recovery after changes in the VLTI or its instruments. It will also be an important pedagogical tool, particularly as it can obtain interference fringes autonomously in Autotest mode.

The design of VINCI is based on the FLUOR beam recombiner (Fiber Linked Unit for Optical Recombination), which is currently routinely operated at the Mount Hopkins Observatory, Arizona.

The conception and design of LdV are provided by the Observatoire de Paris (Meudon), and it is built as an ESO instrument. The HAWAII based infrared camera is built by the MPE Garching.

## 1.1 SCOPE

This document defines the software user requirements specific to LEONARDO da VINCI.

## 1.2 APPLICABLE DOCUMENTS

1. "LdV Technical Specifications", VLT-SPE-MEU-15810-0002, v1.0, 11/07/99
2. "Interface Control Document between the VLTI and its Instruments", VLT-ICD-ESO-15000-1826, v1.0, 23/04/99

## 1.3 REFERENCE DOCUMENTS

3. "LdV Optical Definition", VLT-SPE-MEU-15810-1000, v1.0, 11/06/99
4. "LdV Mechanical Design", VLT-SPE-MEU-15810-2000, v1.0, 12/07/99
5. "LdV Sources and Guided Optics", VLT-SPE-MEU-15810-1001, v1.0, 10/07/99
6. "LdV Electronics Design", VLT-SPE-MEU-15810-3000, v1.0, 13/07/99
7. “Reference, alignment sources and waveguides in LEONARDO/VINCI”, Vincent Coude du Foresto, 27/02/99
8. “Data Acquisition in VINCI : Terminology and Chronology”, Vincent Coude du Foresto , 28/04/99
9. "VLT Software Management Plan", VLT-PLA-ESO-00000-0006, v2.0, 21/05/92
10. "Technical report on Image Processing Algorithms for TCCD systems", VLT-TRE-ESO-17240-1689, 23/10/98
11. "VLTI Software Requirements Specification", VLT-SPE-ESO-15400-0866, 18/12/96

## 1.4 ABBREVIATIONS, ACRONYMS AND TYPOGRAPHIC CONVENTIONS

| | |
|---|---|
| [goal, min] | Numerical requirement (goal value, minimum value) |
| [Req. #] | Numbered requirement (see section 2.19) |
| ADJ | Adjustable |
| ADU | Analog Digital Unit |
| ALIU | The Alignment Unit |
| DCS | Detector Control Software |
| DP | Data Pipeline |
| DL | Delay Line |
| DLCS | Delay Line Control System |
| FSU | Fringe Sensor Unit |
| GUI | Graphical User Interface |
| GEI | Graphical Engineering Interface |
| HW | Hardware |
| ICS | Instrument Control Software |
| IN | Inserted |
| IWS | Instrument Workstation |
| LCU | Local Control Unit |
| LdV | LEONARDO da VINCI, the whole instrument |
| LEONARDO | The artificial star subsystem |
| LISA | The HAWAII-based infrared camera |
| LISA WS | The LISA LCU (workstation) |
| MONA | The fibered recombiner |
| N.A. | Not applicable |
| OPD | Optical Path Difference |
| OS | Observation Software |
| OUT | Removed |
| SNR | Signal to Noise Ratio |
| SW | Software |
| TBC | To Be Confirmed |
| TBD | To Be Defined |
| TCCD | ESO Technical CCD |
| TCS | Telescope Control Software |
| VCM | Variable Curvature Mirror |
| VINCI | The main optical table of LdV |
| VLT | Very Large Telescope |
| WS | Workstation |

## 1.5 GLOSSARY

***Batch*** : a hundred to a thousand scans
In order to decrease the statistical noise, many interferograms are acquired in a row. The term batch designates this collection of scans.

***Detector Control Software (DCS)*** : the DCS is responsible to control one detector system. It resides partly on the LCU (for the direct interface to hw and real-time issues), partly on the Instrument Workstation, for not real-time issues. For LdV we have 2 DCSs, one for the IR science camera (LISA) and one for the TCCD.

***Frame*** : 4 pixel values
A frame is a set of four numbers which are elementary values of the four signals coming out of LISA : 2 interferometric flux values and 2 photometric flux values (dt acquisition~**1 millisecond**). They are the basic information elements provided by LISA.

***Instrument Control Software (ICS)*** : it is responsible to control the whole instrument hw, except the detectors. It resides partly on the LCU (for the direct interface to hw and real-time issues), partly on the Instrument Workstation, for not real-time issues.

***Instrument modes***
LdV is designed both as an engineering and observing instrument. The instrument modes foreseen for LdV are :

- Autotest
- Autocollimation
- Stellar Interferometer
- Pupil Check
- Image Check
- Artificial Star (LEONARDO alone)

***Instrument setup***
The term "setup" designates the hardware setting of the different optical and mechanical elements on LdV. All the LdV setups are associated with an instrument mode. The setups are subsets of the instrument modes. Several setups are associated with a single instrument mode.

***Instrument status***
The current setup of LdV.

***Observation*** : four batches (on source, off source, beam A, beam B)
During an observation (dt acquisition~**1 to 10 minutes**), four batches are obtained :

- off source (about a hundred scans),
- on source (about a thousand scans),
- beam A only (about a hundred scans),
- beam B only (about a hundred scans).

A pointer to the relevant calibrators observation files is included in the header of the file. This is the largest self-consistent data set, and thus it has to be stored in a single, separated file.

***Observation block*** : a few (star observation+calibrators observation)
An observation block consists of interferograms obtained on a science star (the astronomical object of interest) on one hand, and on a calibrator star on the other hand (which is used as a reference to calibrate the science data). The calibrator data is mandatory to produce scientifically significant visibility values from the science target raw data.
The calibrator star gives a reference for the evaluation of the transfer function of the instrument.
During an observation block, a few observation pairs (star+calibrator) are acquired to sample the transfer function variation (dt acquisition ~**15 minutes to 1 hour**). The final estimation of the

transfer function variations takes into account all the calibrators used during the night, by linearly interpolating between the transfer function values. Still, each observed object is associated specifically with one or several calibrators, to which references should be included in the saved file.

***Observation Software (OS)*** : it coordinates the activities of DCSs, ICS and VLTI and interfaces with the VLT Data Flow System. It runs only on the Instrument Workstation. This implies that it cannot deal with any real-time issue, for which DCS and/or ICS must be responsible.

***Optical Path Difference (OPD)*** : this is the difference in the physical length traveled by the stellar light between one arm of the interferometer (i.e. from one telescope) and the other.

***Scan*** : a few hundred frames
The interferogram itself covering a few hundred microns OPD with ~ thousand frames (sampling : ~ 5 pixels / fringe). It shows fringes on the interferometric channels and the photometric variations (dt acquisition~**0.1 to 1 second**).

# 2 LEONARDO DA VINCI SOFTWARE USER REQUIREMENTS

## 2.1 INSTRUMENT CONCEPT

LdV is at the same time an interferometric beam combiner, designed to coherently add the light coming from two telescopes (either test siderostats, auxiliary telescopes or unit telescopes), a reference source system for the VLTI and an alignment toolkit.

The key element of the instrument is the fibered triple coupler MONA, which uses single-mode (in the K-band) fluoride glass fibers to guide and mix the stellar light coming from the two telescopes. It will provide four signals: two interferometric outputs and two photometric calibration signals. The interferometric outputs carry the scientific information, the fringes visibility, while the calibration signals are used to compensate for the perturbations introduced by the atmosphere.

LdV is made physically of two optical tables, separated by a distance of 10 to 15 meters typically:

- **LEONARDO**: a small optical table bearing the reference sources unit (also called artificial star), which can be operated without the main VINCI table. This is the first table in the optical laboratory, just after the telescopes light beams entrance. In this document, LEONARDO will be considered as a single source, but it consists of several distinct light sources (Visible Laser, thermal source, K-band Laser,…),on which a fiber is connected manually to send the light to the other parts of the instrument.

- **VINCI / ALIU**: the main instrument (VINCI), with the fiber injection optics and the alignment tools, including the Technical CCD detector and optics (for ALIU). It is the last optical along the light beams path before the Fringe Sensor Unit (FSU). It is located just before the FSU on the west side of the laboratory. *MONA and LISA* : the fibered beam combiner (MONA), the output optics and the infrared camera (LISA) are located on the VINCI table.

**Figure 1. Optical layout of VINCI**

## 2.2 LdV System Overview

### 2.2.1 Interferometry Room

LdV is located in the VLT interferometry laboratory. The two LdV optical tables LEONARDO and VINCI/ALIU are separated by about 10 to 15 meters. LEONARDO is the first optical table after the beam compressors. The laboratory layout is not yet frozen and the precise positions of LEONARDO and VINCI/ALIU are still TBD.

### 2.2.2 Optical System

The most recent version of the optical design of LdV is presented p.5. The beam diameter which will be accepted by LdV is 18 mm, corresponding to the diameter produced by the beam compressors.

LdV is divided in four functional units:

- **COMBINER (COMU)** : it groups the fiber injection optics (INA, INB), the MONA fiber combiner box, the fiber output optics (OUT) and the filter wheel of LISA (FILT),

- **ALIGNMENT TOOLKIT (ALIU)** : the Technical CCD head and associated optics, the beamsplitter cubes (ALI1 and ALI5), the ALI slide (bearing ALI3 and ALI4),

- **ARTIFICIAL STAR (ARTU)** : the LEONARDO artificial star optics and light sources (lasers, thermal light).

- **INFRARED CAMERA (LISA)** : the main HAWAII based infrared camera of LdV, including its controler.

### 2.2.3 LISA Camera

The infrared detector of LdV is a HAWAII 1024x1024 array, enclosed in a liquid nitrogen cryostat, with a filter wheel, a cold stop and a lens. Only a quadrant (512x512 pixels) will be used by LdV. The four outputs of the optical fibers from the combiner are imaged on four windows (of one or a few HAWAII detector pixels each) of the detector: two for the interferometric outputs and two for the photometric calibration signals. For simplicity, these windows are refered to as 'pixels' in this document. The camera measures the flux on each pixel while the optical path difference is modulated by the fast scan mirror INA3.

### 2.2.4 Mechanical System

The optomechanics of LdV need a main table (VINCI/ALIU) surface of 2.4x1.5 meters, plus another optical table, 1.8x0.9 meters large for the LEONARDO artificial star.

## 2.3 LDV UNITS

Some setup change is required to switch from one instrument mode of LdV to another. In the following section, both manually movable and locally controlled motorized parts are described. The intensity setting of the fibered K-band laser is preset manually in the laboratory by offsetting the attached fiber head. The LdV division in units is **[Req. 55]**.

### 2.3.1 Combiner Unit

#### 2.3.1.1 Manually Movable Devices

| **Element** | **Control type** | **Comments** |
|---|---|---|
| Stellar Beams Folding Mirrors **COMA3, COMB3** | Manual | |
| Folding Mirror for Output Beam **ALI9** | Manual | |
| Injection A Flat Mirror **INA2** | Manual | |
| Injection B Flat Mirror **INB2** | Manual | |
| Injection B Flat Mirror **INB3** | Manual | |
| Output Optics Flat Mirror **OUT2** | Manual | |

#### 2.3.1.2 Computer Controled Devices

| **Element** | **Control type** | **Comments** |
|---|---|---|
| LISA Filter Wheel **FILT** | Motor | 6 positions |
| Output Fiber Head **OUT1** | Motor | 3 translations + 1 rotation |
| Injection A Fast Scan Mirror **INA3** | Piezo | Provides fast OPD modulation (~10 Hz) |
| Injection B Slide **INB** | Motor | 1 translation |
| Injection B On-axis Parabola **INB1** | Motor | 3 micromotors : tip, tilt and focus |
| Injection A On-axis Parabola **INA1** | Motor | 3 micromotors : tip, tilt and focus |

| | | |
|---|---|---|
| Polarization Motors<br>**POLA A, POLA B** | Motor | Two rotating motors : one for each beam |

### 2.3.2 Alignment Toolkit Unit

#### 2.3.2.1 Manually Movable Devices

| **Element** | **Control type** | **Comments** |
|---|---|---|
| Corner Cubes<br>**ALI12, ALI13** | None | Not adjustable |
| Technical CCD Feed Mirrors<br>**ALI3, ALI4** | Manual | |
| Technical CCD Autocollimation Mirror<br>**ALI8** | Manual | |

#### 2.3.2.2 Computer Controled Devices

| **Element** | **Control type** | **Comments** |
|---|---|---|
| Technical CCD Additional Lens<br>**ALI10** | Motor | 1 large translation<br>(short-range focusing) |
| Technical CCD Focus<br>**ALI7** | Motor | 1 translation (focusing motor) |
| Technical CCD Feed Mirrors Slide<br>**ALI** (ALI3 + ALI4 slide) | Motor | 1 large translation |
| Beam Splitters Cubes<br>**ALI1, ALI5** | Motor | 1 large translation, 3 positions |
| Technical CCD<br>**TCCD** (ALI6) | *Section 2.4.4* | The commands are sent to the TCCD DCS |

### 2.3.3 Artificial Star Unit

#### 2.3.3.1 Manually Movable Devices

| **Element** | **Control type** | **Comments** |
|---|---|---|
| Reference Source Folding Mirrors<br>**ARTB1, ARTA1, ARTA2** | Manual | |
| Stellar Beam Folding Mirrors | Manual | |

| **ARTB2, ARTA3** | | |
|---|---|---|
| Artificial Star Injection On-axis Parabola<br>**ART1** | Manual/Local Motor | Adjustment normally not necessary |
| Artificial Star Injection Flat Mirror<br>**ART2** | Manual/Local Motor | adjustment normally not necessary |
| Reference Source Glass Cube<br>**ART4** | Manual | Transmissive at 2.2 and 10 microns |

#### 2.3.3.2 Computer Controled Devices

| **Element** | **Control type** | **Comments** |
|---|---|---|
| Artificial Star Light Source<br>**ART3** | On/Off | Light switches, K Laser |
| Reference Source Beam Splitters<br>**BSA, BSB** | Motor | 1 large translation, 3 positions |

### 2.3.4 Infrared Camera Unit

| **Element** | **Control type** | **Comments** |
|---|---|---|
| Main Infrared Camera<br>**LISA / OUT3** | *See Section 2.9* | The commands are sent to the LISA DCS |

## 2.4 MOVABLE HARDWARE DESCRIPTION

The following sections give the list of the commands related to the opto-mechanical elements **[Req. 56]**, the TCCD and the LISA camera of LdV. For every Element, the current status, as well as the last setup value should be accessible to the user through the GUI (in online modes) or the GEI (in engineering mode) **[Req. 1]**.

In general, any failure when performing setup actions should be reported to the user immediately, through the GUI or GEI **[Req. 2]**.

### 2.4.1 BSA, BSB

These beam splitter cubes are movable in and out of the light beams, in order to clear the stellar light paths of any obstruction during the interferometric observations. The cubes have to be moved in translation to insert or remove them from the beams. Three positions are available :

- Beamsplitter cube sending the light directly to the instruments (BSA1, BSB1) for autotest mode.

- Beamsplitter cube sending the light to the telescopes (BSA2, BSB2) for autocollimation mode.
- Without any optical element in the beam (OUT), for stellar interferometer mode.

The BSA and BSB slides shall be positioned always in the same direction **[Req. 3]**, in order to avoid any backlash in the mechanical motion.

| Element | Range/Values |
|---|---|
| **BSA** | BSA1, BSA2, OUT |
| **BSB** | BSB1, BSB2, OUT |

### 2.4.2 ALI1, ALI5

ALI1 and ALI5 are beam splitter cubes used to redirect the stellar beams to the technical CCD assembly. The cubes have to be moved in translation to insert or remove them from the beams. Three positions are available:

- Beamsplitter cube directing the light to the Technical CCD assembly (ALI1, ALI5), for alignment purposes.
- Shutter blocking the light from the telescopes (ALI1S, ALI5S). In the current definition, the shutter positions will be used in engineering mode only.
- Without any optical element in the beam (OUT), for stellar interferometer mode.

The ALI1 and ALI5 slides shall be positioned always in the same direction **[Req. 4]**, in order to avoid any backlash in the mechanical motion.

| Element | Range/Values |
|---|---|
| **ALI1** | ALI1, ALI1S, OUT |
| **ALI5** | ALI5, ALI5S, OUT |

### 2.4.3 ALI Slide

The two mirrors ALI3 and ALI4 are on the same moving slide. They are used to redirect either the A or the B beam to the technical CCD assembly, after the ALI1 and ALI5 cubes. An intermediate position allows to see the output of MONA after reflection on ALI9 (mirror movable by hand). The ALI slide has to be moved in translation to insert ALI3, ALI4 or no mirror in the beam.

The ALI slide shall be positioned always in the same direction **[Req. 5]**, in order to avoid any backlash in the mechanical motion.

| Element | Range/Values |
|---|---|
| **ALI Slide** | ALI3/ALI4/FREE |

The user should be informed when the slide is moving, and when it has reached the working positions ALI3/ALI4/FREE.

### 2.4.4 TCCD Assembly (head and lens)

In order to focus the TCCD on a point in the laboratory situated about 5 meters away from the TCCD (where the pupil of the VLTI is), it is necessary to insert a supplementary lens in front of the telescope. Two preset focus positions are selectable **[Req. 6]**, one for the infinity focus without TLENS (FOCUS1), and the other for the focus in the laboratory with TLENS, at the foreseen distance of the pupil image projected by the VCM (PRESET2).

The focusing algorithm for the TCCD is a standard one, based on the analysis of the FWHM of a point source (*see section 2.15.1*).

| Element | Range/Values |
|---|---|
| **TCCD Lens** | IN, OUT |
| **TCCD Focus** | [ 0.. 25000 **(TBD)** ] (microns), PRESET1, PRESET2 |

### 2.4.5 INB Slide

The mirrors INB1, INB2 and INB3 are grouped on a moving slide, to allow for the balancing of the optical paths in each arm of the interferometer. The slide position can take continuous values, to allow precise compensation of the residual OPD. This motion will also be used to look for the fringes in the autotest mode. It will allow to scan for the fringes (spread over a length of a few tens of microns) over a few centimeters length.

The INB slide shall be positioned always in the same direction **[Req. 7]**, in order to avoid any backlash in the mechanical motion.

| Element | Range/Values |
|---|---|
| **INB** | [ 0..25000 ] (microns) |

### 2.4.6 INA1, INB1

These on-axis parabolae are used to inject the light in the input fibers of MONA. They are movable in tip, tilt and focus (translation). These motions are used before every fringe acquisition to maximize the flux injected in the optical fibers by placing the star precisely on the fiber head. During this operation, the flux is monitored on the LISA camera pixels.

| Element | Range/Values |
|---|---|
| **INA1 Focus** | [ 0..25000 ] (microns) |
| **INA1 Tip** | [ 0..12500 ] (microns) |
| **INA1 Tilt** | [ 0..12500 ] (microns) |
| **INB1 Focus** | [ 0..25000 ] (microns) |
| **INB1 Tip** | [ 0..12500 ] (microns) |
| **INB1 Tilt** | [ 0..12500 ] (microns) |

### 2.4.7 OUT1

OUT1 is the fiber bundle output, after the beam combination in MONA. The four fibers are grouped in a bundle, and they are imaged on the LISA HAWAII camera through a fixed lens. The position of the bundle head has to be adjusted very precisely, in lateral position, focus and rotation, so as to image the four fiber heads each on a single pixel of the detector. Only the focus and rotation (around the optical axis) are remote controlled, to be adjustable during the observations. The other adjustments will be done during the day.

The goal is to put a maximum fraction of the light from the fiber output on a single pixel of the HAWAII detector. As this may not be possible, due to the small size of the LISA camera pixels, is should be possible to define a window of several pixels (which might not be adjacent) instead of a single pixel **[Req. 50]**. The maximum number of pixels for each of the four windows should be 25, the minimum number 1. See the adjustment procedure section 2.16.2.

| Element | Range/Values |
|---|---|
| **OUT1 Focus** | [ 0..12500 ] (microns) |
| **OUT1 Rotation** | [ 0..20000 ] (10^(-3) degrees) |

### 2.4.8 Polarization Controllers

In order to compensate for differential polarization states between the two beams, the MONA box includes rotative polarization controlers, one for each beam. They are rotated by two motors, whose range has to be defined (about 1 turn).

| Element | Range/Values |
|---|---|
| **POLA A** | [ 0..360 **(TBD)** ] (degrees) |
| **POLA B** | [ 0..360 **(TBD)** ] (degrees) |

### 2.4.9 LISA Filter Wheel

The LISA filter wheel carries four different filters for operation at different wavelengths (K band, K' band, H band, 2.3 microns narrow band) a free position (open) and an obstructed position (closed). The filters, and the associated software names, may change during the life of the instrument. The filter names are fixed arbitrarily for the moment, but should eventually comply with the ESO filter naming system.

| Element | Range/Values |
|---|---|
| **FILT** | K, KPRIME, H, NARROW, OPEN, CLOSED |

### 2.4.10 Piezo Mirror INA3

This is a flat mirror mounted on a piezo stack, which is moved quickly back and forth (0.1-20 Hz) in order to modulate the optical path difference between the two beams. This is done to scan the fringes, while they are recorder by the LISA infrared detector. The synchronization of the motion of INA3 with the LISA detector is a critical real-time process, which is described in the section 2.9.

## 2.5 SUMMARY OF LDV MOVABLE HARDWARE POSITIONS

| Unit | Element | Range/Values |
|---|---|---|
| **ARTU** | **BSA** | BSA1, BSA2, OUT |
| **ARTU** | **BSB** | BSB1, BSB2, OUT |
| **ARTU** | **ART3** | ON/OFF (*See section 2.8.6*) |

| | | |
|---|---|---|
| **ALIU** | **ALI1** | ALI1, ALI1S, OUT |
| **ALIU** | **ALI5** | ALI5, ALI5S, OUT |
| **ALIU** | **ALI Slide** | ALI3/ALI4/FREE |
| **ALIU** | **TCCD Lens** | IN, OUT |
| **ALIU** | **TCCD Focus** | [ 0.. 25000 **(TBC)** ] (microns), PRESET1, PRESET2 |
| **COMU** | **INB** | [ 0..25000 ] (microns) |
| **COMU** | **INA1 Focus** | [ 0..25000 ] (microns) |
| **COMU** | **INA1 Tip** | [ 0..12500 ] (microns) |
| **COMU** | **INA1 Tilt** | [ 0..12500 ] (microns) |
| **COMU** | **INB1 Focus** | [ 0..25000 ] (microns) |
| **COMU** | **INB1 Tip** | [ 0..12500 ] (microns) |
| **COMU** | **INB1 Tilt** | [ 0..12500 ] (microns) |
| **COMU** | **OUT1 Focus** | [ 0..12500 ] (microns) |
| **COMU** | **OUT1 Tip** | [ 0..12500 ] (microns) |
| **COMU** | **OUT1 Tilt** | [ 0..12500 ] (microns) |
| **COMU** | **OUT1 Rotation** | [ 0..20000 ] (10^(-3) degrees) |
| **COMU** | **INA3** | *See section 2.9* |
| **COMU** | **POLA A** | [ 0..360 **(TBD)** ] (degrees) |
| **COMU** | **POLA B** | [ 0..360 **(TBD)** ] (degrees) |
| **COMU** | **FILT** | K, KPRIME, H, NARROW, OPEN, CLOSED |

## 2.6 INSTRUMENT STATES

From the user point of view, the instrument shall be in one of the four states specified in this paragraph **[Req. 57]**.

| Number | Name | Power | Moving Functions | Reference Sources | LISA, TCCD | Status logging |
|---|---|---|---|---|---|---|
| 1 | Off | Off | Motors and encoders off | Off | Off | Off |
| 2 | Loaded | On | Motors and encoders off | Off | On | Active |
| 3 | Standby | On | Motors and encoders on | Off | On | Active |
| 4 | Online | On | Some motors off after reaching position, encoders on | Any | On | Active |

Transition possibilities between instrument states:

1 → 2
2 → 1,3
3 → all
4 → all

Power up/down (from/to state 1 or 2) of the whole instrument, including CCD, will be done manually. Transitions between conditions 2 - 4 will be performed under SW control.

When LdV is set to state 'Online', the motors whose positions are monitored by differential encoders are initialized by sending them to their references.

The instrument has achieved the 'Loaded' state only when all the real motor positions are available to the ICS (either read from absolute encoders, or set to the reference). The switching from 'Loaded' to 'Online' can then be done. No particular starting position is required by the instrument design in the 'Online' mode. The user has the possibility to choose any setup once the instrument is 'Online'. A default starting setup for the 'Online' state could be chosen (a good starting point could be the 'Stellar Interferometer Idle' setup), but this is not mandatory.

Power up following a power failure may leave the instrument in a hazardous condition so there are a number of hardware interlocks for protection of the LISA camera. The motion of the motors and other mechanical systems should be stopped after a power failure.

The commands issued to the ICS and DCS and the corresponding replies from the ICS are logged when the instrument power is on **[Req. 60]**.

The mechanical design of the functions is such that the positions will be kept due to friction. To reduce dissipation of motors, the mechanical devices will be positioned and then the motors switched off. The only remaining dissipation is that of the encoders. They will be left on if the position of the related moving device has to be known to a high precision and if it is moved during the observations. Which encoders will have to be left on has to be checked.

In the OFF, LOADED and STANDBY states, LdV is not directly operational. The BSA and BSB cubes of LEONARDO are placed in positions OUT, where they do not block the light beams, as the other instruments may need to access them. The optical elements on the VINCI table do not require particular positioning, and should be left in the last on-line state setup used.

## 2.7 LdV Engineering and Maintenance Modes

The need for these modes is only to have direct access to all the hardware parameters of the instrument. The normal state for LdV during Engineering and Maintenance operation is "Online".

In the Engineering mode, the user can access and monitor individually the hardware devices (motors, TCCD,…) through the part of the GUI related directly to the ICS and DCS **[Req. 61]**. It is then possible to adjust all the hardware parameters individually (encoders ranges, motor speeds, voltages,…).

## 2.8 LdV Instrument Modes

Here are described the different modes and the associated hardware setups while LdV is in Online State. Setups are assumed to be particular settings of the movable devices of LdV associated with an instrumental mode. The LdV setups allow the user to move the many LdV optical and mechanical elements at the same time as a whole, by entering the corresponding request.

Generally speaking, there is no critical time constraint on the motion of the LdV hardware devices (except for the piezo mirror, see section 2.9.4). No particular hardware incompatibilities are foreseen on the VINCI table.

The software system should then aim at moving the devices as quickly as possible **[Req. 52]** (goal 5 seconds, minimum 15 seconds), in parallel, in order to spare observing time. But there is no critical time limit driven by the conception of the instrument.

The following tables give the setups for each LdV mode.

The setups are named by their function, for example “Autotest Injection Adjust” designates the hardware setup used to make the adjustment of the light injection in the fiber heads, in the autotest mode. The “Idle” setup, which is found in all the instrument modes, is used for engineering purposes or during observations for special needs. It is the default starting setup if no setup is specified by the user when switching to a mode/setup, including the engineering and maintenance modes **[Req. 54]**. In the “Idle” setup, the instrument in online and ready to switch to another setup in the same mode or in another mode.

“IN” = in the optical beam, “OUT” = off the optical beam, N.A. = not applicable, ADJ = adjustable.

### 2.8.1 Autotest

In this mode, LdV can observe fringes without any other VLTI system involved. The LEONARDO artificial star is used to produce the light which is sent directly to the VINCI table.

| Unit | Element | Autotest Idle | Autotest Output Adjust | Autotest Injection Adjust | Autotest Fringe Search | Autotest Data Acquisition |
|---|---|---|---|---|---|---|
| COMU | INB SLIDE MOTOR | OFF | OFF | OFF | ADJ (steps) | OFF |
| COMU | INB1 MOTORS (TIP/TILT/FOCUS) | OFF | OFF | ADJ | OFF | OFF |
| COMU | INA1 MOTORS (TIP/TILT/FOCUS) | OFF | OFF | ADJ | OFF | OFF |
| COMU | INA3 FAST SCAN PIEZO | OFF | OFF | OFF | ON | ON |
| COMU | OUT1 MOTORS (TIP/TILT/FOCUS/ ROTATION) | OFF | ADJ | OFF | OFF | OFF |
| COMU | POLA A, POLA B MOTORS | OFF | OFF | OFF | OFF | OFF |
| COMU | LISA Filter Wheel | N.A. | OPEN | OPEN | ADJ | ADJ |
| ALIU | ALI1 POSITION | OUT | OUT | OUT | OUT | OUT |
| ALIU | ALI5 POSITION | OUT | OUT | OUT | OUT | OUT |
| ALIU | ALI SLIDE POSITION | N.A. | N.A. | N.A. | N.A. | N.A. |
| ALIU | TCCD LENS POSITION | N.A. | N.A. | N.A. | N.A. | N.A. |
| ALIU | TCCD FOCUS | N.A. | N.A. | N.A. | N.A. | N.A. |
| ARTU | BSA POSITION | BSA1 | BSA1 | BSA1 | BSA1 | BSA1 |
| ARTU | BSB POSITION | BSB1 | BSB1 | BSB1 | BSB1 | BSB1 |
| ARTU | LEONARDO light source | ON | ON | ON | ON | ON |
| LISA | LISA Acquisition | OFF | FULL FRAME | 4 PIX, NOT SYNC | 4 PIX, SYNC | 4 PIX, SYNC |

### 2.8.2 Autocollimation

This mode give the capability to send light in the whole VLTI optical system up to the telescopes. This light is then retroreflected to VINCI and fringes are measured. This requires to inject light from LEONARDO, using the BSA2 and BSB2 beamsplitter cubes positions. This mode will be available on-line, without requiring any manual operation in the laboratory. No external access (from the other instruments) is foreseen.

The switching to the autocollimation mode requires to send an OPD offset value to the delay line **[Req. 8]**, compared to the Stellar Interferometer or Autotest modes. The value of this offset is

constant, and depends on the geometry of the artificial star injection. It will be measured during the integration of LdV. It should be possible to change this offset in the software if necessary.

| Unit | Setup name<br><br>Element | Autocoll. Idle | Autocoll. Output Adjust | Autocoll. Injection Adjust | Autocoll. Fringe Search | Autocoll. Data Acquisition |
|---|---|---|---|---|---|---|
| COMU | INB SLIDE MOTOR | OFF | OFF | OFF | OFF | OFF |
| COMU | INB1 MOTORS (TIP/TILT/FOCUS) | OFF | OFF | ADJ | OFF | OFF |
| COMU | INA1 MOTORS (TIP/TILT/FOCUS) | OFF | OFF | ADJ | OFF | OFF |
| COMU | INA3 FAST SCAN PIEZO | OFF | OFF | OFF | ON | ON |
| COMU | OUT1 MOTORS (TIP/TILT/FOCUS/ ROTATION) | OFF | ADJ | OFF | OFF | OFF |
| COMU | POLA A, POLA B MOTORS | OFF | OFF | OFF | OFF | OFF |
| COMU | LISA Filter Wheel | N.A. | OPEN | OPEN | ADJ | ADJ |
| ALIU | ALI1 POSITION | OUT | OUT | OUT | OUT | OUT |
| ALIU | ALI5 POSITION | OUT | OUT | OUT | OUT | OUT |
| ALIU | ALI SLIDE POSITION | N.A. | N.A. | N.A. | N.A. | N.A. |
| ALIU | TCCD LENS POSITION | N.A. | N.A. | N.A. | N.A. | N.A. |
| ALIU | TCCD FOCUS | N.A. | N.A. | N.A. | N.A. | N.A. |
| ARTU | BSA POSITION | BSA2 | BSA2 | BSA2 | BSA2 | BSA2 |
| ARTU | BSB POSITION | BSB2 | BSB2 | BSB2 | BSB2 | BSB2 |
| ARTU | LEONARDO light source | ON | ON | ON | ON | ON |
| LISA | LISA Acquisition | OFF | FULL FRAME | 4 PIX, NOT SYNC | 4 PIX, SYNC | 4 PIX, SYNC |

### 2.8.3 Stellar Interferometer

This is the standard mode for observations with the test siderostats, the ATs or the UTs. The light from the star is directed into the beam combiner wihout going through any transmissive optical element, to reduce the absorption.

| Unit | Element | Stell. Interf. Idle | Stell. Interf. Injection Adjust | Stell. Interf. Fringe Search | Stell. Interf. Data Acquisition | Stell. Interf. Polarization Adjust |
|---|---|---|---|---|---|---|
| COMU | INB SLIDE MOTOR | OFF | OFF | OFF (Main DL) | OFF | OFF |
| COMU | INB1 MOTORS (TIP/TILT/FOCUS) | OFF | ADJ | OFF | OFF | OFF |
| COMU | INA1 MOTORS (TIP/TILT/FOCUS) | OFF | ADJ | OFF | OFF | OFF |
| COMU | INA3 FAST SCAN PIEZO | OFF | OFF | ON | ON | ON |
| COMU | OUT1 MOTORS (TIP/TILT/FOCUS/ ROTATION) | OFF | OFF | OFF | OFF | OFF |
| COMU | POLA A, POLA B MOTORS | OFF | OFF | OFF | OFF | ON |
| COMU | LISA Filter Wheel | N.A. | OPEN | ADJ | ADJ | ADJ |
| ALIU | ALI1 POSITION | OUT | OUT | OUT | OUT | OUT |
| ALIU | ALI5 POSITION | OUT | OUT | OUT | OUT | OUT |
| ALIU | ALI SLIDE POSITION | N.A. | N.A. | N.A. | N.A. | N.A. |
| ALIU | TCCD LENS POSITION | N.A. | N.A. | N.A. | N.A. | N.A. |
| ALIU | TCCD FOCUS | N.A. | N.A. | N.A. | N.A. | N.A. |
| ARTU | BSA POSITION | OUT | OUT | OUT | OUT | OUT |
| ARTU | BSB POSITION | OUT | OUT | OUT | OUT | OUT |
| ARTU | LEONARDO light source | OFF | OFF | OFF | OFF | OFF |
| LISA | LISA Acquisition | OFF | 4 PIX, NOT SYNC | 4 PIX, SYNC | 4 PIX, SYNC | 4 PIX, SYNC |

### 2.8.4 Pupil Check

The light sources (one Light Emitting Diode for each telescope) at the centers of the two mirrors M2 are on.

**This mode, and all the related data, should be accessible from outside of LdV software [Req. 9]**. The LdV instrument is exclusively assigned to the instrument requesting the pupil check. Only the ALIU and ARTU (LEONARDO) units are concerned, but no other operation can be conducted simultaneously. The images and other data (position of the center of the pupil,…) obtained in this mode by an external user instrument should be made available to this instrument.

No real-time constraint is foreseen in this mode.

The pupil check is done by imaging the pupil of the two telescopes on the TCCD. During normal operation, the pupil is situated on the VINCI table, on the parabolae INA1 and INB1. After this image has been saved, the image of the artificial star provided by LEONARDO (star image at infinity) is obtained. By comparing the positions of the pupil and artifial star, the user can evaluate the quality of the pupil alignment.

The LdV TCCD will be used in this mode during the alignment of the pupil of the VLTI, but the control of the mirrors of the optical train is not part of LdV SW, but of VLTI software. It will only provide the coordinates of the pupil and artificial source images to the VLTI alignment software, which will adjust the relevant mirrors. The corresponding interface is **TBD**.

The TCCD can image the pupil from 1 meter to infinity. It is necessary to insert an additional lens (TLENS achromat lens, focal length = 2000 mm) in front of the TCCD in order to focus to pupil distances (to the TCCD refractor lens center) of less than 3900 mm. The focal length of the TCCD refractor is 300 mm. The pupil longitudinal positioning question is adressed in the document [2] section 4.2.4. The detailed description of the optical design for pupil check can be found in the document [3], p 14.

The size of the pupil image on the TCCD will be 6 mm for INA (magnification 0.3) and 8 mm for INB (magnification 0.4), when it is at its nominal position on the on-axis parabolae INA1 (distance from the autocollimator = 2000 mm) and INB1 (distance from the collimator = 1500 mm).

| **Pupil position** | **Additional lens position** |
|---|---|
| 1320 mm to 3900 mm | Inserted |
| 3900 mm to infinity | Removed |

Two preset focus positions are selectable **[Req. 6]**, one for the infinity focus without TLENS (PRESET1) (this is used in the PupilCheck.ArtificialStar* setups) and the other for the focus in the laboratory with TLENS, at the foreseen distance of the pupil image projected by the VCM (PRESET2).

After the rough focus has been achieved, the fine focus procedure can be done if necessary.

| **Unit** | **Element** | **Pupil Check Idle** | **Pupil Check Telescope A** | **Pupil Check Telescope B** | **Pupil Check Artificial Star A** | **Pupil Check Artificial Star B** |
|---|---|---|---|---|---|---|
| COMU | INB SLIDE MOTOR | N.A. | N.A. | N.A. | N.A. | N.A. |
| COMU | INB1 MOTORS (TIP/TILT/FOCUS) | N.A. | N.A. | N.A. | N.A. | N.A. |

| | | | | | | |
|---|---|---|---|---|---|---|
| COMU | INA1 MOTORS (TIP/TILT/FOCUS) | N.A. | N.A. | N.A. | N.A. | N.A. |
| COMU | INA3 FAST SCAN PIEZO | N.A. | N.A. | N.A. | N.A. | N.A. |
| COMU | OUT1 MOTORS (TIP/TILT/FOCUS/ ROTATION) | N.A. | N.A. | N.A. | N.A. | N.A. |
| COMU | POLA A, POLA B MOTORS | N.A. | N.A. | N.A. | N.A. | N.A. |
| ALIU | ALI1 POSITION | IN | IN | IN | IN | IN |
| ALIU | ALI5 POSITION | IN | IN | IN | IN | IN |
| ALIU | ALI SLIDE POSITION | NOMIRROR | ALI3 | ALI4 | ALI3 | ALI4 |
| ALIU | TCCD LENS POSITION | OUT | IN | IN | OUT | OUT |
| ALIU | TCCD FOCUS | N.A. | ADJ PRESET2 | ADJ PRESET2 | ADJ PRESET1 | ADJ PRESET1 |
| ARTU | BSA POSITION | OUT | OUT | OUT | IN | IN |
| ARTU | BSB POSITION | OUT | OUT | OUT | IN | IN |
| ARTU | LEONARDO light source | N.A. | N.A. | N.A. | ON | ON |
| ARTU | LISA Filter Wheel | N.A. | N.A. | N.A. | N.A. | N.A. |
| LISA | LISA Acquisition | N.A. | N.A. | N.A. | N.A. | N.A. |

### 2.8.5 Image Check

The artificial star is off. The setups are the same as the Pupil check, except for the additional lens, which is not used. The pre-position PRESET1 for the TCCD focus is the focus at infinity.

**This mode, and all the related data, should be accessible from outside of LdV software [Req. 9]**. LdV instrument is exclusively assigned to the instrument requesting the image check. Only the ALIU and ARTU (LEONARDO) units are concerned, but no other operation can be conducted simultaneously. The images and other data (position of the center of the pupil,…) obtained in this mode by an external user instrument should be made available to this instrument.

No real-time constraint is foreseen in this mode.

| Unit | Element | Image Check Idle | Image Check Telescope A | Image Check Telescope B |
|---|---|---|---|---|
| COMU | INB SLIDE MOTOR | N.A. | N.A. | N.A. |

| | | | | |
|---|---|---|---|---|
| COMU | INB1 MOTORS (TIP/TILT/FOCUS) | N.A. | N.A. | N.A. |
| COMU | INA1 MOTORS (TIP/TILT/FOCUS) | N.A. | N.A. | N.A. |
| COMU | INA3 FAST SCAN PIEZO | N.A. | N.A. | N.A. |
| COMU | OUT1 MOTORS (TIP/TILT/FOCUS/ ROTATION) | N.A. | N.A. | N.A. |
| COMU | POLA A, POLA B MOTORS | N.A. | N.A. | N.A. |
| COMU | LISA Filter Wheel | N.A. | N.A. | N.A. |
| ALIU | ALI1 POSITION | IN | IN | IN |
| ALIU | ALI5 POSITION | IN | IN | IN |
| ALIU | ALI SLIDE POSITION | NOMIRROR | ALI3 | ALI4 |
| ALIU | TCCD LENS POSITION | OUT | OUT | OUT |
| ALIU | TCCD FOCUS | N.A. | ADJ PRESET1 | ADJ PRESET1 |
| ARTU | BSA POSITION | OUT | OUT | OUT |
| ARTU | BSB POSITION | OUT | OUT | OUT |
| ARTU | LEONARDO light source | N.A. | N.A. | N.A. |
| LISA | LISA Acquisition | N.A. | N.A. | N.A. |

### 2.8.6 Artificial Star

In this setup, LEONARDO can be operated without the main VINCI optical table **[Req. 10]**. As a general rule, LEONARDO should be considered as an integral part of the VLTI infrastructure. The 'user' instrument requests the exclusive assignment of LEONARDO in order to avoid conflicts. The default assignment of LEONARDO should be LdV.

All the LEONARDO light sources are not all immediately accessible on-line. Only one is available remotely at a time, and the switching from one source to another has to be done manually in the laboratory. The following table lists the light sources which are foreseen on VINCI (reference document [7]):

| **Source type** | **Bands** | **Single / multi-mode** |
|---|---|---|
| Red laser diodes (2) | Visible | Single-mode |
| 2.3 microns laser | K | Single-mode |
| Thermal | K | Single-mode |

| | | |
|---|---|---|
| Thermal | K | Multi-mode |
| Thermal | N | Single-mode |
| Thermal | N | Multi-mode |
| Thermal | Visible | Multi-mode |

This mode will be used mainly after the commissioning phase, when the science instruments AMBER and MIDI are operational. The electronic racks of LdV will be on, as well as the WS sw, thus allowing normal operation of the motors and light switches of LEONARDO. The light source can be turned ON without being injected in the optical beams in order to pre-heat it. It can also be turned OFF with the cubes IN to check for the effect of the cubes on the optical transmission. **This mode, and all the related data, should be accessible from outside of LdV software [Req. 11]**.

There is no remote intensity adjustment foreseen for any of the sources on LEONARDO.

The external instruments should access LEONARDO only through the predefined modes (described in the following table) **[Req. 12]**. No low-level command is foreseen to be accessible from outside of LdV software.

| **Unit** | **Element** | **Artificial Star Off Removed** | **Artificial Star On Inserted** | **Artificial Star On Removed** | **Artificial Star Off Inserted** | **Autocollimation On Inserted** |
|---|---|---|---|---|---|---|
| ARTU | BSA | OUT | BSA1 | OUT | BSA1 | BSA2 |
| ARTU | BSB | OUT | BSB1 | OUT | BSB1 | BSB2 |
| ARTU | LEONARDO Light source | OFF | ON | ON | OFF | ON |

## 2.9 DATA ACQUISITION ASPECTS OF LDV

### 2.9.1 Description

The piezo mirror INA3 is used to quickly modulate the optical path difference between the two beams, in order to scan over the fringes. The frequency of its motion is adjustable from 0.1 Hz to 20 Hz **[Req. 13]**. The most common frequency which will be used is 10 Hz. The scan length is also adjustable, from 1 micron to 360 microns **[Req. 14]**. The wave used to control the piezo has a “smooth triangle” shape, which is intermediate between a triangle and a sinusoid. The corresponding factor for the softening ratio is the wave shape factor, whose range will be between 0 (triangle) and 1 (sinusoid) **[Req. 15]**. The generation of this curve is made at the LCU level, based on the defined parameters.

The most important difficulty for the piezo is that it has to be precisely synchronized with the LISA acquisition during the scanning of the fringes, at a submillisecond precision (goal 0.5 ms, minimum 1 ms) **[Req. 16]**. The synchronization does not have to be done at the frame level, but only at the beginning of the scan. This scheme assumes that the internal clockings of the two LCUs (piezo LCU and LISA WS) are accurate enough to guarantee no significant deterioration of the synchronization during the scan duration.

### 2.9.2 Terminology and typical values

There are four fiber outputs in LdV, named I1, I2, P1, P2. The four fibers are arranged (through a fiber bundle) in a square which forms the optical output imaged on the LISA focal plane array. Ideally, each fiber core is imaged onto a single pixel. In case the light cannot be put on a single pixel, it will have to be collected in a window of 1 to 25 pixels **[Req. 50]** (that might not be adjacent). The LISA DCS reads out only those pixels located in the four windows. It then returns four numbers which correspond to the total energy output of I1, I2, P1 and P2 respectively. This operation (readout and sommation) is called a "frame". Frame rates range between a few Hz and a few kHz, a typical value is 1500 Hz.

A "**scan**" is a collection of frames. While observing the astronomical source, they are obtained while the optical path difference (OPD) is modulated by the fast scan mirror INA3. There are real-time issues related to the acquisition of successive scans, which are detailed below.

A "**batch**" is the collection of a number of scans (from about a hundred to a thousand), obtained to reduce the stastical noise. During the batches off-source and with only one of the beams, the piezo mirror could be stopped, as OPD modulation is not relevant, but the data produced is the same as on-source (four series of numbers : I1, I2, P1, P2).

An "**observation**" is a collection of four batches:

- **On-source** : the target is centered in the field and fringes are observed. A few thousand scans are obtained during this phase.
- **Off-source** : the telescopes are offset from the source in order to measure the sky background signal. The number of scans Off-source is aproximately the same as On-Source (but they are acquired faster as no synchronization is need between the piezo mirror and the LISA camera).
- **Beam A** : the beam B is obstructed (by a shutter or by offsetting the telescope B), and a series of about a hundred scans are obtained.
- **Beam B** : the beam A is obstructed (by a shutter or by offsetting the telescope A), and a series of about a hundred scans are obtained.

The order in which these batches will be acquired is not necessarily the one given here. An observation represents 5-10 mm of observing time and its end product is the fundamental VINCI data unit to be saved in the VLTI archive. No time-critical operation is expected to occur between two successive observations.

The fast scan mirror INA3 is mounted on a piezo device which is controled through a command voltage Uc. The following table lists the different scales that relate the command voltage to the OPD generated. The gain factor g takes into account geometric considerations, sign conventions, and the stiffness of the piezo support blades. Its absolute value is typically 1.5 but it has to be calibrated during integration.

| | | |
|---|---|---|
| Piezo command voltage Uc | -5 V (or 0 V) | +5 V (or +10 V) |
| Piezo input voltage Uin | 0 | 1000 V |
| Piezo mechanical extension | 0 micron | +180 microns |
| OPD generated | 0 micron | 180 x g microns |

The voltage ramp that generates the scan is of "smooth triangle" type. The OPD modulation rate v is called the OPD velocity, or fringe velocity. The data are collected only when v is stabilized, i.e. during the linear part of the ramp. Fringe velocity range from 0 to 2500 microns/s. For each observation, the user requests (via the OS) a given velocity and DAQ OPD (typical values are 660 microns/s and 200 microns respectively). Depending on those parameters, the total duration of data collection in a scan $\Delta t_{DAQ} = OPD_{DAQ/v}$ can range between 0.05 s and several minutes. We shall adopt 0.1 s as a nominal (and most common) value. The user also choses a "sample interval", i.e. the OPD interval between two successive frames. This is translated by the OS into a frame rate. The combination of DAQ OPD length, fringe velocity and frame rate determines the number of frames recorded per scan.

After acquisition, a "quick look" analysis is performed by LdV DCS (at the LCU level). Each scan is rearranged in four 1D arrays (synchronous time sequences) that record the intensity evolution at each of the fiber outputs I1, I2, P1, P2. An algorithm (see section 2.9.6) is performed on the arrays I1 and I2 to determine whether fringes have been observed **[Req. 17]** and, if yes, what is the time $t_{ZOPDobs}$ of the observed location of the center of the fringe packet (corresponding to zero total OPD). This time is compared to the expected time $t_{ZOPDexp}$ of zero OPD occurrence, and the quantity $OPD_{OFFSET}=(t_{ZOPDexp} - t_{ZOPDobs}) \times v$ is sent to the VLTI delay line OPD controler as an OPD offset.

For the information of the observer, it would be very interesting to compute a simple estimation of the instrumental visibility as a complement to the OPD offset, and to send it to the LdV WS software. The software should display one computed visibility to the user at a frequency of [2 Hz, 1 Hz] **[Req. 18]**.

Under normal observing conditions, the OPD offset should be smaller than 100 microns. Note that the quick look analysis requires that also reside in memory :

- A dark scan, or a small series of scans acquired off source
- The quick look data reduction parameters

These parameters are updated at the end of each individual observation.

In the current implementation of VINCI it has only one spectral channel (one window for each signal I1, I2, P1, P2). With a typical number of frames per scan of 512, we can estimate the quantity of data contained in one scan : if the data from LISA are coded on 16 bits, one typical scan represents 4 kbytes of data. Only 2 kbytes (256 frames centered on $t_{ZOPDexp}$) per scan are saved.

In a seond generation upgrade of the instrument, it is foreseen to insert a dispersive element in front of LISA to disperse the four output signals. This will result in an increase of the data quantity produced at each scan, by a factor which could be up to 50 (see section 2.20.3). The software system should be able to manage about 100 kbytes per scan **[Req. 19]**, but the associated electronics hardware should not be considered for the first phase of LdV.

A scan I begins at a time ti. We call $\Delta t_{DAQ}=t_{DAQ\_end} - t_{DAQ\_start}$ the duration of useful data collection, the ratio $\Delta t_{DAQ} / (t_{i+1} - t_i)$ defines the duty cycle, i.e. the efficiency of LdV. This duty cycle should be as high as possible : [95%, 90%] **[Req. 20]**.

### 2.9.3 Chronology of data acquisition

The following chronology assumes that the quick look analysis is performed by LISA WS. This is necessary because no real-time processes can be done by the OS.

| Time | Definition | LdV/VLTI event | VINCI ICS event | LISA DCS event |
|---|---|---|---|---|
| | | Wait for :<br>- Delay line in READY status<br>- Piezo in READY status<br>- LISA in READY status<br>- Check that DAQ is requested<br>- Determine tscan_start, tscan_end, tDAQ_start, tDAQ_end and transfer that information to VINCI ICS and LISA DCS | | Reset LISA |
| Ti = tscan_start | Begin scan | | - Start generating voltage ramp | |
| TDAQ_start | Begin data acquisition | | | - Start recording frames |
| TDAQ_end | End data acquisition | Wait for :<br>- Delay Line in TRACK status<br>- LISA in READY status<br>- Piezo in READY status<br>- Check that one more scan is requested<br>- Determine tscan_start, tscan_end, tDAQ_start, | - Wait for tscan_end<br>- Reset piezo status to READY | - End recording frames<br>- Perform quicklook analysis<br>- Transfer offset information to the delay line<br>- Transfer scan data to VINCI OS<br>- Reset LISA |

| | | | | |
|---|---|---|---|---|
| | | tDAQ_end and transfer that information to VINCI ICS and LISA DCS | | |
| Tscan_end | End of piezo motion | | | |
| Ti+1 = tscan_start | Begin scan | | - Start generating voltage ramp | |

The time intervals [Tscan_start, tDAQ_start] and [tDAQ_end, Tscan_end] are used to accelerate and decelerate the piezo mirror. These intervals are not compressible, as they are defined by the hysteresis curve of the piezo itself.

### 2.9.4 Real-time considerations

The critical time interval is $t_{i+1} - t_{scan\ end}$, which corresponds to the 'dead time' during which VINCI is not acquiring data. The software architecture should be designed to, ideally, make it zero or at least minimal **[Req. 21]** : this is the time interval (after the end of the scan) during which the piezo mirror is stopped to wait for the OPD offset computation and correction to finish. After that, the piezo goes backwards to start the next scan in the other direction.

This means that the software system should compute the fringe position quickly enough ('quick look' algorithm), and correct the delay line position, so that it is possible not to waste any time by stopping the piezo at its extremal position (to wait for the computation to end). This puts a constraint on the computation time $t_{OPD\ offset}$ which is : $t_{OPD\ offset} < t_{scan\ end} - t_{DAQ\ end}$. In any case, the 'dead time' $t_{i+1} - t_{scan\ end}$ should be minimized in order to obtain the maximum efficiency of LdV, but the delay line has to be in the 'track' status before starting the next data acquisition.

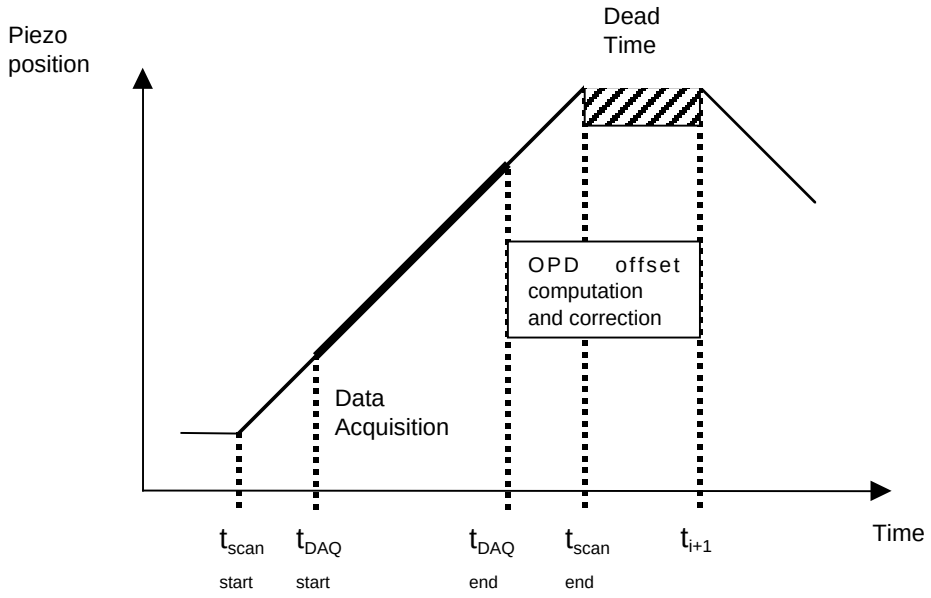


The time critical operations are :
- Transfer of scan data from LISA DCS to LdV OS
- Quick look analysis at the LISA WS level
- Transfer of OPD $_{OFFSET}$ value from LISA WS to the delay line (through the DLCS Interface module)
- Transfer of timing information for the next scan from LdV OS to VINCI ICS and LISA DCS

Meanwhile, the timing information ($t_{scan\_start}$, $t_{DAQ\_start}$,…) should be determined within [0.5 ms, 1 ms] across LdV OS, VINCI ICS and LISA DCS **[Req. 16]**.

### 2.9.5 Delay Line Control

In order to follow the motion of the fringe packet induced by the atmospheric piston effect, it is necessary to send an offset to the position of the delay line. This is done after each scan in which fringes have been detected **[Req. 22]**. The OPD offset is transferred to the delay line control system through the OPD controller.

The OPD offsets shall not be sent to the delay line when the Fringe Sensor Unit (FSU) is used **[Req. 62]**. A switch should allow the user to disable the OPD corrections by LdV.

The total time between the start of the quick-look analysis and the end of the delay line corrective motion (LdV informed that the DL is again in 'track' mode) should be less than the slow-down time of the piezo $t_{scan\ end}$ - $t_{DAQ\ end}$ **[Req. 23]**. This time lapse depends on the shape factor applied to the piezo command signal. It is the shortest when the piezo wave shape is set to its most 'triangular' value. This setting should set the constraint on the OPD offset correction time. Though, not all the scan frequencies can be used with all the wave shapes : generally speaking, the faster the scan, the more sinusoidal the wave shape (to reduce hysteresis). The precise minimum time interval available is thus variable depending on the frequency and wave shape (5-10 ms range).

### 2.9.6 Quick Look Fringe Detection Algorithm

This section describes the algorithm which will be used to detect the fringe packet and then to compute the OPD offset to be sent to the delay line for the next scan.

#### 2.9.6.1 Construction of the Combined Interferometric Signal

The two signals from the interferometric outputs are combined in order to increase the signal to noise ratio. As the two signals are antiphased (max light in one is min light in the other), which means that they are substracted to obtain the combined signal. The simple substraction of the two signals is not optimal because the intensities in the two channels are not exactly the same. It is necessary to compute a coefficient $\alpha$ which minimizes the quantity $I = |I_1 - \alpha.I_2|$, eventually to have the mean of *I* equal zero. The computation of $\alpha$ is done by minimizing the quadratic error on the *I* value.

#### 2.9.6.2 Frequency Filtering

In order to reduce the noise on the combined interferometric signal *I*, the second step of the algorithm is to filter the signal in the frequency space. We know in advance precisely the range of frequencies covered by the fringe signal, from the bandwidth of the K-band (or other) filter used in LISA. So, it is necessary to make a fast Fourier transform of *I*, to cut the frequencies below $F_{min}$ and over $F_{max}$, and then take the inverse Fourier transform of the resulting signal. The number of frames in the scan can be adjusted to optimize the speed of the FFT computation (depends on the algorithm used).

#### 2.9.6.3 Fringes Detection and OPD Offset

The fringe detection follows a simple scheme. The filtered signal *I* is scanned for any point which is over 5 times the standard deviation. If one such point is detected in the signal, then the signal 'fringes detected' can be issued. A list of all these points is built, containing their temporal coordinates (for example : one point over 5 sigmas detected at 0.019 s after the beginning of the scan). If this list is empty, no fringes were detected. The median value of the list is computed, and it corresponds to the position of the fringes centroid center. Finally this temporal position is converted into the OPD offset, taking into account the speed of the piezo scan, and sent to the delay line.

#### 2.9.6.4 Alternative Algorithm for Fringe Detection and OPD Offset

The phase function could be used to determine the precise location of the fringe packet, but this should be considered currently as a second-choice alternative to the previously described algorithm.

### 2.9.7 Synchronized Data Acquisition Parameters (SYNC)

As the fiber outputs of MONA are imaged on a few pixels of LISA, only those pixels are read during observations. The coordinates of the pixels which are to be read are defined by the user **[Req. 50]**. The shapes of the four windows is not necessarily rectangular, as it might be more efficient for example to read an L-shaped figure if the coma is too large.

The rate at which the four windows are read is set by the user **[Req. 24]**, depending on the brightness of the observed target. This setting can be computed by the WS SW from other parameters (described hereafter) entered by the user and that are related to the piezo mirror motion and fringes characteristics.

The "**total OPD range**" is the optical path length covered by the piezo motion, the "**fringe velocity**" is the speed at which the fringes are moving during the scan. There is a direct relationship between the fringe velocity and the piezo mirror scan speed. The "**sample interval**" is the physical OPD length over which the pixel integration is made.

From the user point of view, the parameters of the acquisition should be :

| **Parameter** | **Range/Values** |
|---|---|
| **Data Acq. Total OPD Range** | [ 1..300 ] (microns) |
| **Data Acq. Fringe Velocity** | [ 1..2500 ] (microns/s) |
| **Data Acq. Sample Interval** | [ 0.1..3 ] (microns)<br>[ 1..10 ] (points per fringe) |

After these parameters have been set by the user, the LdV ICS computes the corresponding values of the frequency, voltage range, and optimal wave shape factor for the control of the Fast Scan Piezo :

- the piezo frequency is directly given by : Fringe Velocity (in microns/s) / OPD range (microns),
- the voltage range is a direct function of the sample interval, it include provision for the acceleration and slow down of the piezo (which depends on the wave shape),
- the optimal wave shape is determined based on the OPD range and the frequency, through a decision table (**TBD**).

The integration time for LISA is computed by : Sample Interval (microns) / Fringe Velocity (in microns/s).

The command to start the synchronized acquisition of data can be sent by the user or the WS sw at any time, by switching to the mode 'Stellar Interferometer Data Acquisition'.

### 2.9.8 Signal Check Parameters (NOT SYNC)

In order to precisely center the star image on the fiber head (by moving the injection parabolae INA1 and INB1), it is required to have a continuous estimation of the flux on the four used pixels of LISA **[Req. 25]**. This process is called the "injection optimization". During this phase, the injection mirrors INA1 and INB1 are moved in tip and tilt to position the star image intensity peak exactly on the tiny fiber head (a few microns wide). The flux observed on the LISA pixels gives the

information to know if we are getting close to this maximum: if it rises, we are getting closer, if it falls, we are going the wrong way. Moreover, the atmospheric turbulence causes the flux to vary erratically during this process. Basically, this optimization has to be done before each star observation, that is every 5 to 10 minutes.

*The injection optimization is a hard point for the control software if it is intended to be done automatically. The necessity for an operator to do it manually may not be possible to avoid. A possible algorithm for the automatic injection optimization is described in the section 2.20.1. It is foreseen to achieve the complete automatization of the LdV operations, and this possibility should be left open in the software design.*

From the user point of view, the parameters are the same as for the synchronized mode, except that the signals are displayed in a continuous loop. The only difference is that the piezo mirror might not be moving effectively (if simpler from the SW point of view). Only the computed pixel readout frequency (also called frame rate) is used effectively as a parameter. The difference with synchronized mode is that the camera is read continuously, without the need to wait for the synchronization of the piezo, thus resulting in higher data rate. The parameters used are the same as for the synchronized mode in order to check that they are good with respect to the flux coming from the star (i.e. that the star is not saturating the detector for example).

| **Parameter** | **Range/Values** |
|---|---|
| **Data Acq. Total OPD Range** | [ 1..300 ] (microns) |
| **Data Acq. Fringe Velocity** | [ 1..2500 ] (microns/s) |
| **Data Acq. Sample Interval** | [ 0.1..3 ] (microns)<br>[ 1..10 ] (points per fringe) |

Once the parameters are set, the user or the WS sw can send the starting command for not synchronized acquisition (for example START NOTSYNC).

The possibility to use the synchronized mode for the injection optimization has to be checked, depending on the gain in terms of software development.

### 2.9.9 LISA Full Frame Readout (FULL FRAME)

The positions of the fiber outputs on the HAWAII chip have to be very precisely known and adjusted if necessary. The mount on which the fibers are mounted can drift with time or temperature, and so require a realignment of the outputs on the desired pixels. This is done by taking a full quadrant image (512x512 pixels x 16 bits) from the LISA chip, and fitting the pixel positions with centroids. The position of maxima, together with the FWHM of the pixels are the informations needed to make the necessary adjustements.

In a first implementation, the output optimization will be done manually during daytime, relying on the stability of the camera and fiber mounts to ensure the correct alignment of the fibers on the

LISA pixels. The operator actions will be based on the (maximum, FWHM) informations displayed in near real-time by the system, with a computed value of the percentage of light in a single pixel **[Req. 26]**. The full-frame image should also be available on the display **[Req. 27]**. Checking of the output pixels should be available online during the observations **[Req. 28]**. Eventually, the output optimization could be done before every observation to maximize the effectiveness of the instrument, but this requires that the output optimization process be automatic.

*The output optimization automatization is potentially difficult for the control software. Though, as it is foreseen to eventually achieve the complete automatization of the LdV operations, this possibility should be left open in the software design.*

The readout of the full LISA image should be possible at maximum rate **[Req. 29]**, as a bright artificial source will be used during this process. Though, the command required to start the full frame acquisition should take into account an exposure time setting, in order to accommodate for different artificial light source intensities.

| **Parameter** | **Range/Values** |
|---|---|
| **Full Frame Exposure Time** | [ 1..1000 ] (milliseconds) |

The command to start the exposures automatically one after the other should be available to the user and the WS sw. The computed parameters (maxima positions, FWHM, energy in one pixel) should be displayed to the operator.

Before each observation, the last full-frame image should be saved for reference **[Req. 30]**. This will be necessary at least during the commissioning phase, but this could also be useful afterwards, and in any case, after every automatic optimization when it is implemented.

### 2.9.10 Engineering Mode Data

The data in the Engineering mode is simpler than in the online modes, as no real-time interaction between the LdV and VLTI subsystems (LISA and DL for example) or between LdV LCUs (piezo and LISA) are activated.

The only parameter which has to be accessible in the engineering mode and which does not exist in the other modes is the **fast scan control signal** (proportional to the piezo extension) coming back from the fast scan piezo (INA3) controler **[Req. 31]**. This signal is produced by the piezo itself, and provided as an analog voltage output (amplitude **TBC**) by the piezo controler. It is thus necessary to foresee an analog-digital converter input in the LdV electronics design to access this information.

This will be used to check the performances of the piezo mirror, regarding mechanical hysteresis. There is no real-time access constraint on this requirement : the resulting signal can be displayed after the test cycle is completed. These tests will be done at the ICS level, and will require a dedicated GUI functionnality.

## 2.10 DATA FLOW FROM LDV

The data quantity coming out of LdV is not very large. On a very successful observing night, one can expect to observe during 8 hours. This means 60 targets observed 10 minutes each plus 2 minutes to switch from one target to the other and acquire fringes. Over these 10 minutes of data acquisition, about 5000 scans are obtained, 4 kbytes each. This gives a total science data quantity over one night of : 60x5000x4 kbyte = 1.2 Gbyte. The technical data, instrument parameters and calibration data should a few hundred megabytes at most. This gives a maximum data rate of about 1.5 Gbyte per night. Most probably, the “real life” data rate will be half of this figure, that is ~800 Mbyte **[Req. 32]**.

It is important to keep in mind that an upgrade of VINCI to dispersed fringes mode will increase the data flow from VINCI up to 50 times the previous figure (with a dispersion on 50 pixels taken as a basis). The effective data rate could then theoretically be 60 Gb per night (usually ~30 Gb/night). See section 2.20.3 for further details.

## 2.11 LDV DATA STRUCTURE

The data from LdV will be in two forms : the WS localized data, and the archived data.

### 2.11.1 Workstation Localized Data

The structure of the data on the *LdV* dedicated WS depends mainly on the design of the software itself, and thus will be defined later more precisely.

### 2.11.2 Archived Data

The general requirement reference for the archived data is **[Req. 59]**.

#### 2.11.2.1 Data Hierarchy

The interferometric data can be divided in **frame**, **scan**, **batch**, **observation** and **observation block**, from the most basic information element to the star and calibrator homogeneous data set, which provides the final visibility measurement. These terms are defined page 2.

#### 2.11.2.2 Data Sources

This section gives a list of the data which has to be stored in the final raw data files, sorted by source. The aproximate frequency (frame, scan, observation) at which this data has to be acquired is indicated. All these parameters are available from the LdV LCUs or WS, unless otherwise indicated.

In the future dispersed fringes upgrade, the observational data will be vectors instead of single values.

1. **LISA** :
   - I1, I2, P1, P2 data points (once per frame) or data vectors [intensity, wavelength] in the future spectrally dispersed mode.
   - LISA calibrations (once per observation)
   - LISA full frame (once per observation)
   - LISA Offset of the fringe packet center (quicklook) (meters) (once per scan)

2. **TCCD** :
   - TCCD last images (telescope 1, telescope 2, possibly with the artificial light source on) taken before fringe acquisition (once per observation)

3. **Encoders sensors** :
   - Opto-mechanical computer controled elements positions readings (once per observation) (meters, angular degrees,… see list in the previous sections)

4. **Hardware parameters** (once per observation unless otherwise specified) :
   - Reference UT time (at the beginning and end of each scan)
   - Reference sidereal time (at the beginning and end of each scan)
   - LISA number of frames acquired per scan
   - LISA number of frames saved per scan
   - LISA pixels coordinates associated with I1, I2, P1, P2 (set of coordinates for windows)
   - LISA percentage of the fiber bundle light in each pixel
   - LISA exposure time (seconds)
   - LISA full frame exposure time (seconds)
   - LISA number of data points between the start of the acquisition and the start of the record (left margin)
   - LISA number of data points between the end of the record and the end of the acquisition (right margin)
   - LISA quicklook fringe detection level n sigmas
   - Fast scan piezo mirror incidence angle (radians)
   - Fast scan piezo total OPD range (meters)
   - Fast scan piezo scan OPD range (meters)
   - Fast scan piezo scan OPD / total OPD
   - Fast scan piezo voltage range (Volts)
   - Fast scan piezo voltage offset (Volts)
   - Fast scan piezo waveform signal type (sine, square, sawtooth, triangle)
   - Fast scan piezo waveform stiffness (%)
   - Fast scan piezo waveform frequency (Hz)
   - Fast scan piezo waveform delay (seconds)
   - Fast scan piezo number of waveform samples
   - Fast scan piezo waveform sampling frequency (Hz)
   - Fast scan piezo output sample interval (Hz)
   - Fast scan piezo sample time (seconds)
   - OPD introduced by the Piezo Mirror (meters, can be computed after the acquisition through the piezo motion parameters ) (once per frame)

- Piezo / camera user settings (OPD range, fringe velocity, sample interval)
- FSU usage (with / without)

5. **Object reference data** :

This section describes the data which should be stored as a reference for the data reduction and analysis. The different fields to be stored will depend on the definition of the *VLTI reference catalog of sources and calibrators* which is **TBD**. As a general rule, it is important to store any information which influenced the choices the observer has made for his observations (type of variability, brightness, spectral energy distribution,…). This will be necessary in order to build a posteriori an image of what was the knowledge of the observer about the target at the time the object was observed.

- Names (as taken from Simbad for example, HD, SAO, HR, HIP,…)
- Type : target, calibrator, type of artificial source
- Calibrator quality rating (from 1 (best) to 5 (worse))
- RA, Dec, taken from the Hipparcos catalog or the FK5 (epoch J2000.0)
- Proper motion with uncertainties
- Parallax measurements (Hipparcos,…)
- Separated magnitude estimations in K [min, mean, max], V [min, mean, max]
- All available bands magnitudes (U, B, V, K, L, IRAS, IUE…), [min, mean, max]
- All available color indexes (B-V, J-K,…), with uncertainties
- All available angular diameter estimations (theoretical models, lunar occultations,…) with publications references
- Computed angular diameters, through different methods (spectral type+distance, bolometric flux,…) with uncertainties (in milliarcsec and in radians)
- Variability flag
- Binarity or multiplicity flag
- Variability type (if applicable), code taken from the GCVS for example
- Spectral type(s) determination(s), with publications references
- Period (seconds and days), epoch (julian date), wavelength of measurement (meters), reference publication (for periodic variables)
- Expected amplitude of the angular diameter variation (if applicable) (in milliarcsec and radians)
- Comments entered by the observer

6. **Software parameters** (once per observation, unless otherwise specified) :

- Reference code of the observation (can be sequential, allows to quickly retrieve the data)
- LdV mode name or code
- LdV setup name or code
- Projected baseline length (meters) (once per scan)
- Baseline vector coordinates (u,v,w) (once per scan)
- OPD velocity (meters/second) (once per scan)
- Hour angle (seconds) (once per scan)
- Theoretical RA, Dec
- Theoretical Altitude, Azimuth (once per scan)
- Wavelength range [mini, mean, maxi], coupled to the LISA filter wheel position (meters). This will be replaced by a vector of wavelength ranges (one [min, mean, max] triplet per spectral channel) for spectrally dispersed data.
- Observed internal OPD (meters) (once per scan)

- LdV OPD offset (meters)
- Expected visibility on the current baseline (mean over the observation), with uncertainty (dimensionless)
- Technical CCD extracted parameters (position, brightness of the object) (once per observation)
- Universal time of the beginning and end of the scans (once per scan)
- Number of data points saved in each scan (once per observation)
- Number of scans saved (once per observation)
- Number of scans on source (once per observation)
- Number of scans off source (once per observation)
- Number of scans beam A (once per observation)
- Number of scans beam B (once per observation)
- Name of calibrator(s) and reference code of calibrator files used for this target (once per observation)
- Name of the original file of the observations (once per observation)
- Refraction parameters : air mass, refraction correction applied by the VLTI (beginning and end of each observation)

7. **Delay Line** (once per scan) parameters read from the DL system:
   - Delay line position (meters)
   - Delay line velocity (meters per second)
   - Delay line piezo relative position (meters)
   - Delay line piezo velocity (meters per second)
   - Delay line VCM curvature (curvature radius)
   - Delay line relative pupil position (meters)
   - Delay line error signal (meters)

8. **FSU parameters** read from the FSU system:
   - Piston RMS value measured bu the FSU (once per scan)
   - Residual FSU error signal (once per scan)

9. **Telescopes** (once per observation, unless otherwise specified) parameters read from the telescopes system :
   - VLTI setup (baseline used, telescope types, UT names)
   - Name of the delayed telescope
   - RA, Dec (beginning and end of each observation)
   - Altitude, Azimuth (beginning and end of each observation)
   - Mean tracking error (RA and Dec) over the observation

10. **Observatory** (once per observation, unless otherwise specified) parameters read from the observatory environment monitoring system :
    - Environmental parameters:

    seeing, isoplanetic angle, correlation time, air pressure, air temperature, ground temperature, humidity, wind velocity and direction, seismic activity, seismic flag

### 2.11.2.3 Data Time Scales

In this section, the data produced by LdV is sorted by time scale. The data which is not available locally in the LdV LCUs and WS is indicated.

#### 2.11.2.3.1 Frame

- I1, I2, P1, P2 data points (data vectors in the future dispersed mode)
- OPD introduced by the Piezo Mirror (meters, can be computed after the acquisition through the piezo motion parameters )

#### 2.11.2.3.2 Scan

- Reference UT time (at the beginning and end of each scan)
- Reference sidereal time (at the beginning and end of each scan)
- LISA Offset of the fringe packet center (quicklook) (meters) this value is the one sent the the OPD controller in order to recenter the fringe packet.
- Projected baseline length (meters)
- Baseline vector coordinates (u,v,w)
- OPD velocity (meters/second)
- Hour angle (seconds)
- Theoretical Altitude, Azimuth
- Number of data points saved in each scan
- Observed internal OPD (meters)

Available from the FSU (TBD):

- Piston RMS value measured bu the FSU (once per scan)
- Residual FSU error signal (once per scan)

Available from the DL system:

- Delay line position (meters)
- Delay line velocity (meters per second)
- Delay line piezo relative position (meters)
- Delay line piezo velocity (meters per second)
- Delay line VCM curvature (curvature radius)
- Delay line relative pupil position (meters)
- Delay line error signal (meters)

#### 2.11.2.3.3 Observation

- Reference code of the observation (can be sequential, allows to quickly retrieve the data)
- Names (as taken from Simbad for example, HD, SAO, HR, HIP,…)
- Name of calibrator(s) and reference code of calibrator files used for this target
- Type : target, calibrator, type of artificial source
- Calibrator quality rating (from 1 (best) to 5 (worse))
- Name of the original file of the observations
- Theoretical RA, Dec
- LISA Calibrations
- TCCD last images (telescope 1, telescope 2, possibly with the artificial light source on) taken before fringe acquisition (once per observation)

- Opto-mechanical computer controled elements positions readings (meters, angular degrees,… see list in the previous sections)
- LISA number of frames acquired per scan
- LISA number of frames saved per scan
- LISA pixel coordinates associated with I1, I2, P1, P2 (set of coordinates for windows)
- LISA percentage of the fiber bundle light in each pixel
- LISA exposure time (seconds)
- LISA number of data points between the start of the acquisition and the start of the record (left margin)
- LISA number of data points between the end of the record and the end of the acquisition (right margin)
- LISA quicklook fringe detection level n sigmas
- LISA full frame
- LISA full frame exposure time (seconds)
- Fast scan piezo mirror incidence angle (radians)
- Fast scan piezo total OPD range (meters)
- Fast scan piezo scan OPD range (meters)
- Fast scan piezo scan OPD / total OPD
- Fast scan piezo voltage range (Volts)
- Fast scan piezo voltage offset (Volts)
- Fast scan piezo waveform signal type (sine, square, sawtooth, triangle)
- Fast scan piezo waveform stiffness (%)
- Fast scan piezo waveform frequency (Hz)
- Fast scan piezo waveform delay (seconds)
- Fast scan piezo number of waveform samples
- Fast scan piezo sampling waveform sampling frequency (Hz)
- Fast scan piezo sample interval (meters)
- Fast scan piezo sample time (seconds)
- Piezo / camera user settings (OPD range, fringe velocity, sample interval)
- RA, Dec, taken from the Hipparcos catalog or the FK5 (epoch J2000.0)
- Proper motion with uncertainties
- Parallax measurements (Hipparcos,…)
- Separated magnitude estimations in K [min, mean, max], V [min, mean, max]
- All available bands magnitudes (U, B, V, K, L, IRAS, IUE…), [min, mean, max]
- All available color indexes (B-V, J-K,…), with uncertainties
- All available angular diameter estimations (theoretical models, lunar occultations,…) with publications references
- Computed angular diameters, through different methods (spectral type+distance, bolometric flux,…) with uncertainties (in milliarcsec and in radians)
- Variability flag
- Variability type (if applicable), type code taken from the GCVS for example
- Binarity or multiplicity flag
- Spectral type(s) determination(s), with publications references
- Period (seconds and days), epoch (julian date), wavelength of measurement (meters), reference publication (for periodic variables)
- Comments entered by the observer
- LdV mode name or code
- LdV setup name or code
- Wavelength range [mini, mean, maxi] (meters) (vector for dispersed fringes)

- LdV OPD offset (meters)
- Expected visibility on the current baseline (mean over the observation), with uncertainty (dimensionless)
- Technical CCD extracted parameters (position, brightness of the object)
- Technical CCD refined optimization intensity map
- Number of scans saved
- Number of scans on source
- Number of scans off source
- Number of scans beam A (with one telescope off source)
- Number of scans beam B (with one telescope off source)
- Refraction parameters : air mass, refraction correction applied by the VLTI (beginning and end of each observation)

Available from the telescopes or observatory systems:

- VLTI setup (baseline used, telescope types, UT names)
- Name of the delayed telescope
- RA, Dec (beginning and end of each observation)
- Altitude, Azimuth (beginning and end of each observation)
- Mean tracking error (RA and Dec) over the observation
- Environmental parameters:

seeing, isoplanetic angle, correlation time, air pressure, air temperature, ground temperature, humidity, wind velocity and direction, seismic activity, seismic flag

#### 2.11.2.4 Data Format

After a meeting with representatives of the AMBER and MIDI teams (the two science instruments of the VLTI), and ESO Data Management Division, it has been agreed that the FITS binary table format was the most suitable for the storage of the data. The exact internal formatting and keywords of these files are **currently under definition**.

The header of the FITS file contains all the parameters which are defined less often than every scan (i.e night, observation block, observation). The interferometric data itself is stored in the body of the FITS file. The TCCD images are stored in the body of the data file, before or after the interferometric data.

The following figure shows the typical data acquisition during an observing night, and what is stored in the data files.

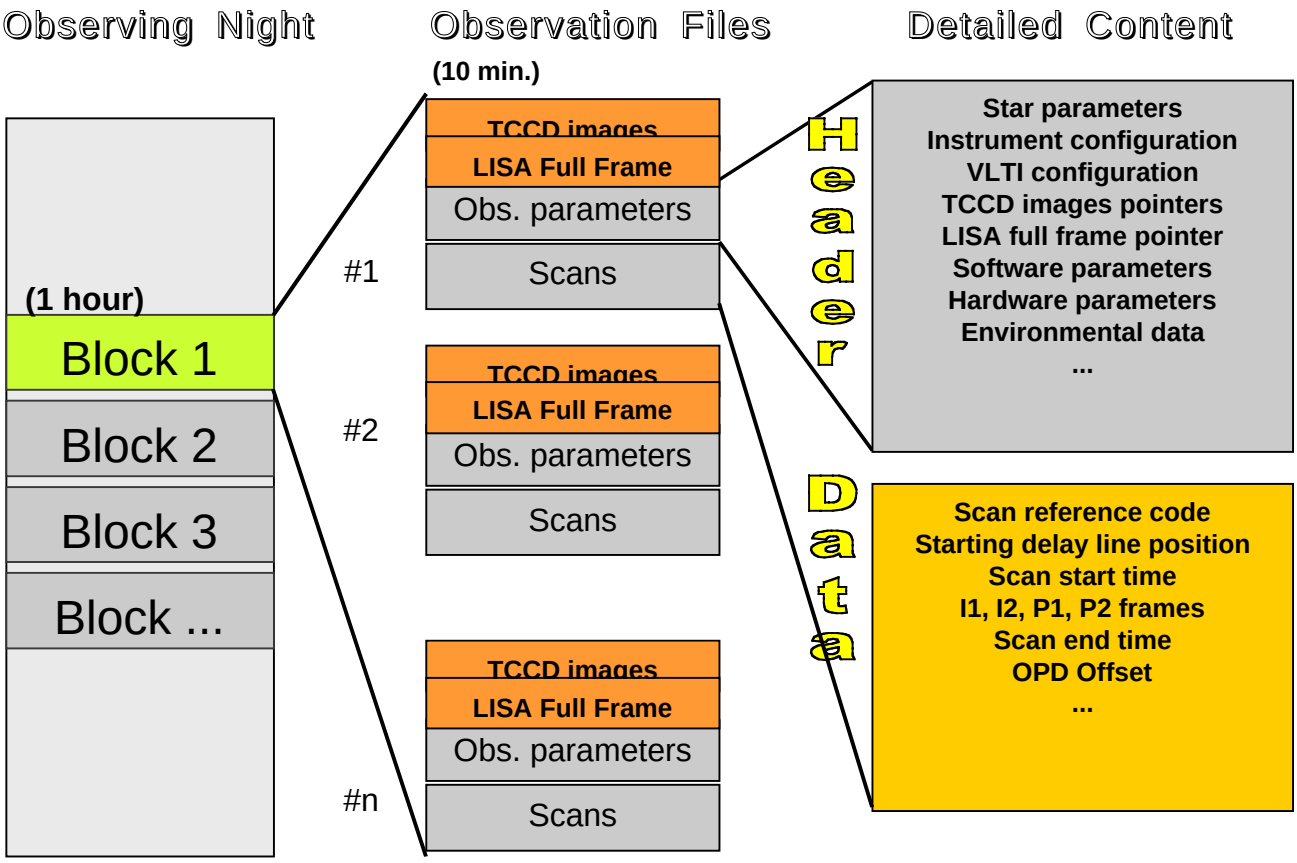


## 2.12 DESCRIPTION OF THE OBSERVATION PROCEDURE

### 2.12.1 Observation Procedure with VINCI

This section gives an overview of a typical observing session.

1. *Observations Scheduling:* the observations scheduling is conducted off-line from the real-time operating system. The creation of a formatted observing list should be possible before on-site arrival through a “front page” software. This system could help the observer determine:
    - which sources are visible
    - the previous observations of his targets
    - the magnitudes (including the K magnitude, if necessary computed from the other bands measurements)
    - the estimated visibility
    - the calibrators used so far
    - the baselines used so far on this target…

    The querying of this database is possible through every field, and it is possible to use the database while on the observing site. The calibrators, selected by the observer with the help of dedicated software, are integrated in the list of the observations to be conducted. Their nature

of calibrators should be apparent in the list. The database is a key element of the VLTI SW. The definition of this database is a point to discuss with the other instruments and the VLTI.

The observation scheduling SW tools are not part of the VINCI SW, but rather part of the general VLTI SW (since they will be used by all the instruments).

2. *LdV Initialization:* the instrument status is changed to “online”.

3. *Short-term Observations Scheduling:* in order to fine-tune the observing program of the instrument, the observer has access to the observing list, and can modify it by hand. The possibility remains of having an automated system to optimize the observing schedule for the night.

4. *Telescopes Pointing:* position the telescopes at the target coordinates.

5. *Telescopes Focusing:* focus the telescopes in order to feed a collimated beam in the Coude train.

6. *Delay Line positioning:* the delay line is sent to the position required for optical path length equalization between the two beams, and it is moved at the computed rate for the observed target.

7. *Technical CCD Images Acquisitions:* images of the target are obtained by the technical CCD on both beams to check for the positioning of the pupil and the image quality. This requires the motion of the LdV mirrors ALI2/ALI3 and ALI4/ALI6.

8. *Positioning of the fiber input:* this is done by maximizing the flux on the camera pixels. The setting of the injection parabolae is motorized, and the flux maximization is done on the stars during the observations. This first setting during the initialization phase will help finding the maximum light position on the scientific targets by giving a reference point. As an upgrade of the system, it should be possible to do this process automatically.

9. *Acquisition of a LISA full frame:* this will enable the observer to check for the quality of the images of the fibers on the HAWAII detector, and track any systematic problem. If the centering of the fiber heads is bad, then an output optimization procedure can be started.

10. *Off source and mixed batches:* In order to compute the transfer matrix of the system, it is necessary to obtain three small batches (about a hundred scans) :

    - off-source : the telescopes are pointed to the background sky,
    - beam A only,
    - beam B only.

11. *Fringes Finding (long scan) and Scanning (fast scan):* **[Req. 51]** during the fringes finding phase, the optical path difference is slowly modulated by moving the delay line while scanning with the fast scan mirror INA3. By doing this motion, a segment of optical path difference is scanned for the presence of fringes. The delay line motion is superimposed to the sidereal speed. The algorithm is simple :

- while fringes are not found, increase the internal OPD by a fixed ammount X (entered by the observer, can be positive or negative)
- once the fringes are found by the quicklook algorithm, the delay line motion speed is set to the sidereal rate, in order to have the fringes at a fixed position.

The fringes are then repeatedly measured and the scans are stored. The duration of the observation is selected by the observer (as a number of 'good' scans for example). At the end of each fringe scan, while on source, a quick look analysis is performed which results in an updated value for the internal OPD, to be communicated to the delay line.

12. *On-line Data Quality Control:* the *LdV* operating system provides the user with an on-line display of the data acquired **[Req. 18]**. This enables the observer to check the quality of the visibility measurements, and gives an estimation of the atmospheric perturbations evolution during the night. The display of these values can be done with a delay of [0.5 s, 1 s] and/or by packets (several scans displayed simultaneously) to reduce the real-time constraints on the system. The basic data reduction should be done by the DCS (quick reduction, in real-time on the LISA WS, but displayed every [0.5 s, 1 s] to the user) and the fine data reduction by the OS (in a near-line regime, after each observation). This implies that the fine data reduction algorithm should be resident on the LdV WS. Since the LdV WS will be essentially idle during an observation, one can expect that the fine reduction can be done during the observations themselves **[Req. 33]**.

    The scenario would be:

| | OS | ICS / DCS |
|---|---|---|
| Observation n | Request obj. pointing<br>Check TCCD, LISA, etc…<br>Request DAQ<br><br><br><br><br><br><br><br><br><br>Receive data from DCS | <br><br><br>Get small batch off-source<br>Get small batch beam A<br>Get small batch beam B<br>Get batch on-source: loop on:<br>- Wait for DL in track<br>- Get one scan<br>- Quick look<br>- Transmit internal OPD value<br>- Quick data reduction<br>- Display scan + vis<br>Get batch off-source<br>Transfer data to OS |
| Observation n+1 | Request obj. pointing<br>Check TCCD, LISA etc.<br>Request DAQ<br><br>Pipeline observation n<br>Store data in archive<br>Display results obs. n<br><br>Receive data from DCS | <br><br><br>Wait for DAQ request<br>Get small batch off-source<br>Get small batch beam A<br>Get small batch beam B<br>Get batch on-source<br>Get batch off-source<br>Transfer data to OS |

If observation n+1 is terminated before observation n is fully pipelined, then observation n is stored in a buffer to be pipelined at the end of the night **[Req. 34]**.

13. During the routine operation of *LdV*, many targets (~50) are observed during the night.

14. *LdV End of the Night:* after the last target has been observed, the termination procedure is started. This includes:
    - saving the opened files, saving the observing log
    - performing a final detector calibration
    - creating a summary of the observations of the night: a summary of the measurements obtained during the observing session is displayed to the observer, and possibly printed or sent by e-mail to the interested users. The final environmental parameters could also be added to the saved data. A summary of all the technical problems and important error messages from the operating system could also be displayed and saved to disk.
    - switching off the instrument: the status of *LdV* is changed to “off”.

15. *Reduction Pipeline:* the automated data reduction process is started after the end of the night. It reduces all the data obtained during the night, which is not already reduced, and saves the resulting files to the *LdV* night data set.

16. *Off-line Data Analysis:* using standard (MIDAS, IDL,…) or specific data analysis tools, the astronomer processes and combines the data.

### 2.12.2 LEONARDO Interface with the VLTI Instruments

The VLTI scientific instruments AMBER and MIDI should have access to LEONARDO artificial star mode **[Req. 11]**.

All the setups of the Artificial Star mode (see desctiptions section 2.8.6) should be available to the VLTI instruments through the VLTI CS :

- **Artificial Star Off Removed**
- **Artificial Star On Inserted**
- **Artificial Star On Removed**
- **Artificial Star Off Inserted**
- **Autocollimation On Inserted**

The switching between these setups will require a few seconds, in order for the motors to achieve the necessary motions. The 'user' instruments should access LEONARDO only through these predefined modes **[Req. 12]**. No low-level command is foreseen to be accessible from outside of LdV software.

The thermal light source can be turned off during normal operations, but if it is required to switch it on again, the preheating will take a few minutes in order to achieve a good stability **[Req. 53]**. This does not apply to laser sources.

The commands issued by the instruments should follow the same format as the commands for the other systems of the VLTI (telescopes, delay lines,…). Generally speaking, LEONARDO should be integrated in the VLTI infrastructure as much as possible and follow the same control procedure **[Req. 35]**. This means that it will act independently from VINCI and the alignment toolkit ALIU.

The user instrument should request the allocation of LEONARDO before sending commands to it, in order to avoid conflicts with the other instruments. By default, LEONARDO should be assigned to LdV. LEONARDO should be automatically allocated to the master observing instrument, so as to avoid the accidental insertion of the LEONARDO cubes in the beams.

### 2.12.3 Alignment Toolkit Interface with the VLTI instruments

The VLTI instruments AMBER and MIDI as well as the alignment software of the VLTI should have access to the Pupil Check and Image Check modes and setups **[Req. 9]**. All the data acquired should be available on request from any system to the VLTI CS (but no real-time constraints are foreseen). The interface requirements are currently under definition (**TBD**).

Generally speaking, the alignment toolkit should be integrated in the VLTI infrastructure as much as possible and follow the same control procedure **[Req. 36]**. The allocation of ALIU (alignment toolkit) to the alignment software or the other instruments should be done by request. By default, it should be assigned to LdV software.

## 2.13 INSTRUMENT USER MANUAL

As LdV will be operated in several ways as a facility for the other VLTI instruments, it is important to foresee a complete User's Manual for this instrument. This will enable the science instruments' teams to have a reference for the proper use of LEONARDO, the alignment unit (those two systems will be used directly by the other instruments) and VINCI.

## 2.14 SETTINGS DATABASE

The operation of LdV on different baselines will require a database of settings (internal OPD, INB slide position, TCCD focus positions,…) to quickly find the fringes after a baseline change. This database should be available on-line on Paranal. It is not part of the VINCI software, and belongs to the VLTI system.

As a general rule for LdV, there is no particular order in which the various functions should be set, and the settings can be done in parallel.

## 2.15 TCCD PROCEDURES

### 2.15.1 TCCD focusing

The focusing of the TCCD is done in a standard way. The image of a point source is obtained, then fitted with a gaussian bidimensional curve, and a correction is computed from the width of this gaussian. Is is iterated a few times if necessary.

In Pupil Check mode, the focus will be achieved on the red LED which is at the center of mirror M2, or on the artificial star image. In Image Check mode, it will be done on the stellar image (either artificial or from the sky). The focusing might be needed from time to time, as a maintenance procedure

In the following sub-sections, the TCCD is supposed focused.

### 2.15.2 TCCD Calibrations

It is necessary to obtain an image of the fiber inputs on the TCCD. This is done by injecting light in the MONA box from one the outputs, and illuminating the fiber input head. Via the ALI1 and ALI5 beamsplitter cubes, the resulting “artificial stars” are imaged on the TCCD. Once the image has been acquired, the precise position of the fiber input is computed by a gaussian fit. These coordinates are the reference on which all the star light has to be concentrated during the observations.

### 2.15.3 Pupil Check

This section refers to the optical configuration described in the reference document [2], section 3.9.2.

At the beginning of the night, and to avoid any loss of stellar light, it is important to check that the light beam arrives unobstructed (= unvignetted) to the instruments. This is done by imaging the pupils of the telescopes on the TCCD chip. The pupils are the images of the secondary mirrors of the feeding optical systems (either siderostats, UTs or ATs). The delay lines system is built so as to keep the beam B pupil plane in the laboratory (this allows an extended field of view for the imaging applications).

Normally, the image of the pupil is obtained by turning on the light source at the center of the secondary mirror. The image obtained on the TCCD is then a point, which has to be centered relatively to the axis of the technical CCD optics. The refractor in front of the TCCD defines the optical axis of the VLTI.

The pupil alignment is expected to occur once per night, or before any observation depending on the stability of the VLTI.

The location of the pupil planes for the two beams will be on the injection parabolae INA1 and INB1. This means that for imaging the pupil, it is necessary to focus at their distance with the TCCD. As it is used also for viewing the stellar images, it is normally focused at infinity.

In order to focus at a few meters, this requires the addition of a converging lens in front of the TCCD. Once this is done, the TCCD can focus on the pupil image which is situated on INA1/INB1.

The OS should get the expected pupil position from VLTI OS **[Req. 37]** and from then:
- insert the bonnette if the pupil is less than 3m away,
- preset the TCCD focus to the expected pupil position.

Once the focusing has converged on the pupil LED, from the focus motor readout the software should derive a measured pupil longitudinal position **[Req. 38]** (which can be compared to the expected pupil position provided by the VLTI OS).

The necessary setups have been described in the section 2.8.4. The focusing of the TCCD is done the same way as for the Image Check, only the starting position (rough focusing) changes.

*In the current design, the role of LdV is not to provide the commands to set the mirrors of the optical train to align the pupil. Only the display and shape measurements of the pupil are a requirement for the LdV software. But this has **TBC** when a clear alignment procedure has been defined.*

The procedure to obtain and measure the pupil with the TCCD is the following:

1. **Obtain an image with the TCCD** in the Pupil Check setup, with the Secondary Mirror red LEDs switched on.
2. **Provide the image to the user**, together with information on the quantity of light available, and the position of the spot.

### 2.15.4 Image Check

This section refers to the optical configuration described in the reference document [2], section 3.9.3.

As a part of the alignment procedure, VINCI's TCCD will be used to measure the alignment of the VLTI regarding the position of the image. It will be done by reimaging a light source (multimode fiber connected to a laser diode) located at the Nasmyth focus of the selected telescope, on the TCCD located in the interferometric laboratory. Then, the position of the image of the source can be modified by tilting a mirror in the VLTI optical train (**TBD** preferably located in a pupil plane or close to it, to limit cross coupling between tilt and OPD).

The image alignment is expected to occur once per night, or before any observation depending on the stability of the VLTI.

The procedure to obtain and measure the image of the Nasmyth light source with the TCCD is the following:

3. **Obtain an image with the TCCD** in the Image Check setup, with the Nasmyth multimode laser diode switched on.

▪

4. **Provide the image to the user**, together with information on the quantity of light available, and the position of the spot.

*In the current design, the role of LdV is not to provide the commands to set the mirrors of the optical train to align the pupil. Only the display and shape measurements of the image are a requirement for the LdV software. But this has **TBC** when a clear alignment procedure has been defined.*

### 2.15.5 Star Image Centering

The Technical CCD is used to check the star image quality and position. During observations in the stellar interferometer mode, the TCCD is used in the following sequence after the telescopes are tracking on the target. The alignment of the VLTI is supposed to be good enough, so as to bring the stellar light up to the VINCI table and on the TCCD chip. The following procedure is foreseen **[Req. 39]** :

1. **The star image is acquired**. The exposure time is computed based on the brightness of the source in the optical wavelengths. It is taken from the observing template or the online catalogs database.

2. **Measurement of the source(s)** : the resulting image shows the source, and possibly other objects, with a calibrated intensity in ADUs. The sources are then measured by fitting two dimensional gaussian curves to the intensity profiles present in the image. This fit could be done via a fast Fourier transform of the image, or other numerical method. The resulting data is a set of coordinates, intensities and profile widths. This information, and the TCCD image will be saved in the observations data.

3. **Identification of the target** : in the observing template, a flag should indicate if a close bright source is expected to be in the same field.
   - In case this flag is up, the identification could be done based on the expected relative brightness of the target compared to the other object(s), or visually by the operator of the instrument.
   - In case this flag is down, the identification is normally unambiguous, though a very slight risk of confusion exists with an unexpected source (other very close star, asteroid,…). This risk should not be taken into account for the design of the software.

4. **Computation of the position error** : once the target is identified, its coordinates are compared to the fiber head input coordinates as measured during the calibration phase. The alignment of the optical train up to the laboratory is supposed to be good, and only the injection optics will be moved to precisely position the star image on the fiber input.

5. **Computation of the tip-tilt mirrors required motions** : the difference is computed and converted to tip-tilt positions of the injection mirrors. The coefficients for this conversion (two for each injection mirror) have been estimated during the commissionning of *LdV*. It will be also necessary to include an offset coefficient in the parameters, due to the different positions of the star images in the visible and in the infrared. This offset varies with respect

to the altitude of the star in the sky. At zenith, this is zero, while near the horizon it is several arcsec (projected on the sky), but a direct mathematical relation allows its computation based on the altitude of the object, the TCCD sensitivity curve mean wavelength and the mean wavelength of the LISA infrared band.

6. **Motion of the INA1 and INB1 mirrors** : commands are sent to the INA1 and INB1 motors to move in order to position the image of the star in the infrared at the same position as the fiber head as measured at the beginning of the night. It is necessary to inject the light at a position offset from the visible outputs of the fibers (as seen on the TCCD), due to differential refraction of the atmosphere. The computed offset will have to take into account the differential refraction, which requires input from VLTI environmental parameters (humidity, temperature...). It is foreseen that the VLTI collecting telescopes send the infrared light directly on-axis, while guiding on the optical image off-axis. This means that the differential diffraction offset has to be taken into account directly at the telescope level. This would make this procedure simpler as no variable offset would have to be applied to the INA1 and INB1 mirrors.

7. **Refined optimization** : At this stage, the star should be positioned on the fiber head, sending light into the MONA box up to the HAWAII detector. The refined injection optimization can then be conducted, see next paragraph.

### 2.15.6 Off-line use of TCCD images and LISA full frames

At least one image of the object (from each telescope) obtained with the TCCD during the acquisition procedure should be saved in the data **[Req. 40]**. This will enable the user during post-processing to check visually the quality of the seeing, the postion of the object relatively to the fiber heads during pre-acquisition,…

As a complement to the TCCD image(s), the computed data on the positions of the sources in the image as well as the refined injection optimization data should be stored in the observation of the star.

The same comments apply to the LISA full frame images, which will help during the data reduction process to track misalignments of the fiber outputs. They should be saved before each observation, and in any case after every output alignment procedure.

## 2.16 INJECTION AND OUTPUT OPTIMIZATION PROCEDURES

### 2.16.1 Refined Injection Optimization

The principle for this optimization is that we are looking for the very precise position of the stellar image peak intensity. The stellar Airy disk size is 0.065 arcsec in FWHM for UT and 0.290 arcsec for AT, and the fiber head projected size on the sky is the same (but the speckle cloud, which replaces the Airy disk without adaptive optics, is about 0.5 to 1 arcsec in size for both). The star image and the fiber head transmissivity have gaussian profiles.

The precision required for the superposition of the two gaussian curves is of the order of 7 milliarcsec for the UTs. It will not be possible to center the images using the TCCD, because the star detection precision is not sufficient. This is a critical point, because all the light which is not injected in the fiber is lost.

As the automation of this procedure is very demanding for the software system, the operator should manually search for the optimum injection in the first phase of the operations of LdV **[Req. 41]**. The main drawback is a slow down of the observations, and the interruption of the automated template observing session.

*Refined injection optimization is a second generation upgrade at this point, but **this is very important** since as long as we do not have automated injection optimization it will not be possible to implement and test fully automated observation templates which is the target operating mode for the VLTI instrumentation. See section 2.20.1 for description of possible algorithms.*

### 2.16.2 Output Alignment Procedure

The four fiber outputs have to be precisely positioned on four pixels of the LISA camera (to a fraction of a HAWAII pixel). This means that the position of the fiber bundle output has to be precisely adjusted with respect to the HAWAII detector pixels. This is done via the OUT1 fiber bundle output, which is adjustable in translation (3 directions) and rotation. Only the focus and rotation aroud the optical axis are remotely controlled. The alignment is checked on the HAWAII camera by acquiring full frames (which cover a quarter of the chip surface, i.e. 512x512 pixels) while light is sent into the fiber bundle with the artificial star light source LEONARDO.

The output alignment is normally done before the observing night, using the Autotest or Autocollimation setups. However, it is possible to do refocusing or rotational adjustment during the night if necessary, as it is remote controlled.

A possible scheme for the output alignment procedure is **[Req. 42]**:

1. **Obtain quick exposures from the LISA camera in full frame mode.**
   ▪
2. **Monitor nearly continuously (frequency of a few Hz) values for :**

   - the total flux arriving on the HAWAII detector
   - the parameters of the four images of the fibers outputs : position of the maximum light, FWHM. This is obtained by fitting gaussian curves to the image.
   - the percentage of the flux (in ADU) concentrated in each maximum light pixels.
   - the global percentage of the light concentrated in the four maximum light pixels. The maximization of this value is the goal of the output alignment procedure.

3. **Adjust OUT1 through paddle control on the WS (z,rotation)**, to move the four fiber outputs on the HAWAII detector. This adjustement is done by the operator. During this motion, the positions of the fiber outputs are adjusted so as to put them on the desired columns of the detector. The precise adjustment of the positions is done using the computed light concentration percentage. The image of the fiber outputs is continuously displayed to the operator. The look-up table for this image is not dynamic, but can be

adjusted by the user. Only focus (z direction) and rotation can be adjusted remotely, while the x and y settings are done by the observer before the observing night and are supposed fixed.

Once this is done, the fiber outputs are well aligned on the detector pixels. The coordinates of the pixels used, as well as the percentages of the light concentrated in each pixel are stored in the WS sw, in order to be added to the data files headers **[Req. 43]**.

A LISA full frame image is stored after this process for reference during the data reduction **[Req. 30]**.

*Automated output focus and rotation alignment is a second generation upgrade at this point, but **it will be mandatory in order to implement fully automated observation templates.** See section 2.20.2 for description of a possible algorithm.*

## 2.17 TEMPLATES

The control software shall allow to build up templates which will carry out in a semi-automated way an observation or a group of observations and use them to measure astronomical, astmospheric or instrumental parameters **[Req. 44]**. *The observations with LdV based on templates are not yet completely defined.*

The sequencing of LdV modes includes the intervention of the observer for some critical tasks, such as injection optimization and output alignment. The steps requiring the operator action are marked with [*operator*].

### 2.17.1 Autotest Mode Observations Standard Template :

- mode Autocollimation Injection Adjust [*operator*]
- mode Autocollimation Output Adjust [*operator*]
- mode Autocollimation Fringe Search
- mode Autocollimation Data Acquisition
- archival of the data

### 2.17.2 Autocollimation Mode Observations Standard Template :

- mode Autotest Injection Adjust [*operator*]
- mode Autotest Output Adjust [*operator*]
- mode Autotest Fringe Search
- mode Autotest Data Acquisition
- archival of the data

### 2.17.3 Pupil check Standard Template

- mode Pupil Check Artificial Star A
- mode Pupil Check Artificial Star B
- mode Pupil Check telescope A
- mode Pupil Check telescope B
- TCCD images are made available to LdV and the external instruments

### 2.17.4 Image Check Standard Template

- mode Image Check telescope A
- mode Image Check telescope B
- TCCD images are made available to LdV and the external instruments

### 2.17.5 Stellar Interferometer Mode Observations Standard Template :

The Pupil Check and Image Check steps require a call to the corresponding standard templates.

- pointing of the telescopes
- initial positioning of the Delay Lines
- standard template Pupil Check
- standard template Image Check
- mode Stellar Interferometer Injection Adjust [*operator*]
- mode Stellar Interferometer Fringe Search
- mode Stellar Interferometer Data Acquisition
- archival of the data

## 2.18 GRAPHICAL USER INTERFACE

The user of LdV shall normally interact with the instrument via the Instrument Workstation and the LdV graphical user interface (GUI) **[Req. 58]**. The user will first have to select the way to operate among three options:

**Standard Observing:** for astronomical targets observations, in the stellar interferometer setup. In this option, the operator will use the GUI to control the observations. LdV will also be used as a measurement tool for internal seeing, optical alignments, internal OPD measurements. This will make use of the standard operating modes defined Section 2.8.

**Maintenance:** to check periodically the performances of LdV at the OS level. The GUI should display the series of tests to be performed, and either perform them automatically or under the user's control. The results of the maintenance tests are then logged for statistical analysis and preventive maintenance.

**Engineering:** to carry out detailed tests or settings regarding the instrument hardware devices, during improvements of the system or in-depth analysis of hardware problems. This is done at the ICS level.

In the first two options, the possibility shall be given to change the instrument state between on-line, stand-by and off **[Req. 45]**. Via the GUI, it shall then be possible to select the instrument mode either **[Req. 46]**:

- Individually via typed commands from the WS sw
- Via the GUI, by form-filling
- Via the GUI, using pre-stored files
- Via a template sequence

The GUI should also display the status information provided by the LdV and TCCD control and acquisition electronics and other relevant data (e.g. meteo and telescope data). The GUI will also generate warnings of hazards or error conditions (e.g. mirrors bad positioning or failure,…) whenever power is on.

*The automated operation of* LdV*, via a template sequence, is a very demanding goal to achieve. Interferometers are very complex technical systems and it is important to realize that no currently working interferometer is completely automated. The option to operate the instrument in a manual or semi-automated way (the first three bullets of the above list) should not be discarded.*

### 2.18.1 Online Modes Interface

The LdV WS sw in Stellar Interferometer Mode should be able to **[Req. 47]**:

- *Interact with the VLTI Control System*, controlling the telescopes and gathering positional and environmental data. The pointing instructions are sent to the VLTI Control System.

- *Interact with the LdV Instrument Control System*. This allows the automatic or semi-automatic setting and monitoring of the:
  - light switches
  - motor commands
  - encoders readout
  - piezo fast scan parameters

- *Control the LISA DCS*. All the acquisition parameters (duration, frequency) are defined by the observer and sent to the camera through the operating system.

- *Control the Technical CCD DCS*. During the acquisition procedure, the WS sw controls the settings of the exposure as well as displays the resulting images and performs the relevant parameters extraction as described in section 2.15. These parameters and data should be displayed in real-time to the operator for quality check.

- *Monitor real-time information about the status of LdV and the VLTI*, including error and warning messages. For example, the position of the delay line, the pointing direction of the telescopes, the status of the movable mirrors, the readings of the encoders and the status of the light switches.

- *Provide the observer with software control* over every computerized element relevant for the Stellar Interferometer Mode, such as the movable mirrors and white light sources.

- *Read and modify the observing list*, to allow for real-time tuning of the observing schedule. The observing conditions can influence the selection of the sources, for example the faint sources will not be observable during bad turbulence periods.

- *Perform basic observational data pre-processing*, such as averaging multiple scans values. The raw data shall be kept safe during these steps and saved together with pre-processed data in the archive.

- *Real-time display the observational data*. This is the key point to allow for a real-time appreciation of the quality of the data, and to check for possible malfunctions. The visibilities could be displayed in chronological order, as well as in the form of an histogram.

- *Allow the user to perform near-line visibility data processing*. To check for unexpected variability in the targets visibilities, and possibly trigger extended observation on the most interesting objects.

- *Access the VLTI archive system*. In order to check for any previous observation of the instrument. To reliably save the observational data, the operating system should access the VLTI Archive at the end of the night, to write the files of the data obtained during the night. It would also be interesting to be able to read in the archive during the observations to check for the previous measurements on the targets.

### 2.18.2 List of Parameters displayed by the Autotest / Autocollimation Modes GUI

| Origin | Description | Typical Update Frequency | Possibility of GUI Setting |
|---|---|---|---|
| VLTI | Seismic activity warning symbol | Continuous | No |
| VLTI | Time signals (Local, UT, Sidereal) | Continuous | No |
| ICS | Status of LdV hw warning symbol (green = ok, red = error) | Continuous | No |
| OS | Data acquisition OPD range | Observation | Yes |
| OS | Data acquisition fringe velocity | Observation | Yes |
| OS | Data acquisition computed sample interval | Observation | No |
| OS | Data acquisition number of points per fringe | Observation | Yes |
| OS | Current LISA filter | Observation | Yes |
| OS | Technical CCD exposure time | Observation | Yes |
| DCS | Last Technical CCD images (beam A, beam B) | Observation | No |
| VLTI | Positions of the Delay Lines (one or two) (m) | [2 Hz, 1 Hz] | Yes |
| OS | Internal Optical Path Difference (m) | [2 Hz, 1 Hz] | Yes |
| OS | Fringe search INB slide OPD increment (millimeters) | [2 Hz, 1 Hz] | Yes |
| DCS | Visibilities plot (time, visibility) | [2 Hz, 1 Hz] | No |
| OS | Visibilities plot settings (axis,…) | Observation | Yes |
| OS | Visibilities plot statistics (last, mean, sigma,…) | [2 Hz, 1 Hz] | No |
| DCS | Visibilities histogram (visibility, number of values) | [2 Hz, 1 Hz] | No |
| OS | Visibilities histogram settings (axis,…) | Observation | Yes |
| OS | Fringes found warning signal | [2 Hz, 1 Hz] | No |
| | | | |
| | | | |
| | | | |
| | | | |
| | | | |
| | | | |

### 2.18.3 List of Parameters displayed by the Pupil / Image Check Modes GUI

| Origin | Description | Typical Update Frequency | Possibility of GUI Setting |
|---|---|---|---|
| VLTI | Seismic activity warning symbol | Continuous | No |
| VLTI | Time signals (Local, UT, Sidereal) | Continuous | No |
| ICS | Status of LdV hw warning symbol (green = ok, red = error) | Continuous | No |
| OS | Technical CCD exposure time | Observation | Yes |
| OS | Current beam on the TCCD (beam A, beam B) | [1 Hz, 0.5 Hz] | Yes |
| DCS | Technical CCD images (one beam at a time) | [2 Hz, 1 Hz] | No |
| OS | Computed pupil / image center coordinates (on the TCCD) | Observation | No |
| | | | |
| | | | |
| | | | |
| | | | |
| | | | |

### 2.18.4 List of Parameters displayed by the Artificial Star Mode GUI

| Origin | Description | Typical Update Frequency | Possibility of GUI Setting |
|---|---|---|---|
| VLTI | Seismic activity warning symbol | Continuous | No |
| ICS | Status of LEONARDO hw warning symbol (green = ok, red = error) | Continuous | No |
| ICS | Status of BSA and BSB slides (BSA1, BSA2, OUT) | Continuous | Yes |
| ICS | Status of the artificial light source (on / off) | Continuous | Yes |
| | | | |
| | | | |
| | | | |

### 2.18.5 List of Parameters displayed by the Stellar Interferometer Mode GUI

| Origin | Description | Typical Update Frequency | Possibility of GUI Setting |
|---|---|---|---|
| VLTI | Telescopes pointing coordinates (RA, Dec, Alt, Az) | Continuous | Yes |
| VLTI | Telescopes status (track, slew,…) | Continuous | No |
| VLTI | Wind load warning symbol | Continuous | No |
| VLTI | Seeing value (arcsec) | [2 Hz, 1 Hz] | No |
| VLTI | Seismic activity warning symbol | Continuous | No |
| VLTI | Time signals (Local, UT, Sidereal) | Continuous | No |
| OS | Target name, target type (scientific object, calibrator) | Observation | Yes |
| OS | Template situation (target list) | Observation | Yes |
| OS | Target coordinates (RA, Dec) | Observation | Yes |
| OS | Target V and K magnitudes | Observation | Yes |
| OS | Target spectral type | Observation | Yes |
| OS | Target expected diameter (mas) | Observation | Yes |
| ICS | Status of LdV hw warning symbol (green = ok, red = error) | Continuous | No |
| OS | Data acquisition OPD range | Observation | Yes |
| OS | Data acquisition fringe velocity | Observation | Yes |
| OS | Data acquisition computed sample interval | Observation | No |
| OS | Data acquisition number of points per fringe | Observation | Yes |
| OS | Current LISA filter | Observation | Yes |
| DCS | Last LISA full frame | Observation | No |
| DCS | Last Technical CCD images (beam A, beam B) | Observation | No |
| OS | Technical CCD exposure time | Observation | Yes |
| VLTI | Positions of the Delay Lines (one or two) (m) | [2 Hz, 1 Hz] | Yes |
| VLTI | Velocity of the Delay Lines (m/s) | [2 Hz, 1 Hz] | No |
| VLTI | Status of the Delay Lines (track, no track) | [2 Hz, 1 Hz] | No |
| OS | Internal Optical Path Difference (m) | [2 Hz, 1 Hz] | Yes |
| OS | Fringe search OPD increment (millimeters) | [2 Hz, 1 Hz] | Yes |
| OS | Internal OPD current relative offset (millimeters) | [2 Hz, 1 Hz] | Yes |
| DCS | Visibilities plot (time, visibility) | [2 Hz, 1 Hz] | No |
| OS | Visibilities plot settings (axis,…) | Observation | Yes |
| OS | Visibilities plot statistics (last, mean, sigma,…) | [2 Hz, 1 Hz] | No |
| DCS | Visibilities histogram (visibility, number of values) | [2 Hz, 1 Hz] | No |
| OS | Visibilities histogram settings (axis,…) | Observation | Yes |
| OS | Fringes found warning signal | [2 Hz, 1 Hz] | No |
| | | | |
| | | | |
| | | | |
| | | | |

### 2.18.6 Interface for the Engineering and Maintenance Modes

The Engineering Mode is generally speaking less complex than the Stellar Interferometer Mode. The user interface for this mode is basically the same as for the online modes, with access to all the instrument parameters **[Req. 48]**, either via a GUI or a command line.

During the maintenance and setup procedures, the needs of the user are mainly to have full control on every element, possibly at the expense of the ease of use. The user interface for this mode is basically the same as for the engineering mode, with access to all the instrument parameters, either via a GUI or a command line.

### 2.18.7 Setting up the Instrument Parameters

The instrument parameters for each standard setup, listed in the section 2.6, should be loaded after the choice of the mode and optical setup of LdV (Autotest, Stellar Interferometer, Pupil Alignment, Image Alignment). They will define the position of each hardware element (motor, light switches, piezos,…) for each mode. The operator should have access via the GUI to the different parameters settings and be able to change them, even after a setup has been loaded **[Req. 49]**.

Use of encoder values to set the functions shall be possible via a dedicated “Hardware Setup” interface.

## 2.19 LIST OF NUMBERED REQUIREMENTS

| Req # | Subject | Section |
|---|---|---|
| **1** | Status of hardware elements | 2.4 |
| **2** | HW warnings and alerts | 2.4 |
| **3** | Slide positioning direction BSA/BSB | 2.4.1 |
| **4** | Slide positioning direction ALI1/ALI5 | 2.4.2 |
| **5** | Slide positioning direction ALI | 2.4.3 |
| **6** | TCCD preset positions | 2.4.4 |
| **7** | Slide positioning direction INB | 2.4.5 |
| **8** | Autocollimation OPD offset | 2.8.2 |
| **9** | Pupil and Image Check accessible from other instruments | 2.8.4, 2.8.5 |
| **10** | LEONARDO stand-alone operation | 2.8.6 |
| **11** | LEONARDO accessible from other instruments | 2.8.6 |
| **12** | LEONARDO high level command | 2.8.6 |
| **13** | Piezo frequency | 2.9.2 |
| **14** | Piezo range | 2.9.2 |
| **15** | Piezo wave shape | 2.9.2 |
| **16** | Piezo-LISA synchro precision | 2.9.2 |
| **17** | Quick look algorithm | 2.9.6 |
| **18** | Visibilities display | 2.9.6 |
| **19** | Possibility of dispersed mode | 2.10 |
| **20** | Duty cycle minimum value | 2.9.2 |
| **21** | Data acquisition 'dead time' | 2.9.2 |
| **22** | OPD offset frequency | 2.9.2 |
| **23** | DL Offset time | 2.9.2 |
| **24** | LISA readout rate selected by the user | 2.9.7 |
| **25** | LISA during signal check | 2.9.8 |
| **26** | LISA percentage of light in a single pixel | 2.9.8 |
| **27** | LISA full frame image | 2.9.9 |
| **28** | LISA output alignment checking | 2.9.9 |
| **29** | LISA full frame readout rate | 2.9.9 |
| **30** | LISA full frame storage | 2.9.9 |
| **31** | Fast Scan control signal in Engineering mode | 2.9.10 |
| **32** | LdV data rate | 2.10 |
| **33** | Online data reduction on the LdV WS | 2.11.1 |
| **34** | Observations buffering | 2.11.1 |
| **35** | Control procedure of LEONARDO | 2.12.2 |
| **36** | Control procedure of the Alignment Toolkit | 2.12.3 |
| **37** | Expected pupil position reading | 2.15.3 |
| **38** | Pupil position from the TCCD focus | 2.15.3 |
| **39** | Star image centering procedure | 2.15.5 |
| **40** | TCCD image storage with the LdV data | 2.15.6 |
| **41** | Manual injection optimization | 2.16 |
| **42** | Output alignment procedure | 2.16.2 |
| **43** | Output parameters storage | 2.16.2 |

| | | |
|---|---|---|
| **44** | Template-based operation of LdV | 2.17 |
| **45** | Instrument state change | 2.18 |
| **46** | Instrument mode setting | 2.18 |
| **47** | Stellar Interferometer user interface | 2.18.1 |
| **48** | Engineering mode GUI | 2.18.6 |
| **49** | Individual Instrument parameters setting | 2.18.7 |
| **50** | HAWAII window shape | 2.4.7 |
| **51** | Fringes search | 2.12.1 |
| **52** | Mode switching time | 2.8 |
| **53** | Preheating of the thermal source | 2.12.2 |
| **54** | 'Idle' as default setup | 2.8 |
| **55** | LdV division in units | 2.3 |
| **56** | LdV opto-mechanical elements | 2.4 |
| **57** | Instrument states | 2.6 |
| **58** | Graphical User Interface | 2.18 |
| **59** | Archived data | 2.11.2 |
| **60** | ICS / DCS commands and answers logging | 2.6 |
| **61** | Engineering mode | 2.7 |
| **62** | No OPD offsets when using FSU | 2.9.5 |

## 2.20 SECOND GENERATION UPGRADES

In this section are described the functions and capabilities that are not necessary for VINCI to work, but which would improve its productivity and ease of use. They could be implemented as an improvement to the current concept after the first fringes have been obtained.

It is important to keep the necessary options opened in the software design.

### 2.20.1 Automated Injection Optimization

In this section, two possible algorithms for automatically peaking the alignment of the star into the fiber are described.

#### 2.20.1.1 Fast image scan algorithm

This algorithm will work only if the motors of the INA1 and INB1 mirrors are replaced by piezos, which is not the case in the current implementation of LdV. It is taken from a proposal by Steve Ridgway (NOAO).

The idea is to scan the image rapidly across the fiber in order to freeze the seeing. But then it takes multiple scans to build up signal to noise. This is not a problem, because you really want the measurement to average over the seeing fluctuations.

Since you have a piezo control, it is possible to put a ramp signal on the piezo and scan repeatedly the fiber head over a range of +/-1 arcsec. Synchronized with the scans, the signal is coadded into a vector. When finished, you should have a peak in the vector which corresponds to the nominal position. You can then move the piezo to the correct position. Then repeat in the other direction. This should be faster, more accurate and more sensitive than alignment by hand.

#### 2.20.1.2 Slow image scan algorithm

Another possible scheme for the automated optimization of the injection in the fibers is :

1. **Obtain quick exposures from the LISA camera in not synchronized mode**, in order to obtain a nearly continuously (frequency of a few Hz) monitored value for the flux arriving on the HAWAII detector. The maximization of this value will be the goal of the optimization.
2. **Start a slow spiral motion** of one of the injection mirrors, say INA1, to slowly move the stellar image disk in front of the fiber head. During this motion, the intensity on the LISA corresponding photometric and interferometric pixels is continuously monitored, as well as the position of the tip and tilt motors. After the spiral motion has reached a radius of one speckle cloud (~ 0.5-1 arcsec projected on the sky), the data acquired is an array of tip and tilt positions (in mm) associated with intensity values (in ADUs).

3. **Do the same thing with the other injection mirror** INB1, which gives you another array of (tip, tilt, intensity) values.

4. **Fit the measured (tip, tilt, intensity) data with a 2 dimensional gaussian curve**, in order to find the precise position of the maximum intensities for the two beams. This gives the offsets to apply to the injection optics to maximize the injected flux. The main source of noise is the intensity variations due to turbulence.

5. **Correct the position with the tip-tilt mirrors** : finally, the computed offsets are sent to the INA1 and INB1 mirrors.

6. **Fringe search** : At this stage, the injection should be optimized, and the fringe search can begin.

### 2.20.2 Automated Output Alignment

This algorithm is **TBD**, but will be, for the focusing part, very similar to the TCCD focus algorithm.

For this procedure, LEONARDO artificial star is on (thermal light source).

The focus setting of the fiber output is remotely adjustable. The precise focusing of the four fiber outputs on the LISA detector requires to monitor precisely their FWHM on LISA full frame images, and then to apply the necessary focus motion on the fiber bundle head OUT1.

To set the rotation of the fiber bundle, it is possible to monitor the light concentrated in the four pixels corresponding to the light maxima, and to compare it with the flux in the surrounding pixels. The target here is to have as much of the incoming light concentrated on a single pixel of the detector. This could result is positioning the four output pixels on four different lines and columns (i.e. on a square with non horizontal and vertical sides).

### 2.20.3 Spectral Dispersion

The optical design of LdV makes it possible to disperse the light from the four fiber outputs before it enters the LISA camera. This feature is very interesting, because it would greatly extend the capabilities of LdV, in the field of stellar and extrasolar planets observations. It is thus important to keep in mind that the LdV software has to be able to accommodate for four lines readout of LISA instead of four pixels.

The dispersion would cover about 50 pixels. This would mean for the LdV software a proportional increase in the quantity of raw data produced. The LdV software should be able to read 200 (50x4) individual windows on the HAWAII detector. The fiber output alignment procedure would also be affected in this configuration of the instrument.

### 2.20.4 Sensors

A number of optical elements are moved manually. If they are forgotten in a wrong position, this could cause data to be lost. The monitoring of their position, with the possibility to send alerts to the user in case of mispositioning, might be required in order to ensure the reliable operation of the instrument.

The particular question of the fiber type sensors is adressed here with respect to the reference document [7]. They are not essential for the operation of the instrument, but they could make the operation of LdV easier and more straightforward. In the following table, the name of each fiber connector to be monitored is indicated in the column 'Measured Physical Parameter' (for example, the ART3 connector on the artificial source,...). The names of the fibers that can be plugged on each connector are listed in the column 'value' (for example, it is possible to plug WG1X1, WG1X2, WG2X1, WG2F1, WG2F2,... on the ART3 connector). Each fiber is designated by its coded name (for example WG1X2 means WaveGuide 1 connected to the X coupler number 2 on one end).

| **Measured Physical Parameter** | **Measured every...** | **Range/Values** | **Comments** |
|---|---|---|---|
| ART3 FIBER | Observation | WG1X1, WG1X2, WG2X1, WG2F1, WG2F2, WG2F3, WG2F4, WG2F5, WG2F6, WG2F7, WG3F1, WG3F2, WG3F3, WG3F4, WG3F5, WG3F6, WG3F7, WG4F1, WG4F2 | The main light source fiber feed |
| ART2 FIBER | Observation | WG1X2, WG2X1, WG3F1, WG4F1, WG5F1 | Focus of parabola ART1 |
| INA2 FIBER | Observation | WG1X1, WG2F2 | Focus of parabola INA1 |
| INB2 FIBER | Observation | WG2F6, WG3F6 | Focus of parabola INB1 |
| MONA IN 1 FIBER (A BEAM) | Observation | WG1X2, WG2F4, WG3F2 | Injection of light from the “in” side of MONA, beam A |
| MONA IN 2 FIBER (B BEAM) | Observation | WG1X2, WG2F5, WG3F3 | Injection of light from the “in” side of MONA, beam B |
| MONA OUT 1 FIBER (A BEAM) | Observation | WG2X1, WG3F4 | Injection of light from the “out” side of MONA, beam A |
| MONA OUT 2 FIBER (B BEAM) | Observation | WG2X1, WG3F5 | Injection of light from the “out” side of MONA, beam B |
| OUT1 FIBER | Observation | WG2F6, WG2F7, WG3F6, WG3F7 | Output of the MONA box (4 fibers bundle) |
| COMA3 POSITION | Night | IN, OUT | Present in normal operations |
| COMB3 POSITION | Night | IN, OUT | Present in normal operations |

| | | | |
|---|---|---|---|
| ALI9 POSITION | Night | IN, OUT | Used only for engineering |

### 2.20.5 Photometric Calibrations for the TCCD

At the beginning of the night, it would be interesting to obtain flat field images of the bright sky with the TCCD in order to calibrate the images obtained during the night. Once the object image has been acquired, a dark field should be acquired, of the same exposure duration as the object exposure, to be substracted from the object image.

Moreover, it is desirable to obtain once or twice per night the image of a photometric reference, in order to estimate broadband magnitudes of the targets. The procedure to obtain these measurements is not different from the pointing of the science targets. The desired magnitude precision is 0.1 mag. It is understood that this magnitude is not directly comparable to the standard systems magnitudes, as it is a broadband integration, based on the sensitivity curve of the TCCD. This measurement could be useful to estimate the parameters for the infrared camera exposures.

*Page laissée vierge intentionnellement*

# 3. LISA Test Report

EUROPEAN SOUTHERN OBSERVATORY

Organisation Européenne pour des Recherches Astronomiques dans l'Hémisphère Austral
Europäische Organisation für astronomische Forschung in der südlichen Hemisphäre

# VERY LARGE TELESCOPE

## LEONARDO da VINCI

### LISA Test Report

Doc. No.: VLT-TRE-ESO-15810-2330

Issue: 1.0

Date: 5 October, 2000

Prepared: P. Kervella
. . . . . .
Name Date Signature

Approved: A. Glindemann
. . . . . .
Name Date Signature

Released: M. Tarenghi
. . . . . .
Name Date Signature

CHANGE RECORD

| Issue | Date | Section/Page affected | Reason/ Initiation/Remarks |
|---|---|---|---|
| 1.0 draft | 7 August, 2000 | All | First draft, alignment procedure. |
| 1.2 draft | 6 September, 2000 | All | Includes first tests with the windowed readout mode. |
| 2.0 draft | 21 September, 2000 | Sections 5, 6, 10, 11 | Detector tests using the 64x64 pixels and windowed readout modes. |
| 1.0 | 5 October, 2000 | Sections 6-9 | The results obtained with the chopping device (memory effect) are included, and the filter wheel order is corrected. Readout noise level error corrected. |

# TABLE OF CONTENTS

# Figures



# Tables

# 1. INTRODUCTION

## 1.1 SCOPE

This document describes both the procedures and results of the tests conducted on the LISA camera in Garching, using the collimated light source provided by the Observatoire de Paris-Meudon.

## 1.2 GENERAL PHILOSOPHY

VINCI makes a particular use of the HAWAII detector of LISA, reading only a few of its pixels at a high frequency. The tests described here aim at validating both the optical concept and performances of the camera.

These tests are preliminary to the acceptance of LISA in Garching and also to the AIV of the whole LEONARDO da VINCI instrument.

## 1.3 APPLICABLE DOCUMENTS

| | | | |
|---|---|---|---|
| 1. | LISA Maintenance Manual (Draft), MPE | | 06/2000 |
| 2. | LISA User's Manual (Draft), MPE | | 06/2000 |
| 3. | LISA Acceptance Plan (Draft), MPE | | 06/2000 |
| 4. | LISA Drawings, MPE | | 06/2000 |
| 5. | LISA Statement of Work | VLT-SOW-ESO-15810-1xxx v.1.0 | 28/07/1999 |
| 6. | LISA Technical Specifications | VLT-SPE-ESO-15810-1xxx v.1.0 | 31/08/1999 |
| 7. | OUT Alignment Procedure, DESPA | | 17/07/2000 |
| 8. | ICD between VLTI and Instruments | VLT-ICD-ESO-15000-1826 v.1.0 | 16/11/1999 |

## 1.4 REFERENCE DOCUMENTS

## 1.5 ABBREVIATIONS AND ACRONYMS

| | |
|---|---|
| ADU | Analog Digital Unit |
| AIV | Assembly, Integration and Verification |
| ALIU | The Alignment Unit |
| DCS | Detector Control Software |
| DP | Data Pipeline |

| | |
|---|---|
| GUI | Graphical User Interface |
| GEI | Graphical Engineering Interface |
| GOL | Garching Optical Laboratory |
| HW | Hardware |
| ICS | Instrument Control Software |
| IRTD | Infrared Real Time Display |
| IWS | Instrument Workstation |
| LCU | Local Control Unit |
| LdV | LEONARDO da VINCI, the whole instrument |
| LEONARDO | The artificial star subsystem |
| LISA | The HAWAII-based infrared camera |
| LISA WS | The LISA LCU (workstation) |
| MONA | The fibered recombiner |
| N.A. | Not applicable |
| OPD | Optical Path Difference |
| OS | Observation Software |
| ROF | Raw Observation File |
| SNR | Signal to Noise Ratio |
| SW | Software |
| TBC | To Be Confirmed |
| TBD | To Be Defined |
| TCCD | ESO Technical CCD |
| VINCI | The main optical table of LdV |
| WS | Workstation |

# 2. DEWAR GENERAL CHARACTERISTICS

## 2.1 COLD TEMPERATURE AUTONOMY

The measurements presented on Figure 1 have been done with an external temperature of about 20 degrees C. The upper tank capacity is about 6 liters, and the lower tank capacity is about 3 liters.

**The real autonomy is 24 hours, *but not more*.**

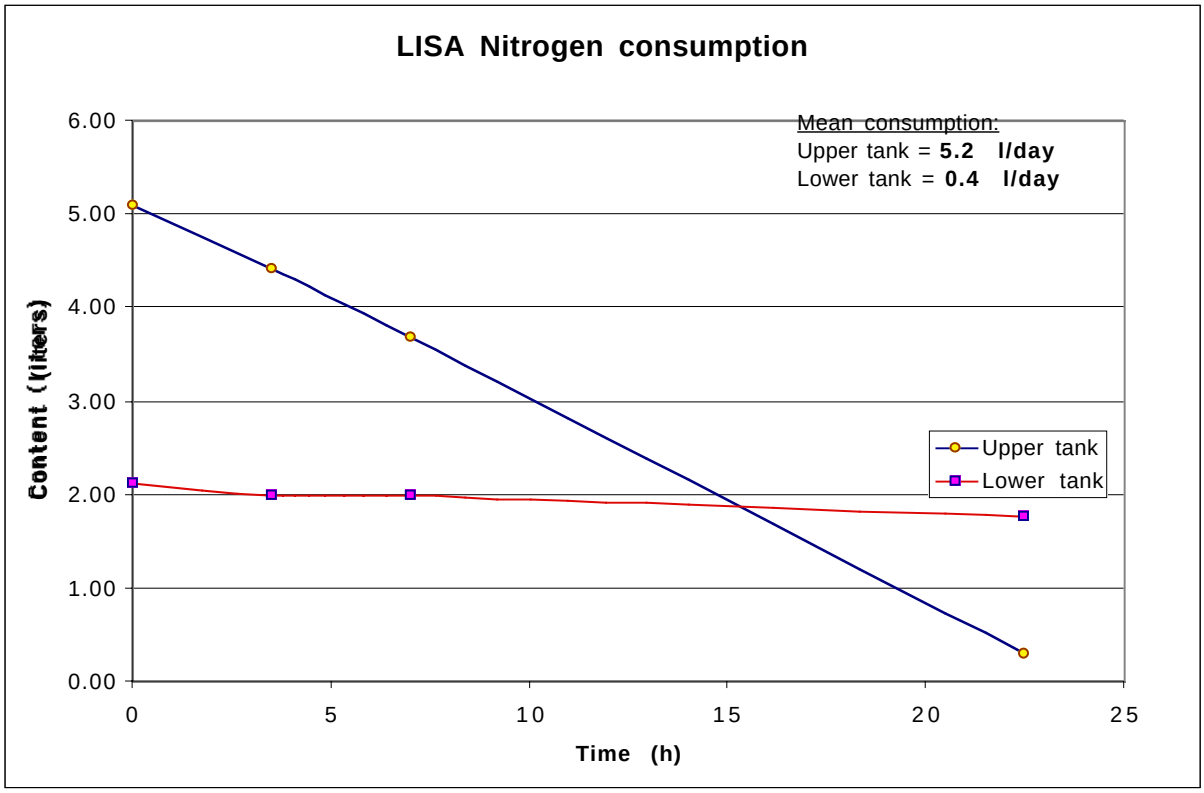


**Figure 1. LISA Nitrogen consumption**

## 2.2 NITROGEN FILLING

The filling of the two tanks was achieved without problem following the instructions of the manual provided by MPE. It is difficult to fill the upper and lower tanks to more than 5 and 2 liters respectively.

## 2.3 VACUUM TIGHTNESS

The tightness of the dewar is relatively good, but condensation was observed occasionally on the metallic surface of the dewar. The addition of a vaccuum gauge (by ESO) to the dewar has made it possible to evaluate precisely the tighness of the camera. When the camera is not cooled down, the molecular sieve releases the gas it has trapped, and the vacuum becomes worse. After pumping and cooling down, the level of vaccuum is very satisfactory (pressure less than 10^-6 mbar), and stays at low values until the camera is warmed up again.

# 3. MECHANICAL ALIGNMENT

## 3.1 DESCRIPTION

The LISA dewar is attached to its dedicated mechanical support, that is installed on the main VINCI table. The height of the LISA support alone is not correct for the required height of the beams, and therefore it is installed on four aluminium cylinders. The whole system is not attached to the VINCI table, and is therefore not compliant to the seismic resistance specifications of ESO. Clamps have to be installed for the acceptance of the system.

The support is made of machined aluminum plates. The rigidity of this system was tested with respect to the required accuracy on the detector (maximum displacement of the fiber image on the detector has to be negligible compared to the pixel size). See Section 4.6.5 for a detailed report.

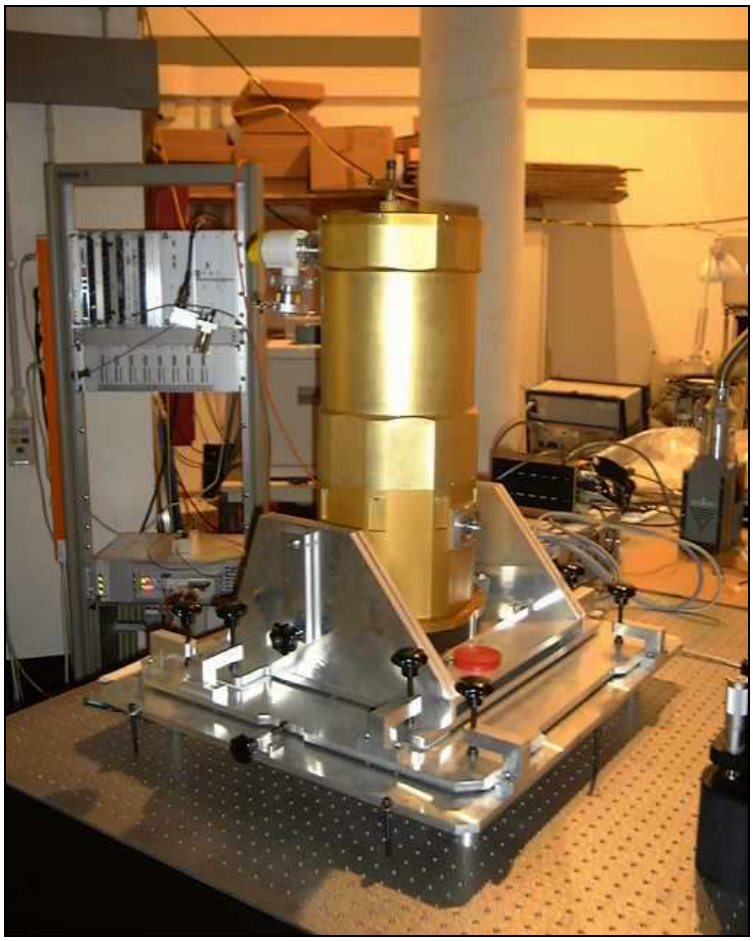

**Figure 2. LISA installed on its support.**

## 3.2 ALIGNMENT PROCEDURE

◊ Check that the VINCI table is horizontal.

◊ Set all the mechanical adjustments of the LISA camera to central position.

◊ Check that the LISA support bottom plate is horizontal, relatively to the VINCI table. For this, use a slide caliper to measure the height of the four corners of the support relatively to the VINCI optical table.

◊ Check that the upper plate of the dewar is horizontal (with a bubble level). Pay special attention to the setting of:
- the “cradle” part of the support,
- the direction pointed by the dewar window.
These two settings directly impact the position of the beam on the detector.

◊ Measure the height of the entrance window of LISA and of the output mirror of the artificial light source OUT relatively to the VINCI table surface. This can be done directly by using a square and measuring the height from the table surface, or by using a slide caliper to measure the heights of all the supports. The center of the dewar window is located aproximately 149 mm above the bottom surface of the dewar.

◊ Adjust if necessary of the height of LISA, by using the three pads below the dewar. Be careful to maintain the same height for all pads. The height of the center of the entrance window of the dewar should be 320 mm.

◊ Check precisely the horizontality of the off-axis parabola using the two reference pods on the back of its support. This can be done with a micrometric comparator or, as an alternative, with a precise slide caliper. The reference for the measurement should be the optical table itself, but as a second choice, the base plate of the OUT source can also be used.

# 4. DOUBLET FOCUSING

## 4.1 ALIGNMENT PROCEDURE

◊ Collimate roughly the artificial light source following the Meudon procedure (on a distant wall for example). The adjustement is done by moving the fiber head itself. The image produced by the laser should be a tiny spot of light less than 1 mm across, with round shape and sharp edge. Two small, fainter dots on each side of the main spot should be visible (they are due to the microgrooves of the off axis parabola). Turn back the source in the correct direction.

◊ Measure the relative positions of the two benches on the VINCI table. The references are the center of the LISA dewar window and the center of the OUT2 flat mirror. The precision required depends on the distance between the source and the dewar (the further, the lower the required precision). A precision better than 1 mm (relatively to the table edge) should be sufficient assuming a distance of 1 or 2 m between LISA and OUT2.

◊ Send the laser in the OUT system and adjust the OUT2 mirror *only* to have the red dot centered on the entrance window of the LISA camera. This will set the reference for the alignment of the optical axis of the autocollimator. **Be careful to switch off the laser after use.**

◊ Install the autocollimator and adjust its height precisely. For that it is necessary to have a correct horizontality of the autocollimator optical axis. There is an integrated bubble level for that purpose. The height of the center of the input lens should be set at 320 mm above the table surface.

◊ Position the axis of the autocollimator between the OUT2 mirror and the LISA camera window (mm precision). This part is not very easy, as there is no reference to set the direction of the refractor. One possible method is to use the laser of the OUT source:

- send the laser light into the OUT source,
- check that the laser dot is at the center of the entrance lens of the autocollimator, but **do not look into the eyepiece**,
- **be careful to switch the laser off** and plug in the thermal light source,
- do a first rough autocolimation of the refractor by using a flat mirror in front of the entrance lens. The goal here is to focus the image of the cross.
- while looking into the eyepiece, move the back of the autocollimator until you can see the fiber head near the center of the autocollimator,

◊ Do a second autocollimation to focus precisely the autocollimator to infinity.

◊ Move the OUT2 mirror to center the fiber image on the cross of the autocollimator.

◊ Adjust finely the fiber position to have a focused, aberration-free fiber image in the autocollimator. **The aberration-free field of the off-axis parabola is only of the size of the fiber core**, so the precision of positioning must be very good. The image should be a small yellowish disk of light, with round shape and clean edge. If the fiber is moved vertically or laterally, use the OUT2 mirror to center the image back on the center of the autocollimator field of view.

◊ Note the exact focus position of the micrometric knob used to move the fiber in focus (and also in other directions). This measurement can be done to a precision of 1 micron on the adjustment knob. Be careful to have a precise reading.

◊ Remove the autocollimator from the beam. There should be a somewhat fuzzy image on the LISA detector.

## 4.2 FOCUSING PROCEDURE

The measurement procedure is based on the idea that we know the magnification factor between the fiber off-axis parabola and the doublet inside the LISA dewar. The knowledge of the focus offset between infinity and correct detector focus enables to compute the motion to give to the doublet (or to the detector) to focus the dewar optics correctly to infinity.

Therefore, the measurement is done several times using the following procedure:

◊ Focus the fiber at the focal point of the off-axis parabola, to produce a clean collimated beam (procedure explained in paragraph 4.1).

◊ Take down precisely the position of the micrometric knob P1. The reading can be done at a 1 micron precision, but the final precision is probably something like +/- 10 microns.

◊ Position the beam on the detector at the position where the focus is necessary.

◊ Obtain the best possible focus by adjusting the focus knob on the fiber head mount.

◊ Take down the new position of the micrometric knob P2. The difference with the previous reading (P2-P1) gives the focus difference between infinity and the current position of the doublet. A multiplicative factor corresponding to the magnification factor has to be applied to have the physical motion to give to the doublet (or the detector). See Section 4.4 for the complete computation.

## 4.3 EXPERIMENTAL RESULTS

**Table 1. Fiber head motion to obtain the focus on the Hawaii array.**

| Test # | X (pix) | Y (pix) | R (pix) / lower left | Autocollimator | Fiber Infinity (mm) | Fiber Pos. Focus (mm) | Delta (mm) | Energy in one pixel (%) | Comments |
|---|---|---|---|---|---|---|---|---|---|
| 1 | (550)38 | 20 | 42.9 | White | 4.911 | 4.615 | **0.296** | **48** | Old autocollimator |
| 2 | (550) 38 | 20 | 42.9 | Black | 4.951 | 4.614 | **0.337** | **65** | New autocollimator, background evaluation problem |
| 3 | (550) 38 | 20 | 42.9 | Black | 4.949 | 4.619 | **0.330** | **64** | New autocollimator, background evaluation problem |
| 4 | (530) 18 | 44 | 47.5 | Black | 4.952 | 4.659 | **0.293** | | Difficult reading of focus |
| 5 | (529) 17 | 43 | 46.2 | Black | 4.950 | 4.709 | **0.241** | **50** | Very difficult measurement (slow) and new lateral positioning of the fiber |
| 6 | (548) 36 | 35 | 50.2 | Black | 4.942 | 4.730 | **0.211** | **54** | Precise measurement |
| 7 | (548) 36 | 35 | 50.2 | Black | 4.937 | 4.723 | **0.214** | **54** | Precise measurement |

The mean ΔFocus is 0.275 mm (standard deviation of 0.053 mm), but the focus point is different for different parts of the detector. The reason for this could be a curved focal plane for the doublet, or a bad parallelism between the detector and the doublet, or even a non-planeity of the detector surface (due possibly to decay of the indium layer observed near the edges).

A plot of the evolution of the focus position as a function of the distance to the center of the detector (lower left corner of the used quadrant) is presented on the following figure. X axis is the radius in pixels (18 microns) from the center of the detector (lower left corner of the quadrant used), Y axis is the fiber displacement in millimeters.

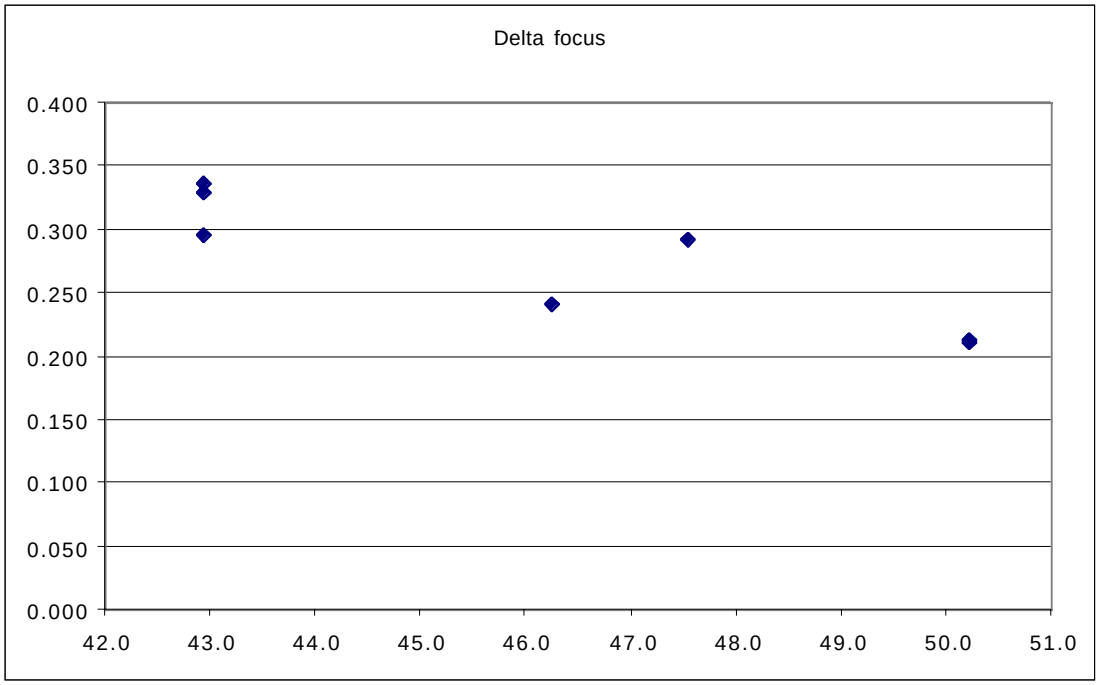


***Delta (millimeters) = -0.01408 R(pixels of 18 microns) + 0.924***

Using this formula, it is possible to compute the focus correction to give to the doublet (or to the detector), depending on the part of the detector that will be used for the actual observations. Though, it is necessary to evaluate the usable area of the detector to determine the best focus to apply.

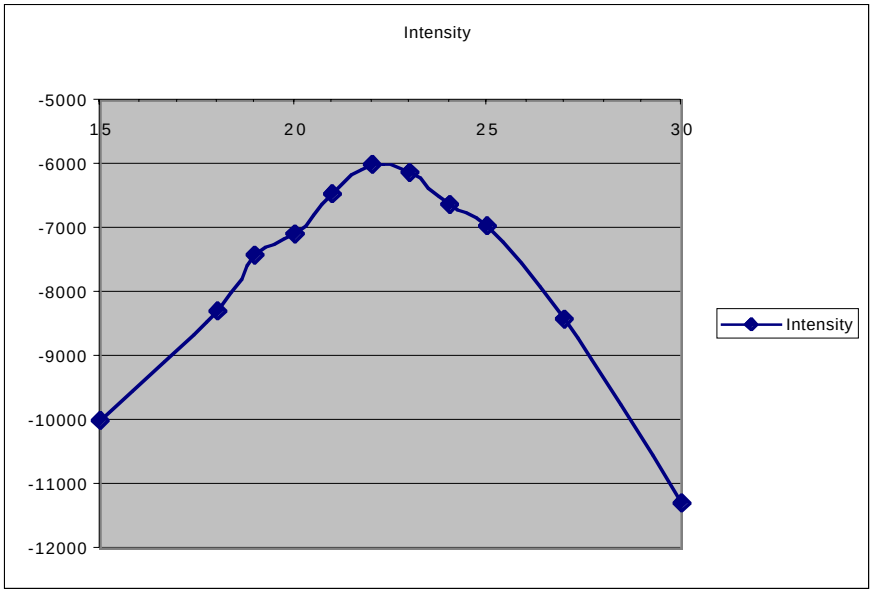


**Figure 3. Example of a focusing done by moving the fiber (test #7, X scale in tens of microns, Y in ADUs).**

The direction of the focus motion necessary is **towards** the off axis parabola (**See Figure 4**).

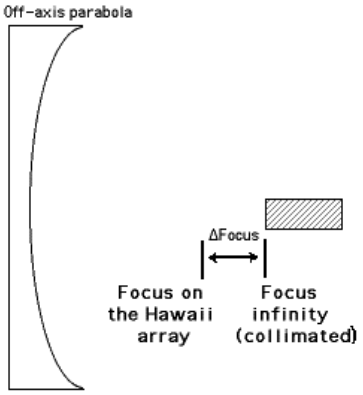


**Figure 4. Direction of the applied focus motion**

## 4.4 FOCUS CORRECTION TO APPLY TO THE DOUBLET

As described in Section 5.1.5, the usable area of the detector is centered on the pixel (X=33,Y=38). The focusing tests #6 and #7 (see Section 4.3) have been done on pixel (X=36,Y=35), which is very close to the center of the usable area. **Therefore, the focus motion to give to the doublet should be computed assuming a measured focus offset of 0.214 millimeters on the fiber position**, as test #7 gives the best percentage of light in a single pixel, and is very coherent with the measurement obtained on test #6.

The direction of the motion to give to the doublet has to be determined knowing that the fiber focus correction has been done in the adequate direction (Figure 4):

It is mandatory to take into account the correct **magnification factor** between the off-axis parabola and the doublet.

The focus correction has to move the doublet **closer** to the detector. The ammount of motion is computed using the following formula:

$$\Delta X_{doublet} = G^2.\Delta X_{fiber}$$

with

$$G = 9 \times 18.5 / 125 = 1.332$$

the nominal longitudinal magnification factor (the fiber images are separated by 9 pixels of 18.5 microns, while the fibers in the bundle are separated by 125 microns). The real value may differ by a few percents from this value. Therefore, the resulting motion for the doublet is:

$$\boxed{\Delta X_{doublet} = 1.332^2 \times 214 \sim 380\ \mu m}$$

## 4.5 RESULT OF THE FOCUSING

### 4.5.1 Procedure

The focusing correction computed (380 microns) was applied to the detector mount towards the doublet, by machining the positioning reference device. After this step, the OUT light source was collimated precisely using an autocollimator, and the resulting beam was sent to the detector, on pixel (545,38) (coordinates

(33,38) from the lower left corner of the detector, corresponding to the center of the usable field. The beam position was adjusted at sub-pixel precision to maximize the flux in the target pixel.

### 4.5.2 Intensity profiles

The resulting profiles in the X and Y directions are presented in the following figures (measurement #10). In this measurement, the 64x64 window readout mode was used at the maximum frequency. The spot was not saturated on the detector.

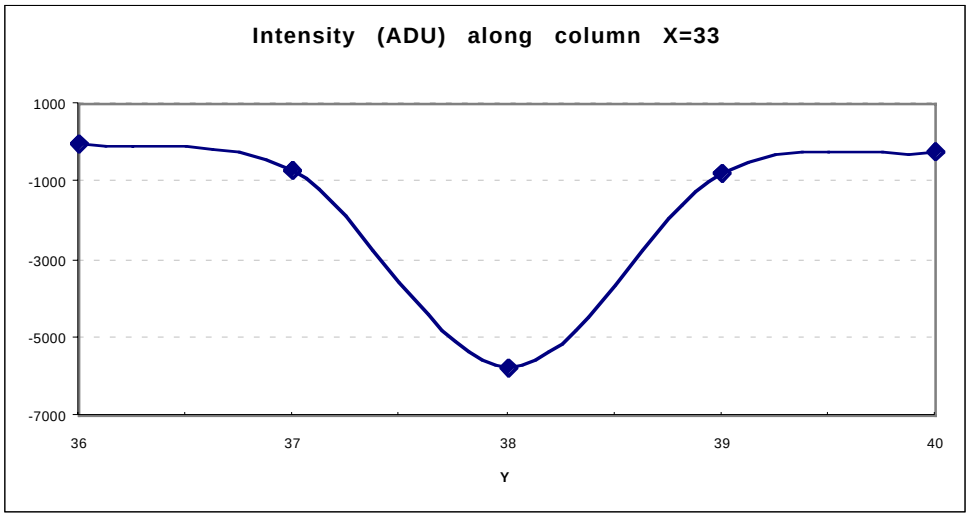


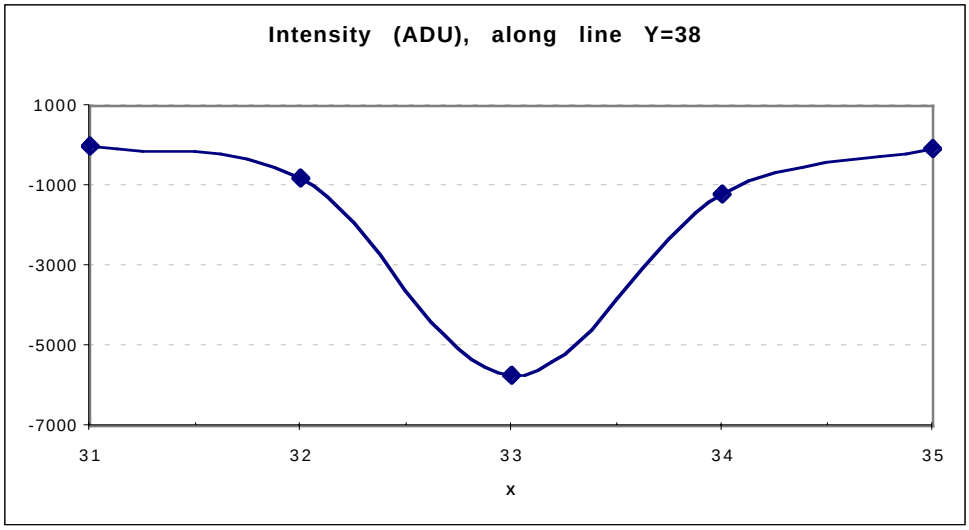


### 4.5.3 Energy in the target pixel

The energy contained in the target pixel is 56 % (see Table 2), for test #10 (the most significant). This result is about the same as for the best focus obtained previously (tests #6 and #7). It is suspected that the previous tests were done with the detector in the saturated regime, on the strongly non linear part of the sensitivity curve, but the focusing could (fortunately) still be achieved correctly in this regime.

**Table 2. Result of the in-focus test on LISA.**

| Test # | X (pix) | Y (pix) | R (pix) / lower left | Autocollimator | Fiber Infinity (mm) | Fiber Pos. Focus (mm) | Delta (mm) | Energy in one pixel (%) | Comments |
|---|---|---|---|---|---|---|---|---|---|
| 8 | (545) 33 | 38 | 50.3 | Black | 4.904 | - | - | **54** | Collimated beam, suspected saturation.. |
| 9 | (545) 33 | 38 | 50.3 | Black | 4.904 | - | - | **53** | Unsaturated pixel, but very high background. |
| 10 | (545) 33 | 38 | 50.3 | Black | 4.904 | - | - | **56** | Short exposure time (64x64 readout mode), and no saturation plus fixed pattern removal. BEST EVALUATION. |

### 4.5.4 Optical efficiency

Due to electronic leaking of the target pixel into its neighbors, **only 58% of the energy brought effectively by the photons into this pixel are present in electronic form for readout** (*ref*: study by Gert Finger on the HAWAII chip). The other 42% are present in the four neighbors of the target pixel, in the fast and slow shift register directions (horizontal and vertical). 15% of the energy is lost in each neighbor pixel along the fast shift register, and 6% in the neighbor pixels along the slow shift register.

Therefore, the 56% measured with the detector in focus (test #10) correspond to a very good optical efficiency.

## 4.6 PROBLEMS

### 4.6.1 Clamping of the camera mount

Currently the camera is not attached at all on the VINCI optical table. It is important to foresee an addition to the current design to fasten the mount securely to the table. In the current status, the camera is very unstable, and can be moved easily by hand.

### 4.6.2 Sign of the ADU counts

All the counts in ADU delivered by the camera when in double correlated mode are negative. Higher flux gives lower negative ADU counts. This was a misleading behavior, and the sign of the subtraction of the two readouts in double correlated windowed readout mode was modified in the last version of the software (as of 11/09/00). The 64x64 and 512x512 pixels modes were not corrected.

### 4.6.3 Filters order in the filter wheel

Counted *counter clockwise, seen from the front of the dewar towards the detector*, the correct order is the following:

**Table 3. Filters positions in the filter wheel.**

| Position | Filter |
|---|---|
| 1 | CLOSED |
| 2 | OPEN |
| 3 | K BAND (green color) |
| 4 | H BAND (orange color) |
| 5 | OPEN |
| 6 | OPEN |

### 4.6.4 Connector surface

During these experiments, the connector of the fiber was apparent on the detector, as a darker spot. The explanation seems to be that the detector is seeing itself in the connector polished surface, therefore it appears much colder than the surroundings.

Generally speaking, the background level is very high, due to the absence of a real cold stop for the detector (see section 5.2 for details).

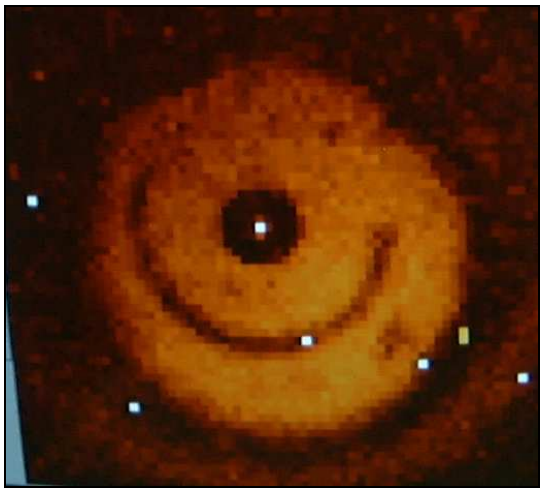

**Figure 5. Image of the OUT fiber as seen on the detector of LISA. The fiber core (bright, saturated point near center, should be dark if not saturated) is surrounded by the envelope (dark), and the surface of the connector (brighter halo). The scale being inverted, the connector appears in reality darker than the background.**

### 4.6.5 Camera mount stability

After the focusing of the beam on the detector, it was possible to do the first stability tests of the mount. First the long-term stability of the mount, if not charge is applied, seems satisfactory, with no visible motion of the spot over one night.

A concern was the difference in the position of the camera when it is loaded with nitrogen and when it is empty. For this purpose, a ~3 kg mass was put on top of the dewar to simulate the presence of a load of nitrogen. When the load is positioned precisely on the dewar axis of symetry, then there is no apparent motion of the spot on the detector (no variation in the intensity of the illuminated pixel). This is due to the fact that a translation of the dewar in the plane of focus will not cause any shift of the spot.

When the load is added slightly offset from the center of the dewar upper plate, then the load is asymetric, and in this case, there is a motion of the spot on the detector of one to two pixels. This case will normally not happen under normal observation conditions, as the nitrogen load is purely axisymetric.

A second test with a higher mass (5 kg) positioned precisely at the center of the upper plate did not provoke a visually detectable motion of the spot on the screen.

As a conclusion, the stability of the dewar mount seems satisfactory, except for non axisymetric loads, which should be avoided as much as possible. A concern might be for example the presence or not of the vacuum pump. For normal observations, absolutely no lateral load should be put on the dewar, and no cable should be moved, in order to avoid any tilt of the dewar.

# 5. OPTICAL AND BASIC DETECTOR TESTS

## 5.1 FIELD OF VIEW

### 5.1.1 Description

The Hawaii array is illuminated by the cold doublet lens in front of the camera. It is necessary to evaluate the field of view seen by the detector, in order to position the fiber images in an unvignetted part of the field.

### 5.1.2 Procedure

◊ First roughly evaluate the LISA detector field of view by putting a diffuse, extended light source just in front of the camera window while running the full-frame acquisition.

◊ Evaluate the uniformity of the light on the dectector.

◊ Make a focused image of the fiber head on the LISA detector (see Section 4.2).

◊ Measure the peak intensity of the spot as it is moved over the detector (by turning the knobs on the *flat* mirror of the OUT source).

The center of the field is located at the lower left corner of the detector (as seen on the RTD screen), in order to have the best possible readout speed. Though, there are a number of dead or bad pixels in that region, that should be avoided.

### 5.1.3 Diffuse illumination

The illumination of the detector with a diffused source gave a uniformly decreasing intensity from the center to the edge of the detector (radial). The decrease is nearly perfectly linear, and the noise level seems to be approximately constant. It is difficult to estimate the impact of this effect on the fringe measurements, before the noise tests have been conducted on the system.

### 5.1.4 Focused saturated spot

As a second step, the focused light source spot was moved over the array, in order to estimate what fraction of the detector is usable to image the fiber head. The problem here is that the beam is easily vignetted by the window of the dewar if its direction is too much tilted. The practical experiment was done by measuring the intensities across one line and one column.

**A problem was identified after the measurement: the spot was heavily saturated due to a too long exposure time (more than 2 seconds). Therefore, the usable area defined in this section will have to be checked with a lower intensity beam and the LdV four fibers bundle.**

**It is important to bring the spots as close as possible to the lower left corner of the array to optimize the readout frequency.**

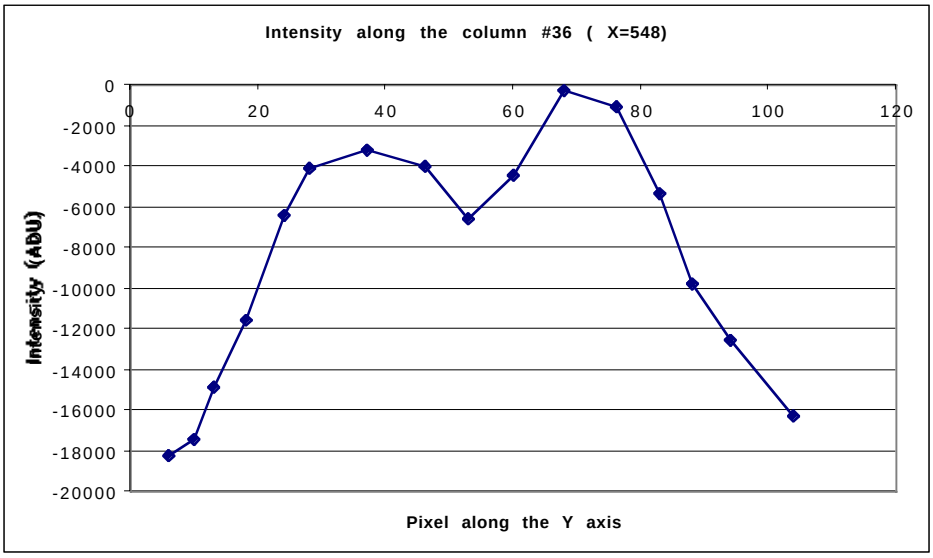


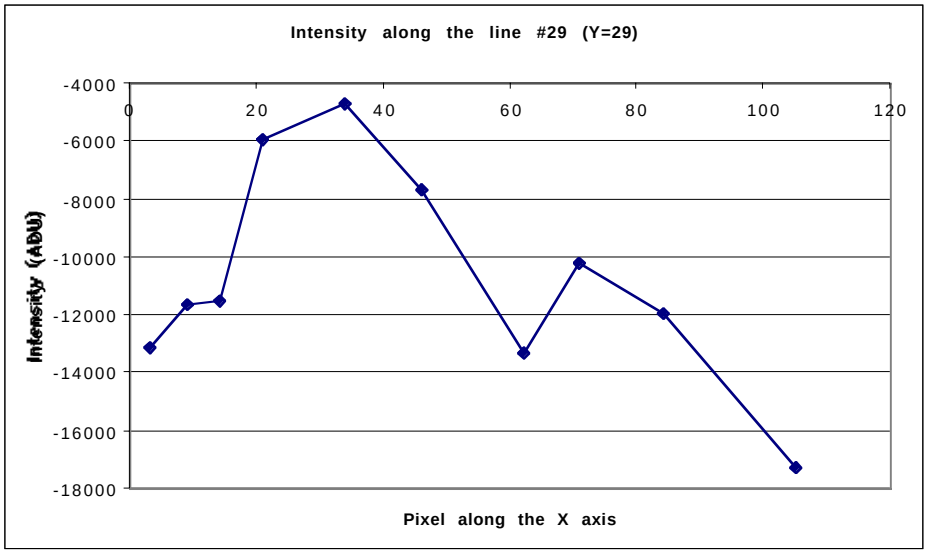


The structure of the array is nearly symetric relatively to the diagonal of the quadrant, with the first lines and columns not as reactive as the others. The explanation for this behavior may be the same as for the presence of dead pixels around the outer edges of the detector (indium layer decay ?).

The best area for the positioning of the four scientific spots seems therefore to be approximately [20 < X < 45, 25 < Y < 50], intersected with a quarter disc of radius ~ 45 (centered on the lower left corner).

### 5.1.5 To be checked: Usable detector area

In the following figures, the usable part of the Hawaii detector is indicated on the quadrant (“OK” square area). The size of this area is small, but this is the best location with the current optical design.

This zone has to be verified using a *non saturated* spot moved across the detector.

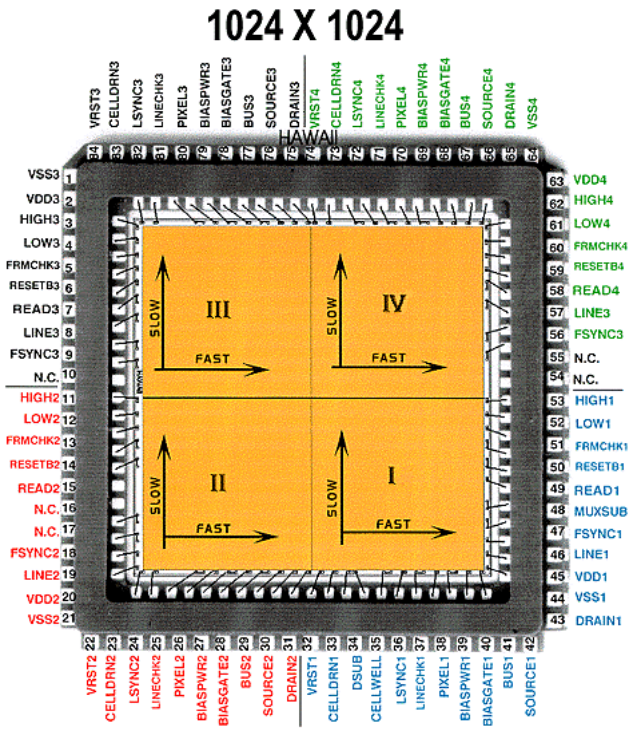


**Figure 6. The HAWAII array. LISA detector uses quadrant IV (picture from Rockwell). The X axis of the LISA camera is along the fast shift register (positive direction), and the Y axis is along the slow shift register (positive direction).**

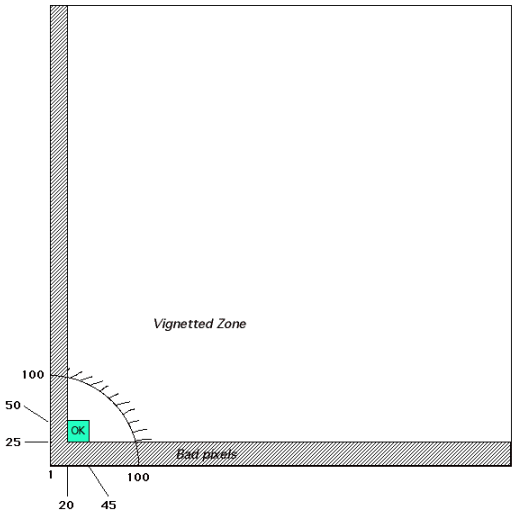


**Figure 7. LISA Hawaii detector usable part**

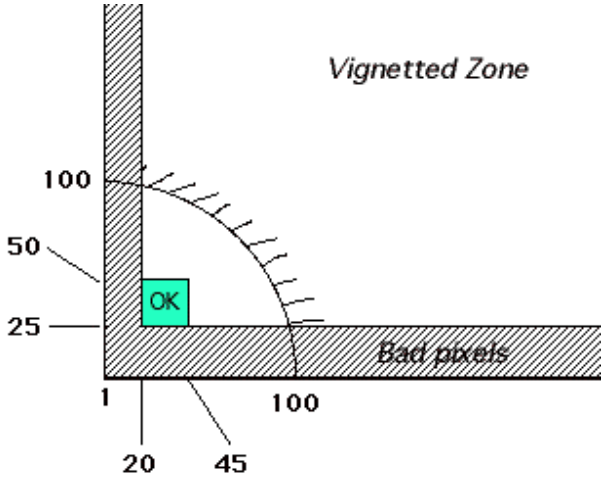


**Figure 8. Zoom on the usable part of the array.**

## 5.2 BACKGROUND LEVEL

During the tests of the detector, the background was very apparent and variable depending on the environment in a wide cone (maybe about 50 degrees angle) in front of the dewar. All the tests presented in this section were done using the full quadrant integration mode, giving an **exposure time of 2 seconds**. This is very long, and therefore *not really significant of the normal acquisition regime*.

A test was conducted by putting a soldering iron 30 cm off the detector axis, and 70 cm away from the window (angle from the dewar window ~25 degrees). It was installed as a low intensity light source for the fiber. The intensity of the background on the detector shows clearly the temperature variations of the soldering iron due to the temperature regulation loop (Figure 9). For all the tests (except when mentioned otherwise), the K band filter (green in aspect) was put in front of the detector.

Even after shutting off all the lights in the room, the background level on the detector is still very high, causing the saturation of the detector even with a very faint additional light source.

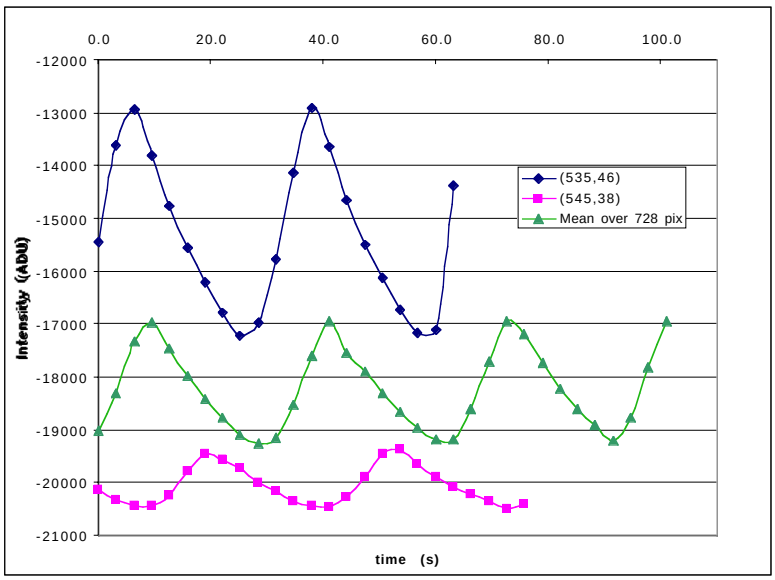

**Figure 9. Variation of the background due to stray light from a soldering iron about 25 degrees off axis. The curves correspond to three different test sequences.**

Tests have also been conducted with the soldering iron hidden from direct view to the detector by a metal piece, but the variations are still very visible (several thousand ADUs), due to reflections on the laboratory walls and other optical elements.

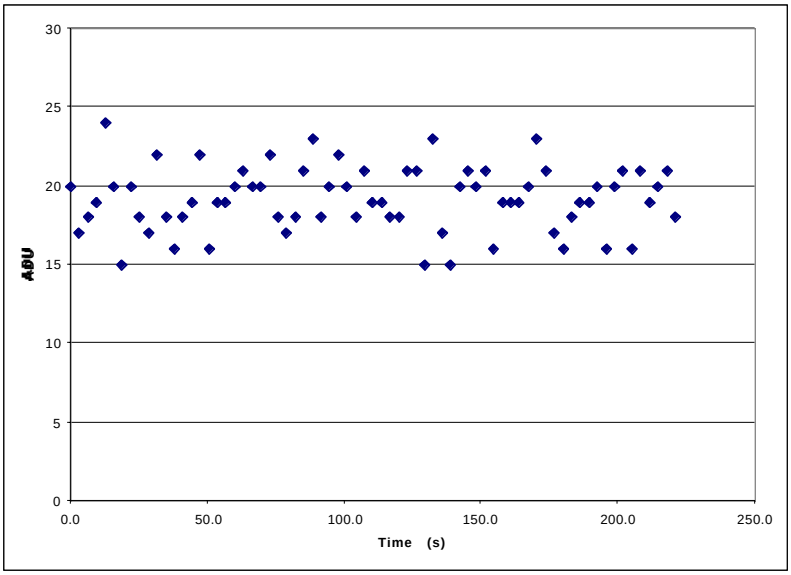


**Figure 10. Background with cold shutter closed (Mean = 19.28, RMS = 2.07 ADUs) .**

When the cold shutter is closed the variations of the background signal are inexistent, as visible on Figure 10. This shows that the baffling defect takes place optically between the dewar window and the filter wheel.

These tests show that the background is as computed in the study phase of the camera at about **40000 e-/s/pixel**. The solution to reduce this background would be to add a cold stop in front of the doublet lens. Currently, only the filter wheel is playing the role of an imperfect cold stop. Though, it is expected that the short exposure times will not suffer from this background.

A picture of the LISA cold mechanics is presented on Figure 11 and Figure 12. They show the cold mechanics down to the detector support. A possible location for an additional cold stop would be close to the black part on the left of Figure 11.

As a conclusion, the addition of a cold stop is not absolutely required for now, but would be an important plus to the current design. It will be mandatory for an upgrade of the camera to a lower readout noise detector.

**Figure 11. LISA cold mechanics and baffling, seen from the front (photo MPE).**

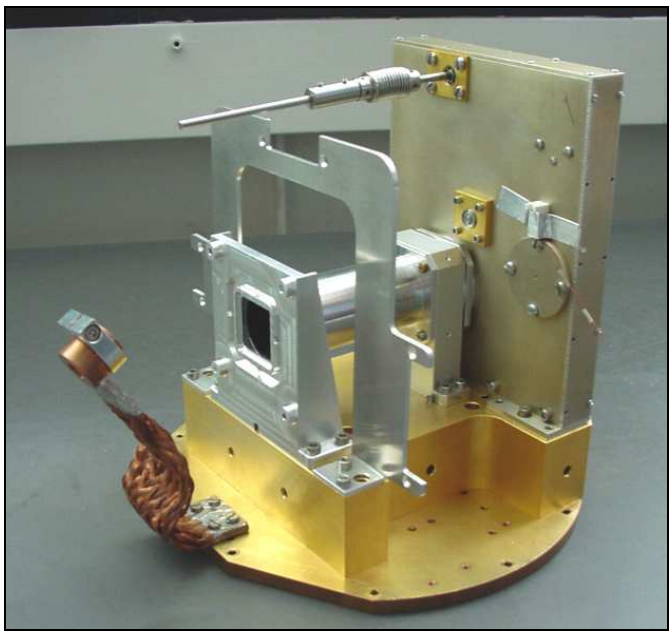

**Figure 12. LISA detector support and baffling, seen from the back (photo MPE).**

## 5.3 DETECTOR READOUT NOISE IN FULL FRAME MODE

All the measurements described below are done in **double correlated readout mode**, which is the one used for the scientific observations.

### 5.3.1 Aproximate gain factor

The gain factor is computed from the slope of the Signal vs. Noise curve. It is expressed in ADU/electron. The measurements were done in full quadrant, double correlated readout mode. The light source used was simply the background light (it is nearly saturating the detector, see section 5.2 for discussion). The intensity was varied by (very) slightly opening the cold shutter in front of the doublet lens. Temporal series of a few tens of values were obtained for each light level.

The gain is given by the inverse square root of the slope of the linear fit (shown on Figure 13):

g ~ 2.9 electrons/ADU.

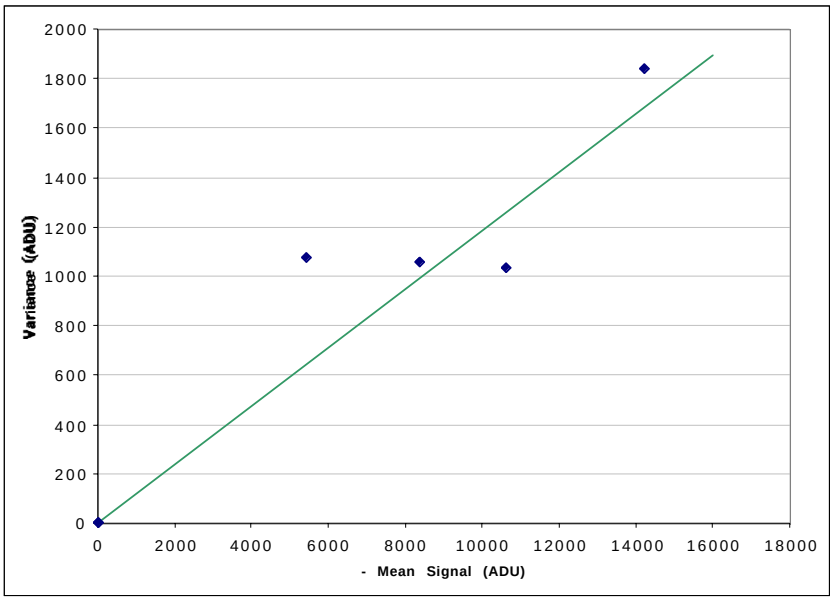


**Figure 13. Variance as a function of signal for LISA. The slope is 0.1182, giving a gain factor of 2.9 electrons/ADU. X axis is the mean signal in ADU. Y axis is the observed variance of the temporal sequence in ADU$^2$.**

The overall distribution of the points on the curve may not be linear. It seems that a plateau occurs at least from -4000 to -12000 ADUs. This point will be checked more thoroughly in the 64x64 and windowed readout modes (fast readout). Please see Section 7 for a much more precise study.

### 5.3.2 Readout noise in full quadrant mode (512x512 pixels)

The shutter being closed, a time sequence of pixel values is acquired. The graph presented on Figure 10 shows that the signal mean value is 19.18 ADU (inverted scale in double correlated mode: the higher values values are negative), and the standard deviation is 2.06 ADU. Using the gain factor computed in section 5.3.1, the resulting read-out noise in double correlated mode is ~ 6 electrons.

This value is a very rough first estimate of the effective readout noise of the array. Please refer to Section 0 for precise measurements.

## 5.4 READOUT MODES

### 5.4.1 List of modes

The useful modes for the camera operation are listed in the following table. They include the possibility to switch from one windowed readout mode to another, to adapt the size of the read windows to the brightness of the star for example. This list is likely to be updated.

**Table 4. LISA readout modes**

| |
|---|
| Uncorrelated, 512x512 pixels |
| Double Correlated, 512x512 pixels |
| Uncorrelated, 64x64 pixels |
| Double correlated, 64x64 pixels |
| Double correlated, 4 windows of 1x1 pixel |
| Double correlated, 4 windows of 2x2 pixels |
| Double correlated, 4 windows of 3x3 pixels |

### 5.4.2 Off-line windows generator

In order to define the windows for the Beam readout mode (four windows), an off-line generator was delivered by MPE. This tool is especially useful during the commissioning and test phases. The clock pattern files generated contain some syntax errors, and require some manual correction to work properly.

### 5.4.3 Full quadrant, double correlated

The readout in full quadrant mode worked properly during the tests. The intensity values follow a negative scale. The minimum exposure time is a bit more than 2 seconds, due to the intrinsic readout speed limitations of the detector.

Three dark quadrants are displayed by the Infrared Real Time Display (IRTD), in addition to the useful quadrant. This is a bit confusing, and should be corrected.

### 5.4.4 64x64 window, double correlated

Tis readout mode works properly once the window dimensions are selected. The options to activate on the control panel are the following, to read the lower-left corner 64x64 window:

1. HW-window selected (green)
2. StartX: 1 NX: 128
3. StartY: 1 NY: 128

The readout frequency is much higher in this mode than in full quadrant mode (see section 6).

The display on the Infrared Real Time Display (IRTD) is correct, but presents the same three dark quadrants as in the full quadrant readout mode.

### 5.4.5 Windowed readout, double correlated

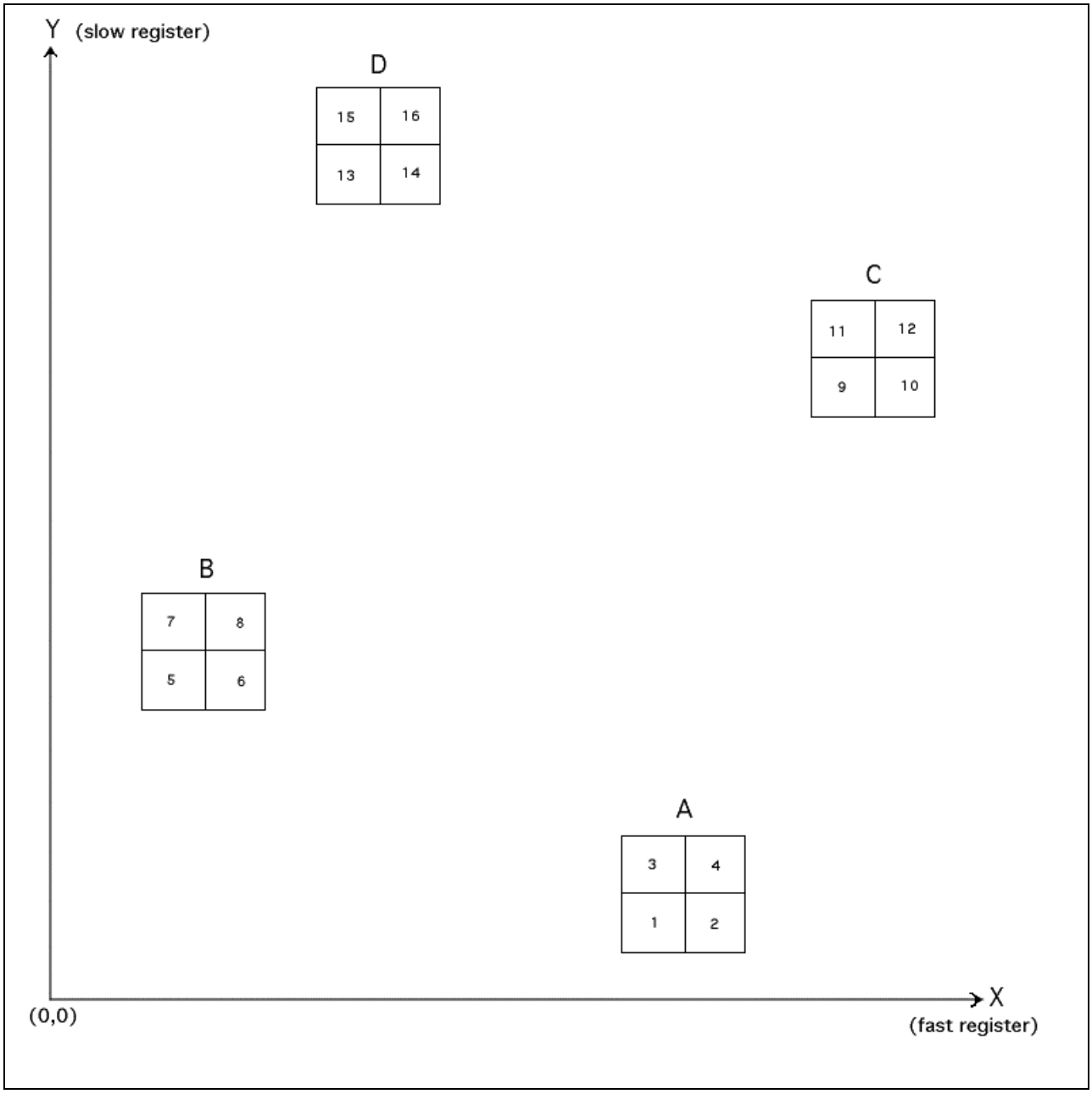


**Figure 14. LISA windowed mode readout order.**

The order of the data in the IRTD and in the data file is presented in the following sections.

5.4.5.1 Beampix data

During the tests of the windowed readout mode (four beams each of 2x2 pixels), the system behaved correctly, showing the intensity of the light in the 16 pixels at the first and second reads of the detector (32 data points). The waterfall display on the IRTD was correct. To ascertain that the correct pixels were listed at the correct positions, the fiber spot was moved from one pixel to the other in the same window (fourth window).The pixel showing the spot was always correct in the Beampix data submode.

The order in which the data is output is the following, using the naming convention of the Figure 14, with [A2,2] meaning the second read of the A2 pixel:

```
[A1,1] [A1,2] [A2,1] [A2,2] [A3,1] [A3,2] [A4,1] [A4,2] [B5,1] [B5,2] [B6,1] [B6,2]…
```

On the IRTD, these values are displayed as a temporal sequence starting from the bottom of the screen to the top, in a kind of “reversed waterfall” display.

To obtain the fluxes in ADU (positive sign) for example on pixel A1:

```
Flux A1 = [A1,1] – [A1,2]
```

The actual fluxes from the DCS are computed using this formula, and therefore have the correct sign.

#### 5.4.5.2 Flux data

In this data submode, the fluxes in each of the four windows (first read minus second read to give a positive value) is summed to give one value per window. The result is a series of four numbers, plus two additional numbers containing the total flux in all windows and TBC. The display in the RTD shows the following values (as displayed on the screen):

| **Line #** | **Name** | **Order** |
|---|---|---|
| 6 | [?] | O(t1) O(t2) O(t3)… |
| 5 | [Total flux] | F(t1) F(t2) F(t3)… |
| 4 | [Flux beam D] | D(t1) D(t2) D(t3)… |
| 3 | [Flux beam C] | C(t1) C(t2) C(t3)… |
| 2 | [Flux beam B] | B(t1) B(t2) B(t3)… |
| 1 | [Flux beam A] | A(t1) A(t2) A(t3)… |

#### 5.4.5.3 Quicklook data

A vector containing the processed scans (TBC) is also produced. In the tests we have conducted, the quicklook algorithm was not implemented, and therefore the data produced was not meaningful.

# 6. READOUT FREQUENCIES

## 6.1 INTRODUCTION

The readout of the camera in double correlated mode is based on five steps:

1. Reset of the four windows
2. Optional wait time
3. First readout of the four windows
4. Exposure time
5. Second readout of the four windows

The execution of these five steps produces two numbers for each pixel corresponding to the first and second reads. Both numbers are accessible in the Beampix data submode for each pixel of each window. In the Flux output mode, the fluxes are summed over each window. The order of the pixels in the data output from the camera is explained in section 5.4.5.

The minimum exposure time *Min DIT* is computed automatically, and displayed on the control panel. This minimum time corresponds to the time needed to complete a single scan, with the specified number of frames. It does not include the overhead time necessary to compute the delay line offset, and therefore it is strictly the time necessary to acquire one frame multiplied by the number of frames. From this number, it is easy to compute the effective frame frequency through:

Frequency = [Number of Frames in Scan] / [Min DIT]

## 6.2 EFFECTIVE MAXIMAL READOUT FREQUENCIES

The maximal frequency reachable by the detector depends on the position of the four windows on the detector and on their size. The smaller and the closer to the lower left corner, the faster the readout. The selected pixel windows for the windowed readout tests were centered (for the 1x1 or 3x3 pixels) or had their lower left corner (for the 2x2 pixels windows) on the pixels **[29,26], [25,34], [33,38], [37,30]**. The distance between these pixels was chosen to be 9 pixels, to mimic as much as possible the behavior of the real spots readouts.

**Table 5. Maximum readout frequencies for LISA**

| Mode | Maximal frequency (Hz) |
|---|---|
| 4 windows 1x1 pixel each | 2545 |
| 4 windows 2x2 pixels each | 1656 |
| 4 windows 3x3 pixels each | 1062 |
| 64x64 double correlated | 28.6 |
| 64x64 uncorrelated | 54.1 |
| 512x512 double correlated | 0.48 |
| 512x512 uncorrelated | 0.95 |

The maximum frequency reachable with the 1x1 pixel mode is better than 2.5 kHz, therefore fulfilling the requirements stated in the 'LISA Technical Specifications' document.

For information, the pixel readout rate in 64x64 mode was 117 kHz. This means that 4 windows of 1x1 pixel located in the lower left corner of the array ([0,0] [0,1] [1,1] [1,0]) could theoretically be read at a maximum frame rate of 29 KHz.

# 7. BEST PHOTOSITES SELECTION

## 7.1 PRINCIPLE

To select the best possible photosites for the light detection, it is necessary in principle to measure the noise level of all the pixels in the frequency range used by the DCS. The detector useful readout frequency range is about 2 - 2000 Hz.

It is possible to use the special 64x64 readout mode of LISA to have a sampling rate of about 30 Hz on every pixel in the selected window, in double correlated mode. It is reasonable to assume that the noise level of the LISA camera does not depend on the readout frequency of the detector (this assumption was checked a posteriori and is valid). The selection can therefore be done in two steps:

1) first construct a map of the lower left corner 64x64 region indicating the bad and noisy pixels. Using the 64x64 readout mode gives access to the power spectral density up to a frequency of 14.3 Hz.

2) do a finer selection of the best pixels in this area, by acquiring a series of scans at the highest possible frequency. In this case, the maximum reachable frequency in the power spectral density can be of more than 1000 Hz.

For these tests, the data was acquired using the control panel of the camera, and saved into standard FITS format data files. The data processing was done using the IDL software (including the ASTRON package).

## 7.2 PIXEL GAINS

### 7.2.1 Measurement procedure

To obtain the values of the gains for all the pixels, the detector was exposed to an increasing light level by opening slightly the cold shutter. Cubes of 500 frames of 64x64 pixels were recorded (150 ms exposure time), of which 256 were processed (adequate number for fast Fourier transform computation). This test was conducted at seven different light levels, of which six were kept for processing (the seventh contained some saturated pixels).

$$\sigma^2_{total} = \sigma^2_{photons} + \sigma^2_{RON}$$
$$= \frac{S_{ADU}}{G} + \sigma^2_{RON} \approx \frac{S_{ADU}}{G}$$

The gain was estimated as the inverse of the slope of the linear regression of the Variance = f(Signal) curve.

All the processing was done using IDL. The listing of the procedures is included in the Appendix.

### 7.2.2 Examples of gain curves

The following curves show the fits achieved for three typical pixels.

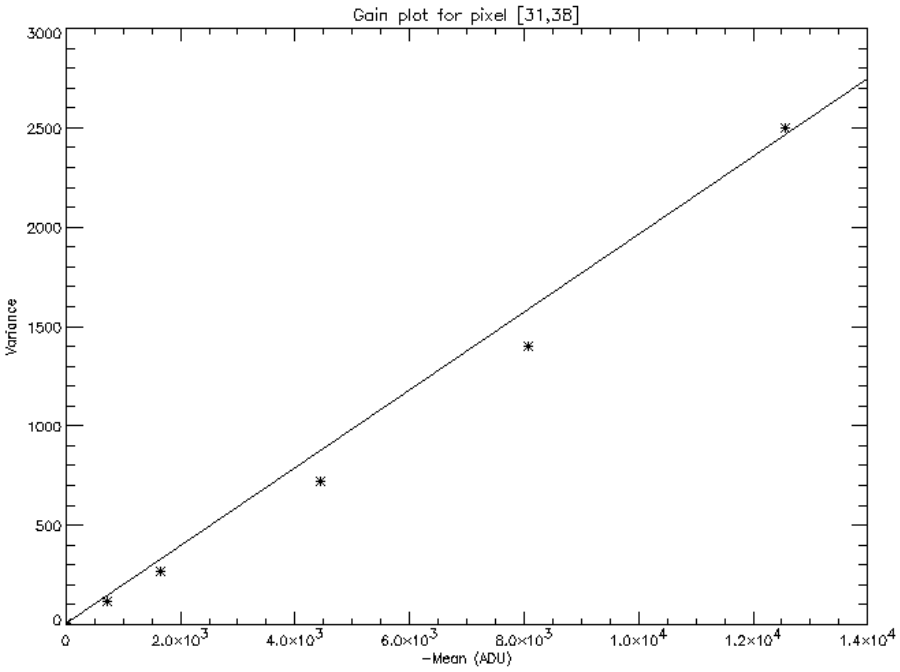


**Figure 15. Gain plot for pixel [31,38] (G=5.1096)**

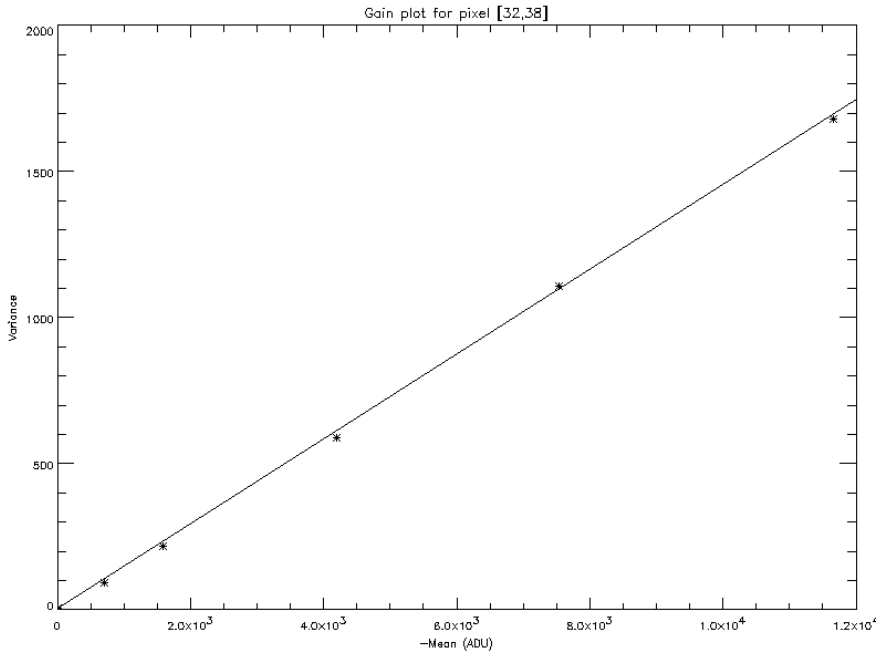


**Figure 16. Gain plot for pixel [32,38] (G=6.8939)**

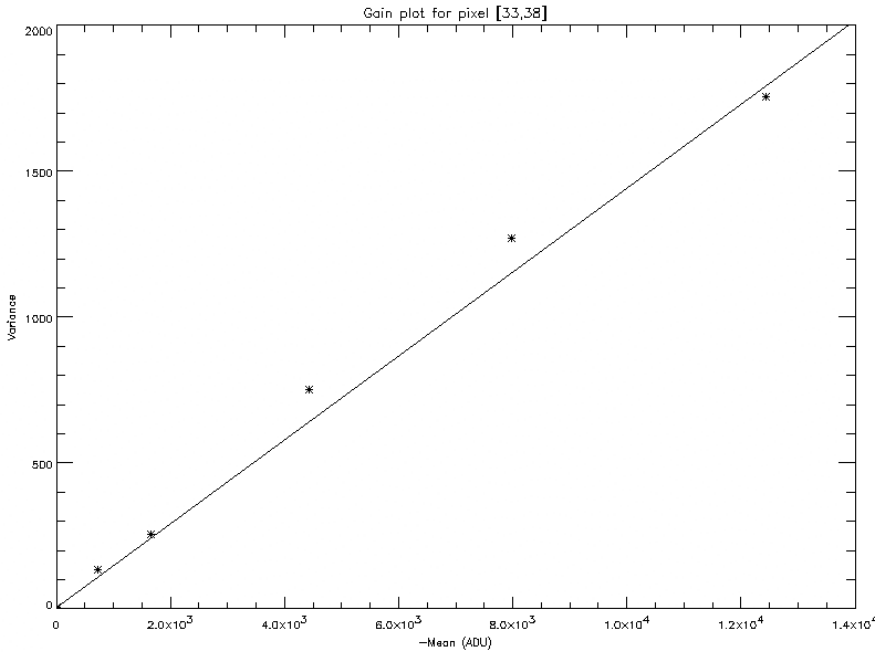


**Figure 17. Gain plot for pixel [33,38]. (G=6.9652)**

### 7.2.3 Gain map

The gains are available numerically for all the pixels in the lower left 64x64 area of the detector. Figure 18 shows a graphical plot of the gains over the array (linear scale). Typical values are between 5 and 10.

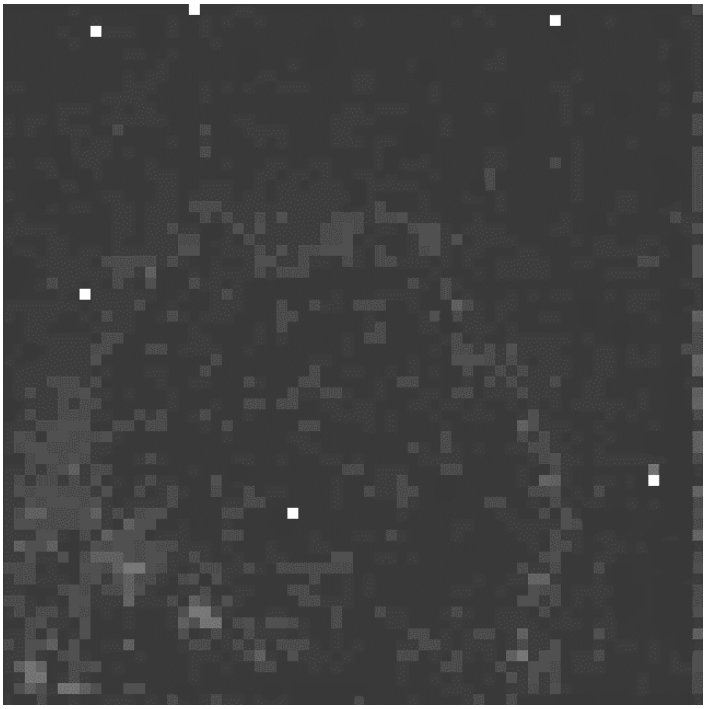

**Figure 18. Gain map over the 64x64 pixels lower left area. Pixel [0,0] is in the lower left corner, X axis is to directed the right, Y to the top.**

### 7.2.4 Histogram of pixel gains

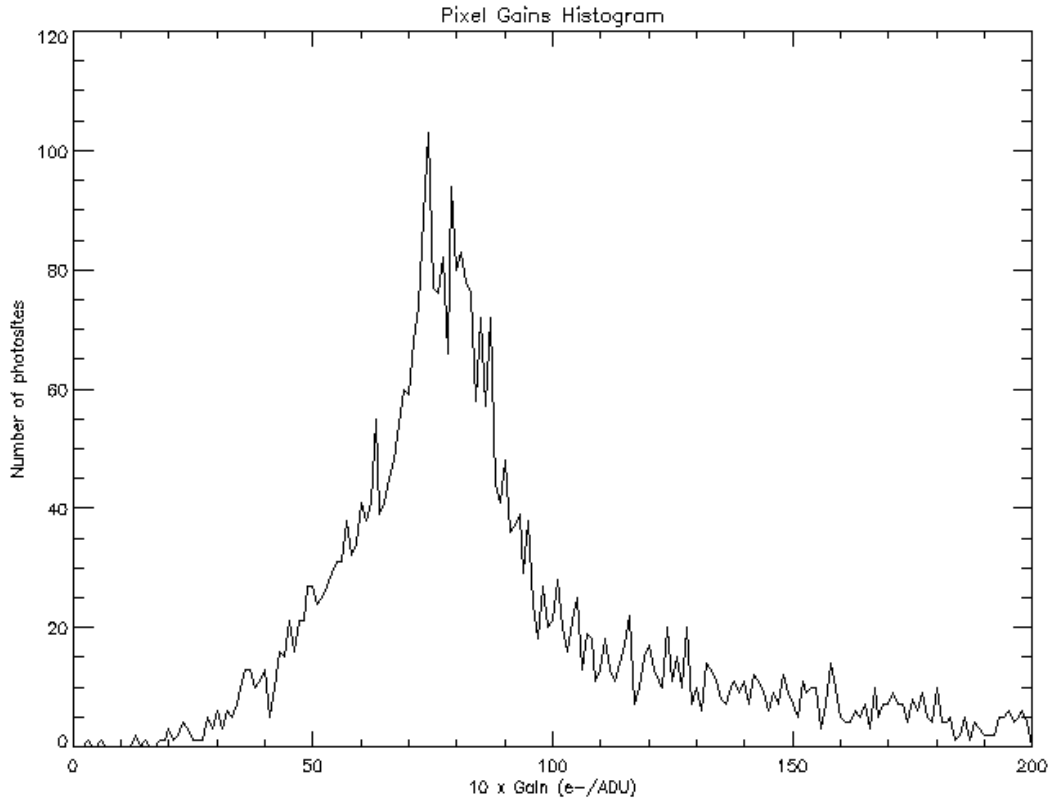


**Figure 19. Histogram of the 64x64 lower left pixels gains (measured at 6.66 Hz frame frequency).**

## 7.3 PIXEL READOUT NOISES

### 7.3.1 Measurement procedure

The readout noise RON is easily computed from the standard deviation of the noise sigma(N) in ADU at zero light level (cold shutter closed) and the gain G in electrons/ADU through the formula:

$$RON = sigma(N) \times G$$

sigma(N) is directly the time sequences standard deviation (obtained with the cold shutter closed), and G is already known for each pixel from the previous measurement.

### 7.3.2 Readout noise map

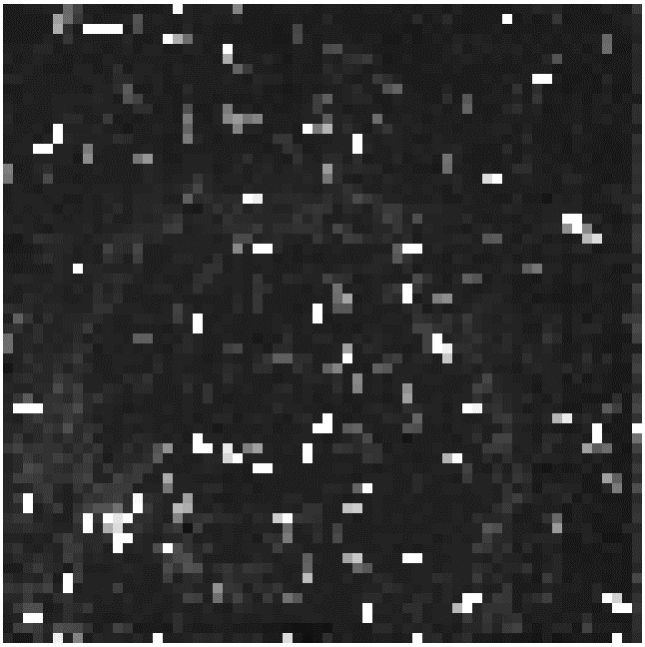

**Figure 20. Readout noise map of the lower left 64x64 area, at 6.66 Hz frame frequency. The image grey scale is linear between 0 and 30 electrons.**

### 7.3.3 Histogram of pixel readout noises

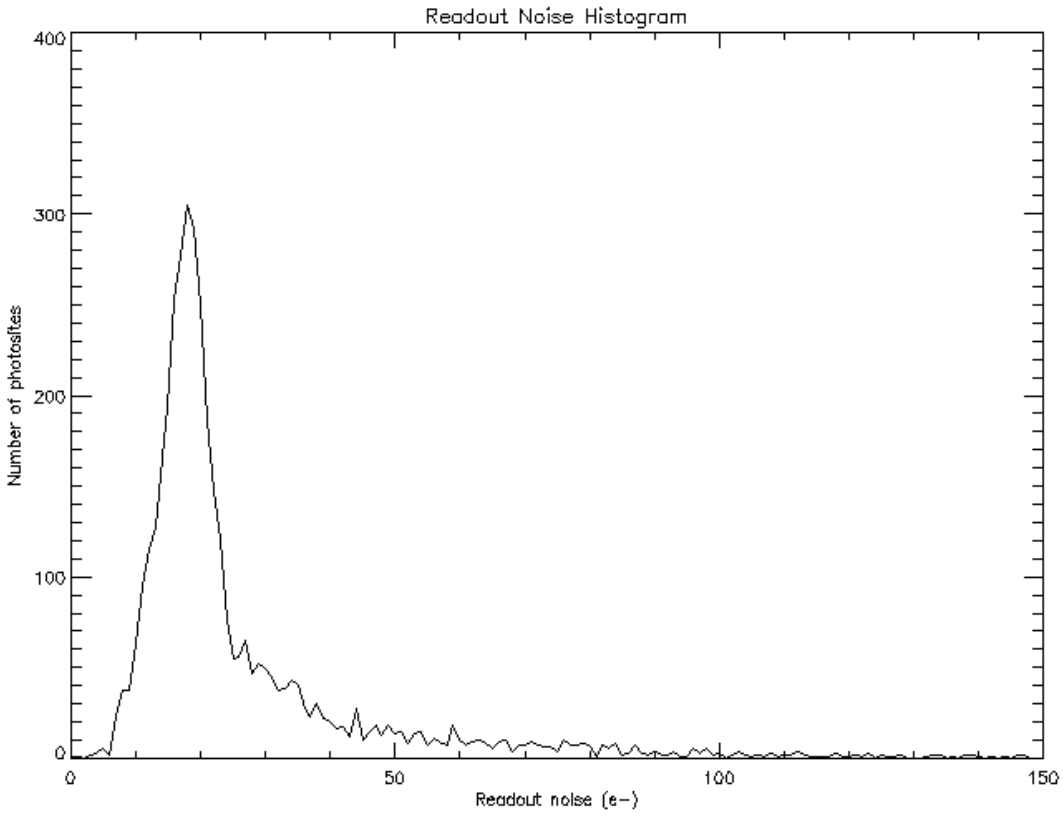


**Figure 21. Histogram of pixel readout noises at 6.66 Hz frame frequency. The median value is 20.18 e-, and the maximum number of pixels is found at 18 e-. There are still a number of pixels at less than 15 e-.**

The pixel [33,38] has a readout noise of **17.76 electrons**. There is an indication that the readout noise varied with the frequency, being lower for higher frame rates (see next section).

#### 7.3.4 Readout noise at the highest frame frequency

A series of scans was acquired at the highest possible frequency for four 1x1 pixels windows, with the cold shutter closed. The readout noise from this data was found to be **12.24 electrons** (assuming a constant gain of 6.9652 e-/ADU).

Compared to the **17.76 electrons** value obtained for the same pixel at 6.66 Hz frame rate, it seems that the readout noise is significantly lower (30%) when acquiring at a higher frequency.

| **The reason for this behavior is ???** |
|---|

### 7.4 PIXEL NOISE POWER SPECTRAL DENSITY

The second step in the photosites selection is to evaluate the “color” of the noise, i.e. the absence of power peaks at certain frequencies that would betray the incorrect behavior of the detector noise.

### 7.4.1 Low frequency (0–3.33 Hz)

7.4.1.1 Data analysed

For the low frequency evaluation, the power spectral density (PSD) was computed for all the pixels up to the Nyquist frequency of 6.66 / 2 = 3.33 Hz. This frequency is half of the inverse of a single 64x64 frame exposure time. The power spectral density was computed simply as the squared modulus of the fast Fourier transform along the time sequence axis for each pixel in the temporal data cube (64x64x256).

7.4.1.2 Examples of individual pixels PSD

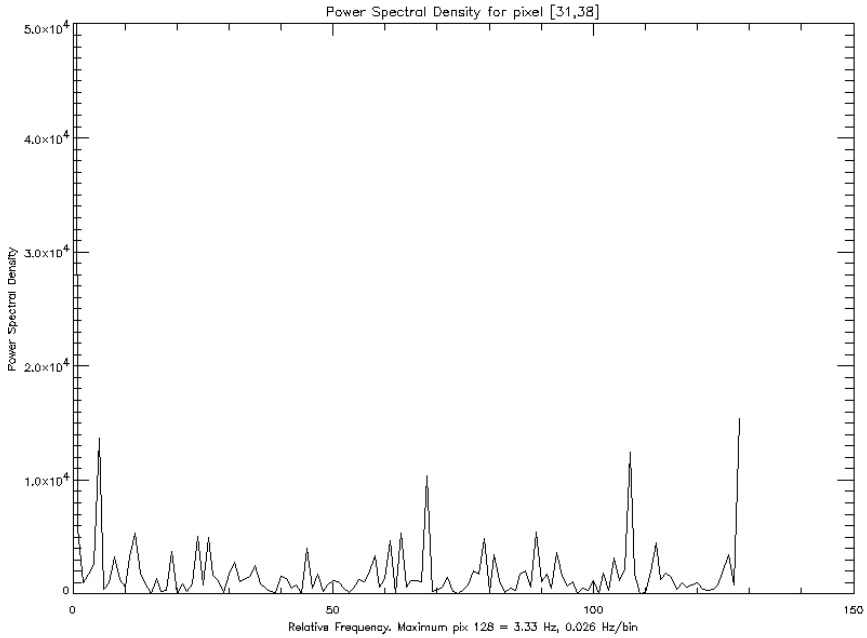


**Figure 22. Power spectral density for pixel [31,38] from 0 to 3.33 Hz (X=128). Y scale arbitrary.**

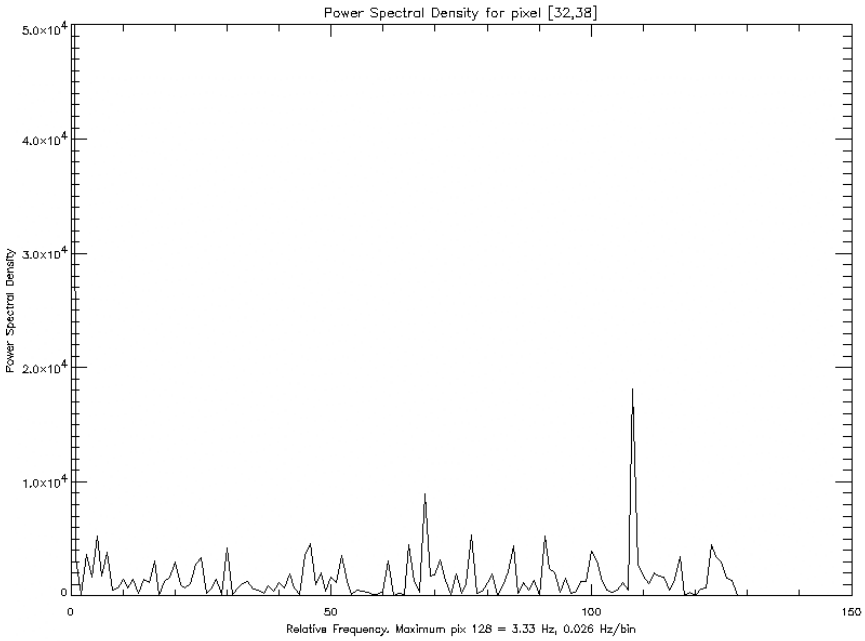


**Figure 23. PSD for pixel [32,38] from 0 to 3.33 Hz (X=128). Y scale arbitrary.**

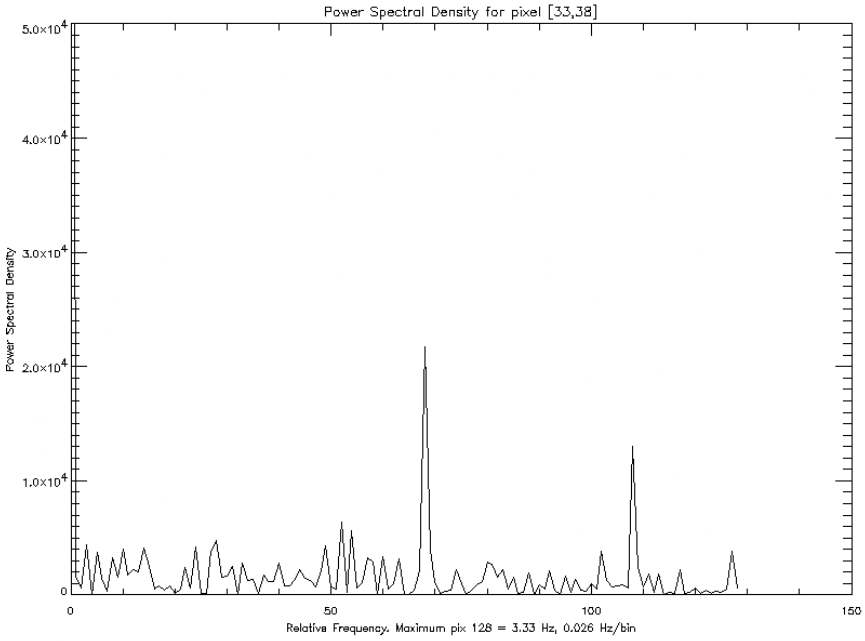


**Figure 24. PSD for pixel [33,38] from 0 to 3.33 Hz (X=128). Y scale arbitrary.**

7.4.1.3 Median low frequency PSD over the 64x64 pixels

Figure 25 shows the median PSD obtained over the 64x64 pixels area. Two peaks are clearly visible, but the very low frequency of these peaks make them not very problematic for the detection of the interference fringes (which frequency is usually set to about 100Hz).

When using LdV with a fringe tracker, it will be necessary to decrease the fringe frequency down to very low values for faint objects, possibly interfering with these peaks. In this case they could become an important problem.

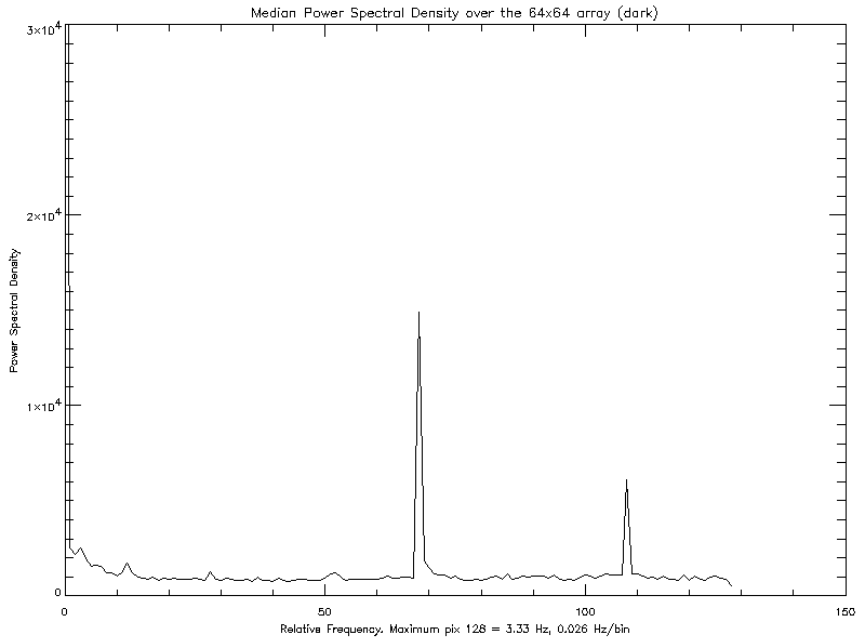


**Figure 25. Median Power Spectral Density for the 64x64 pixels, from 0 to 3.33 Hz (X=128). The Y scale is arbitrary.**

### 7.4.2 High frequency (0–828 Hz)

7.4.2.1 Data analysed

This second type of measurements is done using the windowed readout mode of LISA. This is necessary because the readout frequency of the camera in the 64x64 pixels mode is limited to less than 30 Hz, which is too low for the study of the behavior of the detector at the frequencies used for the detection of the fringes.

The windows used were 2x2 pixels in size, giving 16 pixels. For each pixel, a series of 20 scans of each 1024 frames was analysed. The frame frequency was set to the maximum possible value (at the selected configuration, see Section 6 for details), e.g. 1656 Hz. Therefore, the frequencies investigated by computing the PSD of the sequences were in the range 0-828 Hz.

7.4.2.2 Example of pixel [33,38]

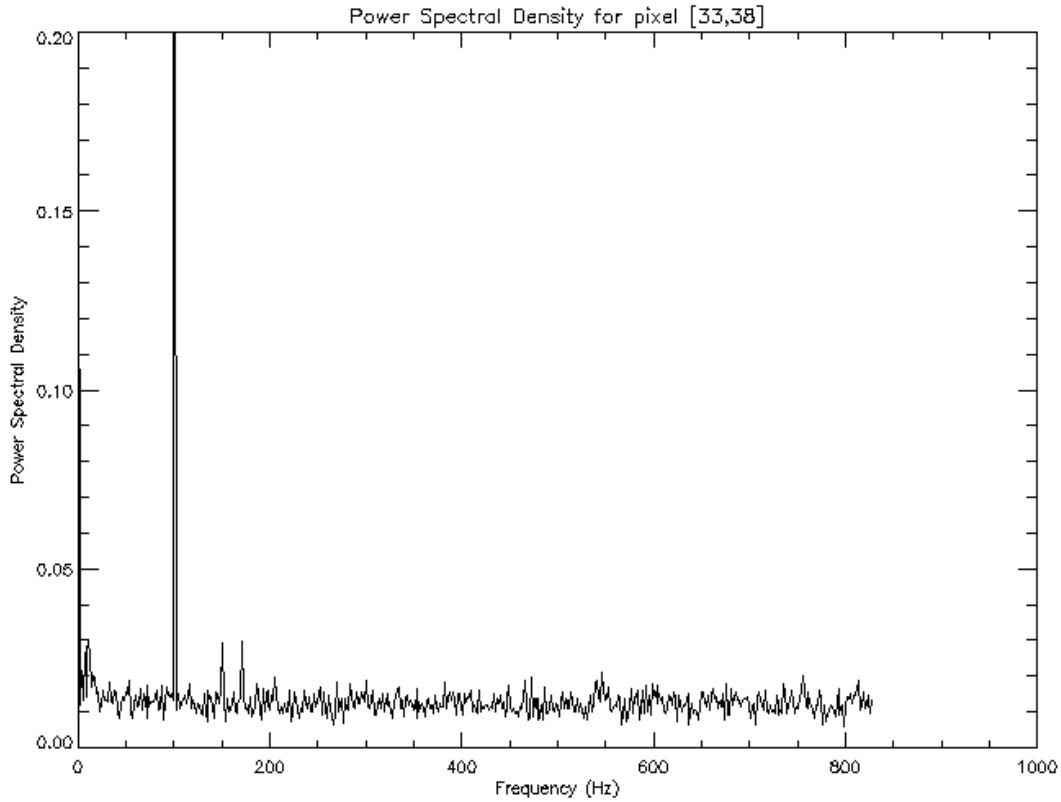


**Figure 26. Overview of the PSD for pixel [33,38] read at 1656 Hz frame rate (frequencies between 0 and 828 Hz). The shutter was open (background light present), but the fiber spot was not illuminated. The large peak on the left is precisely in the bin containing the 100 Hz frequency. (mean over 20 scans).**

### 7.4.3 Maximum frequency (0–1223 Hz)

7.4.3.1 Data analysed

This measurement is done using the windowed readout mode of LISA. The windows used were 1x1 pixel in size, giving 4 pixels. For each pixel, a series of 20 scans of each 1024 frames was analysed. The frame frequency was set to the maximum possible value (at the selected configuration, see Section 6 for details), e.g. 2545 Hz. Therefore, the frequencies investigated by computing the PSD of the sequences were in the range 0-1223 Hz.

7.4.3.2 Example of pixel [33,38]

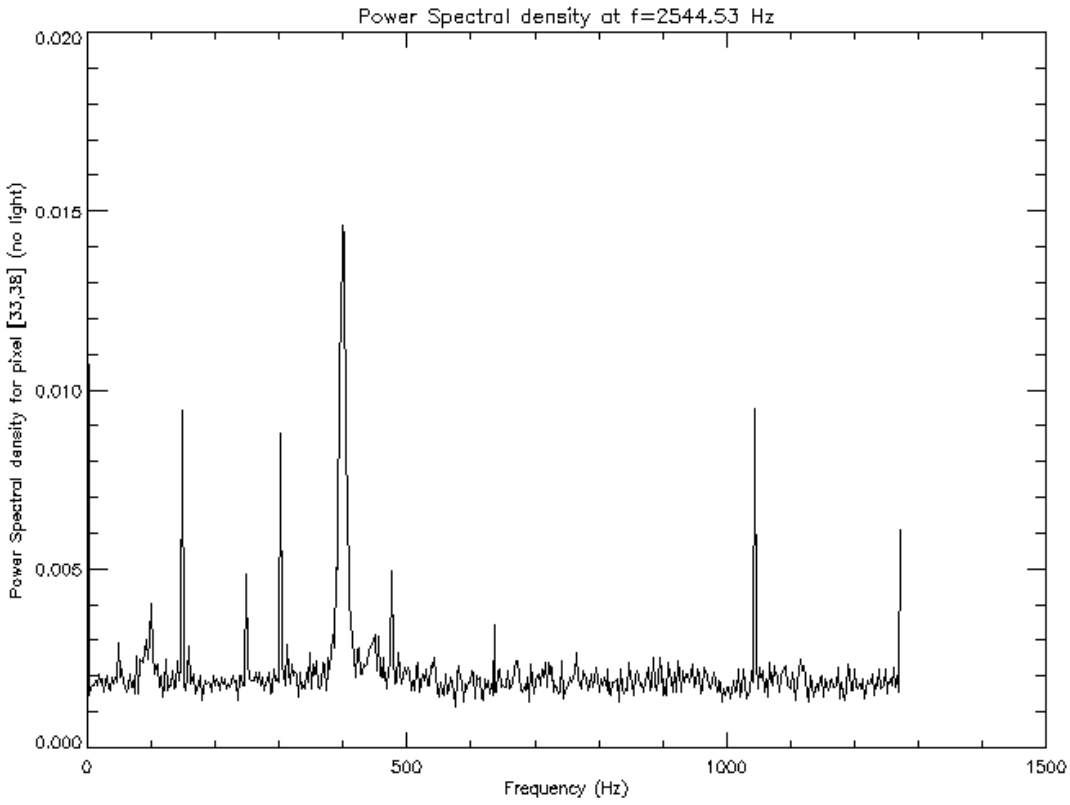


**Figure 27. Power spectral density at maximum acquisition frequency for pixel [33,38], with cold shutter closed. Notice the overall very low level compared to the previous case (1656 Hz frequency). Ths frequencies of the peaks are mostly multiples of 50 Hz, therefore suspected to be associated with power supply pickups (grounding problems ?).**

## 7.5 DISCUSSION

A strong peak is visible precisely at 100 Hz on the 1656 Hz data, and several smaller peaks are visible on the 2544.5 Hz data. The presence of this peak is difficult to explain. This could be a pickup of the electric power distribution (?).

Otherwise, the noise is very clean (“white”), showing no particular increase with the frequency.

# 8. INDIUM LAYER STABILITY

The array used in LISA is an engineering grade detector and suffers from dead pixels at the external edges of the array. This is caused by the destruction of the indium layer connecting the photosites. The evolution of this defect has to be followed carefully, as it may evolve after each cooling of the camera.

The procedure is simply to save an full frame image produced by the array after cooling it down. The detection of possible dead pixels can be done by subtracting the images obtained from a reference image, and by adjusting the display levels to check for the pixels having no evolution between the two frames (no noise associated with them).

During the tests of the camera, a series of images of the full 512x512 quadrant have been saved for future reference. No obvious variation of the dead pixels positions have been observed visually during the tests.

# 9. MEMORY EFFECT

## 9.1 DESCRIPTION

As stated in the LISA User's Manual, the Hawaii detector may be subject to a memory effect, which could affect the visibility measurements and even the observational procedure.

The symptom of the detector memory is that after a bright illumination of the photosite (causing or not a saturation of the pixel), a residual signal is kept for a while and affects the readouts for the following cycles.

Three kinds of behaviors are tested:

- **Minute timescale**: Saturation of the detector followed by closure of the cold shutter. This test ensure that the array does not need a rest time between a bright source and a faint source observation. The effect of the saturation should disappear completely in a short time. The tests were not conducted on the LISA camera, but measurements have already been obtained by Gert Finger on the HAWAII detector. His measurements show that the signal intensity is divided by 100 in 150 seconds.

- **Millisecond timescale**: Array response to a chopped signal stimulus cut very quickly to zero (in less than 1 integration time). This measurement makes it possible to evaluate if the fringe visibility could be degraded by a memory effect of the detector. The only delicate point in this test is that the shut-off of the light intensity has to be very fast. This is achieved easily by masking quickly the fiber head with an opaque material on the light injection side. The very small diameter of the fiber core allow to achieve sub millisecond closing times. A chopping device was used for that purpose.

## 9.2 MEASUREMENT PROCEDURE

◊ Align the light source in order to have a good quality, point-like source on the detector.

◊ Adjust the intensity of the light source to obtain an intensity on the detector just below saturation.

◊ Close the cold mask of the detector for a while, in order to avoid contamination by a possible long-term memory effect.

◊ Open the cold mask and select the K band filter.

◊ Start the chopper wheel, in front of the fiber injection.

◊ Start the data acquisition at the maximum data rate on a four windows set containing the illuminated pixel.

◊ Acquire two sets of data shutter open and shutter closed to have the top and bottom levels.

## 9.3 GEOMETRY OF THE CHOPPING SYSTEM

The geometry of the chopping system determines the shape of the input signal sent to the camera. Figure 28 shows the geometrical configuration of the chopper used to modulate the signal sent to the camera. This system is installed at the **injection** side of the artificial light source. This allows to have a sharper cutting of the beam than in the collimated part after the off-axis parabola.

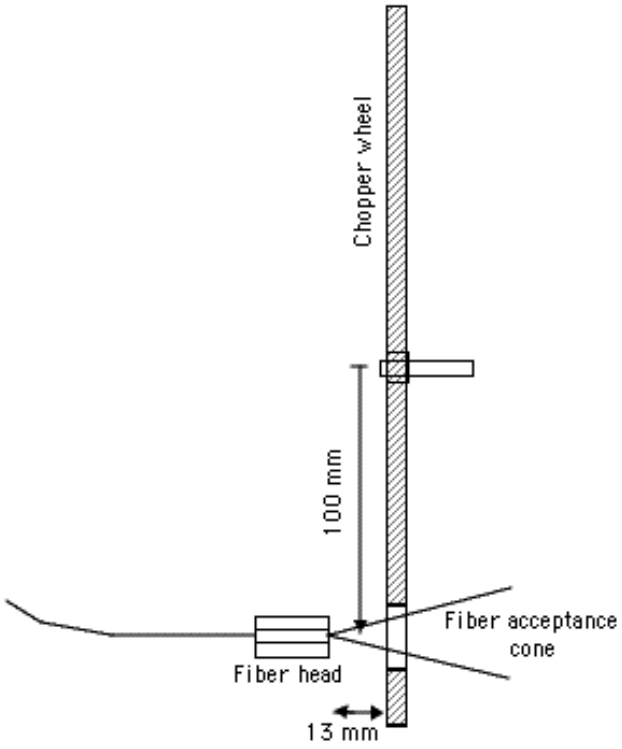


**Figure 28. Chopper geometrical configuration.**

The chopping frequency, as measured on the detector, is 22.7 pixels at the highest frequency of 2544.53 Hz. This corresponds to a chopping frequency of 2544.53/22.7 = **112.09 Hz**. There are 5 holes on the chopping wheel, which means that the wheel is rotating physically at $f_0$ = 22.418 Hz. The linear speed of the wheel at the radius of 100 mm corresponding to the position of the fiber head is therefore $f_0$ x 2 x *pi* x 0.1 = 14.086 m/s. The numerical aperture of the fiber is 2.8, meaning that the fiber accepted beam has a diameter of 13/2.8 = 4.6 mm at a distance of 13 mm.

The time necessary to shut completely the beam is therefore 0.0046/14.086 = **0.327 ms**.

At the 2544.53 Hz frequency, the single frame time is **0.393 ms**. This means that the beam is cut by the shutter in **0.832 frame**. We can therefore consider that the shutoff of the light is instantaneous (less than 1 pixel) and adopt a “square” input signal model.

## 9.4 DATA REDUCTION

The goal of the data reduction here if to produce a graph of the modulation transfer function of the camera, as a function of frequency, at the maximum data acquisition rate. It uses a series of IDL procedures that are listed in the appendix. The resulting curve is presented on .

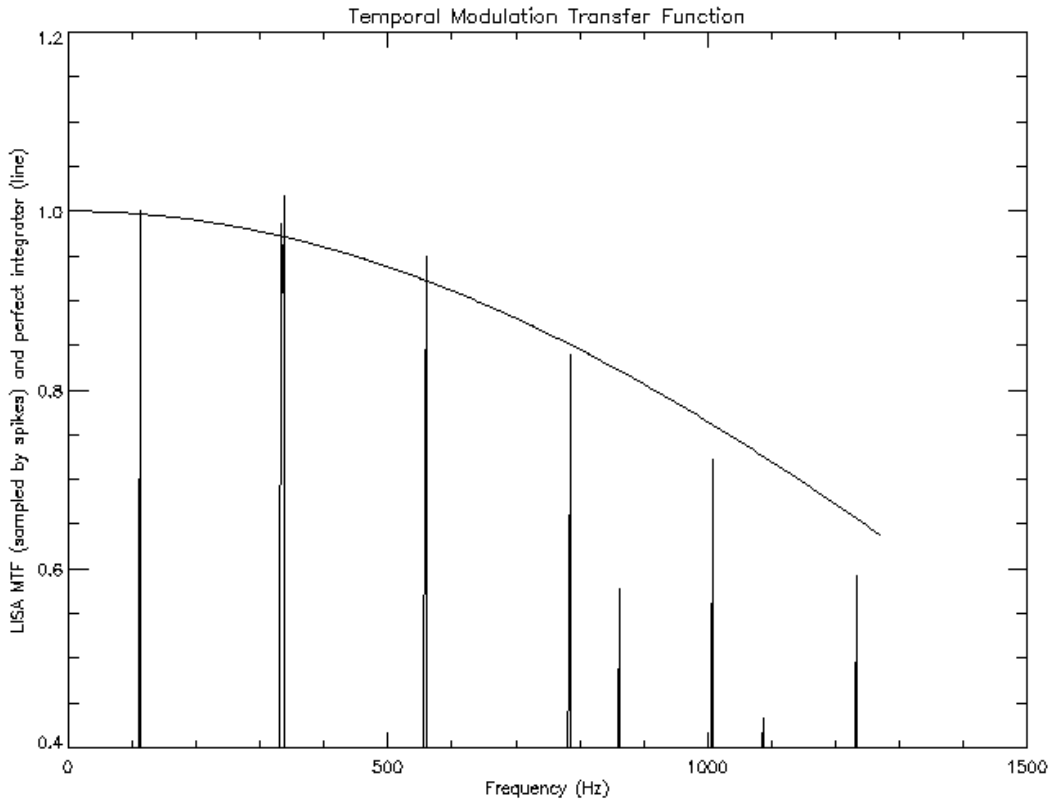


**Figure 29. Modulation transfer function of the LISA camera (spikes) compared to a perfect integrator (solid line).**

The behavior of the camera is **close to the perfect integrator** curve.

**Table 6. Modulation transfer function of LISA**

| Frequency (Hz) | Absolute MTF value | Perfect Integrator | Ratio |
|---|---|---|---|
| 111.8 | 1.001 | 0.997 | 1.004 |
| 336.7 | 0.963 | 0.971 | 0.991 |
| 561.6 | 0.948 | 0.922 | 1.028 |
| 785.2 | 0.839 | 0.851 | 0.985 |
| 1008.9 | 0.722 | 0.761 | 0.949 |
| 1232.5 | 0.592 | 0.656 | 0.902 |

## 9.5 DISCUSSION

The conslusion of this study is that **the camera response is not affected by memory effect** in a way that could disturb the detection of the interference fringes. Especially, the Modulation Transfer Function at high frequency is very close to the ideal case.

# 10. SUMMARY OF PROBLEMS

The following table lists the major problems encountered during the installation and tests of LISA in stand-alone mode in Garching. The mention "NA" (not applicable) in the "Solved" column means that the problem was not solved but is not a concern in the actual status of the camera.

**Table 7. Apparent problems in the LISA system during the tests in Garching.**

| # | Problem | Suspected Cause | Solved |
|---|---|---|---|
| **1.** | Negative values for increasing incoming flux in double correlated mode | Wrong sign in the subtraction of the two readouts for the double correlated mode. | **Yes** |
| **2.** | Filters in the filter wheel are not in the documented order | Wrong mounting of the filters | **Yes** |
| **3.** | Blurred image of the collimated light source on the detector | Incorrect focusing of the doublet relatively to the HAWAII array. | **Yes** |
| **4.** | Impossible to mount the cryogenic security device for the upper nitrogen tank | Damage to the threading on the dewar. | **NA** |
| **5.** | Insecure fastening of the camera support on the table | No briddling currently available. | **No** |
| **6.** | Very high level and variable background | Improper cold stop. | **NA** |
| **7.** | Three dark quadrants displayed together with the useful one | Data is not discarded early enough in the computer system (only for 64x64 and 512x512). | **No** |
| **8.** | Dark stripes in the widowed readout mode (missing data) | Program code problem | **Yes** |
| **9.** | First few pixels of a frame are brighter than the others | Reset before the scan (removed) | **Yes** |
| **10.** | Generation of the windows for the four beams mode is tedious | Off-line generator has bugs (see Section 5.4.2) | **No** |
| **11.** | Data content in the "flux" data mode is not correct for the two additional channels | (the four windows total fluxes are correct) | **No** |
| **12.** | Presence of a strong frequency peak in the noise at a frequency of ~ 100 Hz | Interference with electroluminescent light tubes through power supply? | **Yes (TBC)** |
| **13.** | Presence of low frequency peaks in the camera noise | Ground loops producing "waves" on the detector? | **Yes (TBC)** |

**Table 8. Points to be clarified**

| # | Question | Suggested solution | Solved |
|---|---|---|---|
| **1.** | Structure of the data produced by IRACE not clear | The DCS to IRACE SW interface document should be completed | **Yes** |
| **2.** | Possibility to save a data cube of 64x64 images for photosites selection | | **Yes** |
| **3.** | Effective exposure time and frame time are not available in the keywords | Modify dictionnary | **Yes** |
| **4.** | 3x3 windows generation and readout | Generate and check clock paterns | **Yes (still pb)** |

# 11. APPENDIX: IDL SIGNAL PROCESSING PROCEDURES

## 11.1 READ DATA

```
pro read_data, flux
;pro read_data, cube, flux
;
; Reads the test data from LISA
;
; version: 13/09/2000

;=============================================================================
;
; Reads the data cubes into the memory
;
;print, '* Data Files are being read into memory...'
;cube_0_full = mrdfits('dark_1_DIT.fits',0)
;cube_700_full = mrdfits('level_700_1_DIT.fits',0)
;cube_1800_full = mrdfits('level_1800_1_DIT.fits',0)
;cube_4400_full = mrdfits('level_4400_1_DIT.fits',0)
;cube_9000_full = mrdfits('level_9000_1_DIT.fits',0)
;cube_14000_full = mrdfits('level_14000_1_DIT.fits',0)
;cube_20000_full = mrdfits('level_20000_1_DIT.fits',0)

;=============================================================================
; Extracts the lower right corner of the data, and keeps only 256 points
; to compute the Fourier transform faster.
;
;cube = intarr(7,64,64,256)
;print, '* Extracting the useful data (64x64x256)...
;print, '   -> Cube 0'
;cube(0,0:63,0:63,0:255) = cube_0_full(64:127,0:63,0:255)
;print, '   -> Cube 1'
;cube(1,0:63,0:63,0:255) = cube_700_full(64:127,0:63,0:255)
;print, '   -> Cube 2'
;cube(2,0:63,0:63,0:255) = cube_1800_full(64:127,0:63,0:255)
;print, '   -> Cube 3'
;cube(3,0:63,0:63,0:255) = cube_4400_full(64:127,0:63,0:255)
;print, '   -> Cube 4'
;cube(4,0:63,0:63,0:255) = cube_9000_full(64:127,0:63,0:255)
;print, '   -> Cube 5'
;cube(5,0:63,0:63,0:255) = cube_14000_full(64:127,0:63,0:255)
;print, '   -> Cube 6'
;cube(6,0:63,0:63,0:255) = cube_20000_full(64:127,0:63,0:255)

;=============================================================================
; Reads the scan records
; The beampix data gives the two values for the two reads of the double
; correlated readout mode.
; The order of the data in the 'scan' variable is the following:
; first axis : readouts for one frame
; second axis : frame sequence
; third axis : scan sequence

scan = mrdfits('scan_mini_fiber_off_1_BeamPix.fits',0)

;
; Computes the fluxes for each pixel
;
n_pix = n_elements(scan(*,0,0))/2
n_frames = n_elements(scan(0,*,0))
n_scans = n_elements(scan(0,0,*))
flux = intarr(n_pix,n_frames,n_scans)
```

```
for pix=0,(n_pix-1) do begin
        flux(pix,*,*) = scan(2*pix,*,*) - scan(2*pix+1,*,*)
endfor

end
```

## 11.2 PROCESS 64X64 DATA

```
pro process_64, cube, means, variances, gain, readout_noise, fourier, psd, median_psd,
mean_psd_per_pix, median_RON, median_gain
; SYNTAX:
; process_64, cube, means, variances, gain, readout_noise, fourier, psd, median_psd,
mean_psd_per_pix, median_RON, median_gain
;
; Processes the test data acquired with the LISA camera in order to
; extract the best possible pixels for the VINCI beams. This procedure
; makes the computations for the 64x64 windows data cubes and produces
; the power spectral density for all pixels, at different lighting levels.
;
; This is the first step of the best pixels selection, as described in the
; document 'LISA tests in Garching'
;
; It also computes the gain factor and the read-out noise for every pixel
; at the frequency used for the tests.
;
; version: 28/09/2000

;
; Computes the mean value and variance of each pixel over the sequence
; It excludes the last acquisition (partly saturated).
;
print, '* Means and variances...'
means = fltarr(6,64,64)
variances = fltarr(6,64,64)
for n=0,5 do begin
       print, '+++'
       for i=0,63 do begin
              for j=0,63 do begin
                     means(n,i,j) = mean(cube(n,i,j,*))
                     variances(n,i,j) = variance(cube(n,i,j,*))
              endfor
       endfor
endfor
;
;=============================================================================
; Computes the gain factor and the read-out noise for each pixel
;
weights = replicate(1.0,n_elements(means(*,0,0)))
results = fltarr(64,64,2)
gain = fltarr(64,64)
readout_noise = fltarr(64,64)
print, '* Computing gains and readout noises for each pixel...'
for i=0,63 do begin
       for j=0,63 do begin
              results(i,j,*) = regress(transpose(-
means(*,i,j)),variances(*,i,j),weights,$
                     yfit,const,/RELATIVE_WEIGHT)
              gain(i,j) = 1/(results(i,j,0))
              readout_noise(i,j) = sqrt(variances(0,i,j))*gain(i,j)
       endfor
endfor
print, 'Gains'
print, gain(1:10,1:10)
print, 'RON'
print, readout_noise(1:10,1:10)
median_RON = median(readout_noise)
```

```
median_gain = median(gain)
print, 'Median RON ='
print, median_RON
print, 'Median gain ='
print, median_gain
;
;============================================================================
; Computes the Power Spectral Density (PSD) for each pixel and each light
; intensity
;
print, '* Power Spectral density for each pixel...'
fourier = complexarr(6,64,64,256)
psd = fltarr(6,64,64,129)
for n=0,5 do begin
       for i=0,63 do begin
              for j=0,63 do begin
                     fourier(n,i,j,*)=fft(cube(n,i,j,*),1)
                     for k=0,128 do begin
                            psd(n,i,j,k) = abs(fourier(n,i,j,k))^2
                     endfor
              endfor
       endfor
endfor

;
; Computes the mean PSD for each pixel over the different light intensities
;
print, '* Mean PSD for each pixel over the different light levels'
mean_psd_per_pix = fltarr(64,64,129)
for i=0,63 do begin
       for j=0,63 do begin
              for k=0,128 do begin
                     mean_psd_per_pix(i,j,k) = mean(psd(*,i,j,k))
              endfor
       endfor
endfor
;
; Computes the median PSD over the 64x64 pixels, for dark exposures
;
print, '* Median PSD over the array at light level 0'
median_psd = fltarr(129)
for k=0,128 do begin
       median_psd(k)=median(psd(0,*,*,k))
endfor

;============================================================================
; Prints some data for checking
;
print,' Gains'
print, gain(0:10,1)
print,' RON'
print, readout_noise(0:10,1)
print,' ==='
print, means(0:1,32,32)
print, variances(0:1,32,32)
print, psd(0:1,32,32,121)
end
```

### 11.3 PROCESS SCANS

```
pro process_scans, flux, means, variances, fourier, psd, mean_psd
; SYNTAX:
; process_scans, flux, means_scans, variances_scans, fourier_scans, psd_scans,
mean_psd_scans
;
; Processes the test data acquired with the LISA camera in order to
```

```
; extract the best possible pixels for the VINCI beams. This procedure
; makes the computations for the ***scans*** data cubes and produces
; the power spectral density for all the pixels used.
;
; This is the second step of the best pixels selection, as described in the
; document 'LISA tests in Garching'
;
; Version: 13/09/2000
; Author: P. Kervella


; Computes the mean value and variance of each pixel over the sequence
; It excludes the last acquisition (partly saturated).
;
n_pix = n_elements(flux(*,0,0))
n_frames = n_elements(flux(0,*,0))
n_scans = n_elements(flux(0,0,*))

print, '* Means and variances...'
means = fltarr(n_pix)
variances = fltarr(n_pix)
print, '+++'

for n=0,(n_pix-1) do begin
       means(n) = mean(flux(n,*,*))
       variances(n) = variance(flux(n,*,*))
endfor

print, flux(0:5,0:20,2)

;============================================================================
; Computes the Fourier Transform for each pixel and each scan
;
print, '* Fourier transform for each pixel and each scan...'
fourier = complexarr(n_pix,n_frames,n_scans)
psd = fltarr(n_pix,n_frames/2+1,n_scans)

for i=0,(n_pix-1) do begin
       for j=0,(n_scans-1) do begin
              fourier(i,*,j)=fft(flux(i,*,j))
       endfor
endfor

;============================================================================
; Computes the Power Spectral Density (PSD) for each pixel and each scan
;
print, '* Power Spectral density for each pixel and each scan...'

psd = fltarr(n_pix,n_frames/2+1,n_scans)

for i=0,(n_pix-1) do begin
       for j=0,(n_scans-1) do begin
              for k=0,(n_frames/2) do begin
                     psd(i,k,j) = abs(fourier(i,k,j))^2
              endfor
       endfor
endfor

;============================================================================
; Computes the mean Power Spectral Density (PSD) for each pixel
; over the scans
median_psd_scans = fltarr(n_pix,(n_frames/2 +1))
print, '* Mean PSD over the scans'
for i=0,(n_pix-1) do begin
       for j=0,(n_frames/2) do begin
              mean_psd(i,j)=mean(psd(i,j,*))
       endfor
```

```
endfor
end
```

### 11.4 PLOT 64X64 DATA

```
pro data_plot, means, variances, gain, readout_noise, fourier, psd, median_psd
; SYNTAX:
; data_plot, means, variances, gain, readout_noise, fourier, psd, median_psd
;
; Plots the processing results for the selection of the best pixels for
; the LISA camera.
;
; This ends the first step of the best pixels selection, as described in the
; document 'LISA tests in Garching'
;
; version: 12/09/2000
;
;============================================================================
; Variance of the pixel as a function of flux (gain plot) for one good pixel
;
window, 0, title='Gain plot for pixel 33,38', xsize=800, ysize=600
plot, -means(*,33,38), variances(*,33,38), psym=2, xtitle='-Mean (ADU)',$
       ytitle='Variance', title='Gain plot for pixel [33,38]'
x_fit_gain = [0,20000]
y_fit_gain = fltarr(2)
y_fit_gain(*) = x_fit_gain(*)/gain(33,38)^2$
              +variances(0,33,38)
oplot, x_fit_gain, y_fit_gain
write_bmp, 'gain_plot_X33_Y38.bmp',tvrd()
;
; Variance of the pixel as a function of flux (gain plot) for one good pixel
;
window, 0, title='Gain plot for pixel 32,38', xsize=800, ysize=600
plot, -means(*,32,38), variances(*,32,38), psym=2, xtitle='-Mean (ADU)',$
       ytitle='Variance', title='Gain plot for pixel [32,38]'
x_fit_gain = [0,20000]
y_fit_gain = fltarr(2)
y_fit_gain(*) = x_fit_gain(*)/gain(32,38)^2$
              +variances(0,32,38)
oplot, x_fit_gain, y_fit_gain
write_bmp, 'gain_plot_X32_Y38.bmp',tvrd()


; Variance of the pixel as a function of flux (gain plot) for one good pixel
;
window, 0, title='Gain plot for pixel 31,38', xsize=800, ysize=600
plot, -means(*,31,38), variances(*,31,38), psym=2, xtitle='-Mean (ADU)',$
       ytitle='Variance', title='Gain plot for pixel [31,38]'
x_fit_gain = [0,20000]
y_fit_gain = fltarr(2)
y_fit_gain(*) = x_fit_gain(*)/gain(31,38)^2$
              +variances(0,31,38)
oplot, x_fit_gain, y_fit_gain
write_bmp, 'gain_plot_X31_Y38.bmp',tvrd()


; Power Spectral Density
;
window, 0, title='PSD for pixel 33,38', xsize=800, ysize=600
plot, psd(0,33,38,*), xrange=[0,128], yrange = [0,50000], xtitle='Relative Frequency.
Maximum pix 128 = 3.33 Hz, 0.026 Hz/bin',$
       ytitle='Power Spectral Density', title='Power Spectral Density for pixel [33,38]'
write_bmp, 'psd_X33_Y38.bmp',tvrd()

; Power Spectral Density
;
```

```
window, 0, title='PSD for pixel 32,38', xsize=800, ysize=600
plot, psd(0,32,38,*), xrange=[0,128], yrange = [0,50000], xtitle='Relative Frequency.
Maximum pix 128 = 3.33 Hz, 0.026 Hz/bin',$
       ytitle='Power Spectral Density', title='Power Spectral Density for pixel [32,38]'
write_bmp, 'psd_X32_Y38.bmp',tvrd()

; Power Spectral Density
;
window, 0, title='PSD for pixel 31,38', xsize=800, ysize=600
plot, psd(0,31,38,*), xrange=[0,128], yrange = [0,50000], xtitle='Relative Frequency.
Maximum pix 128 = 3.33 Hz, 0.026 Hz/bin',$
       ytitle='Power Spectral Density', title='Power Spectral Density for pixel [31,38]'
write_bmp, 'psd_X31_Y38.bmp',tvrd()

;
; Histogram of the noises of the pixels
;
window, 0, title='Histogram of the pixel readout noises', xsize=800, ysize=600
plot, histogram(readout_noise, min=0, max=30, bin=1,/nan),$
       title='Readout Noise Histogram', xtitle='Readout noise (e-)',$
       ytitle='Number of photosites'
write_bmp, 'Noise_histogram.bmp',tvrd()
;
; Histogram of the gains of the pixels
;
window, 0, title='Histogram of the pixel gains', xsize=800, ysize=600
plot, histogram(gain, min=0, max=5, bin=0.1,/nan),$
       title='Pixel Gains Histogram', xtitle='10 x Gain (e-/ADU)',$
       ytitle='Number of photosites'

write_bmp, 'Gain_histogram.bmp',tvrd()

;
; Gain factors image
;
window, 0, xsize=64, ysize=64
tv, gain
write_bmp, 'gain_map.bmp', tvrd()
;
; Readout noises image
;
window, 0, xsize=64, ysize=64
tv, readout_noise
stretch, 0, 60
write_bmp, 'readout_noise_map.bmp', tvrd()
;
; Median PSD for all pixels
;
window, 0, title='Median PSD over the 64x64 pixels', xsize=800, ysize=600
plot, median_psd(*), xrange=[0,128], yrange = [0,30000], xtitle='Relative Frequency.
Maximum pix 128 = 3.33 Hz, 0.026 Hz/bin',$
       ytitle='Power Spectral Density', title='Median Power Spectral Density over the
64x64 array (dark)'
write_bmp, 'median_psd.bmp',tvrd()

end
```

### 11.5 PLOT SCAN DATA

```
pro scan_data_plot, frequency, mean_psd
; SYNTAX:
; scan_data_plot, frequency, mean_psd_scans
;
; Plots the processing results for the selection of the best pixels for
; the LISA camera.
;
```

```
; This ends the first step of the best pixels selection, as described in the
; document 'LISA tests in Garching'
;
; version: 12/09/2000
;
; Power Spectral Density
;
set_plot, 'X'
;set_plot, 'PS'
;device,/inches, xsize=7.0, ysize=7.0
!p.position=[0.15,0.1,0.9,0.9]

n_pix = n_elements(mean_psd(*,0))
n_frames = 2*(n_elements(mean_psd(0,*))-1)

window, 0, xsize=800, ysize=600

plot, frequency, mean_psd(12,*), yrange = [0,1], $
       xtitle='Frequency (Hz)',$
       ytitle='Power Spectral Density', title='Power Spectral Density for pixel [33,38]'
write_bmp, 'psd_scan_X33_Y38_overview.bmp',tvrd()

plot, frequency, mean_psd(12,*), yrange = [0,0.2], $
       xtitle='Frequency (Hz)',$
       ytitle='Power Spectral Density', title='Power Spectral Density for pixel [33,38]'
write_bmp, 'psd_scan_X33_Y38.bmp',tvrd()

plot, frequency, mean_psd(12,*), yrange = [0,0.05], $
       xtitle='Frequency (Hz)',$
       ytitle='Power Spectral Density', title='Power Spectral Density for pixel [33,38]'
write_bmp, 'psd_scan_X33_Y38_zoom.bmp',tvrd()
wdelete, 0
end
```

## 11.6 TRANSFER FUNCTION COMPUTATION

```
pro transfer, fft_model, fft_chop, transfer_function, transfer_function_table
; SYNTAX: transfer, fft_model, fft_chop, transfer_function, transfer_function_table
;      ;,fft_const_mean
;
; Computes the modulation transfer function of the camera. fft_chop contains
; the individual ffts of each scan
;
; version: 21/09/2000
;
; Identification of the frequencies sampled
;
table_freq=fltarr(1024)

limit = 180
limit2 = 130
limit3 = 80

for i=0,100 do begin
       if abs(fft_model(i)) GT limit then begin
;      if (((i*2.48486) mod 112.09) LE 0.05) then begin
              table_freq(i)=1.0
       endif else begin
              table_freq(i)=0.0
       endelse
endfor

for i=100,300 do begin
       if abs(fft_model(i)) GT limit2 then begin
;      if (((i*2.48486) mod 112.09) LE 0.05) then begin
              table_freq(i)=1.0
```

```
       endif else begin
              table_freq(i)=0.0
       endelse
endfor

for i=300,513 do begin
       if abs(fft_model(i)) GT limit3 then begin
;      if (((i*2.48486) mod 112.09) LE 0.05) then begin
              table_freq(i)=1.0
       endif else begin
              table_freq(i)=0.0
       endelse
endfor

transfer_function_table = complexarr(1024,100)

for i=0,1023 do begin
       for j=0,99 do begin
       transfer_function_table(i,j) = (fft_chop(i,j)/fft_model(i))

;      Normalization to the noise of the open shutter...
;      transfer_function_table(i,j) = (fft_chop(i,j)/fft_model(i))$
;      /fft_const_mean(i)

       endfor
endfor

for i=0,512 do begin
       transfer_function(i)=mean(abs(transfer_function_table(i,*)$
                                     *table_freq(i)))
endfor
plot, transfer_function, xrange=[0,600], yrange=[0.5,1.5]

end
```

## 11.7 MODEL GENERATION

```
pro gen_model, period, size, min_level, max_level, rise, model
; SYNTAX: gen_model, period, size, min_level, max_level, rise, model
;
; generates a model of the chopping, with a defined rise time, period, and size.
;
; version: 21/09/2000
;

for n=0,(fix(size/period)-2) do begin
       i = period*n
       for j=fix(i),fix(i+rise/2) do $
                     model(j)=max_level/2 - $
                     (max_level-min_level)*(j-fix(i))/rise
       for j=fix(i+rise/2),fix(i+period/2-rise/2) do model(j) = min_level
       for j=fix(i+period/2-rise/2),fix(i+period/2+rise/2) do $
                     model(j)=min_level + $
                     (max_level-min_level)*(j-fix(i+period/2-rise/2))/rise
       for j=fix(i+period/2+rise/2),fix(i+period-rise/2) do model(j)=max_level
       for j=fix(i+period-rise/2),fix(i+period) do $
                     model(j)=max_level - $
                     (max_level-min_level)*(j-fix(i+period-rise/2))/rise
endfor
plot, model
end
```

## 11.8 TRANSFER FUNCTION PLOT

```
pro memory_plot, transfer_function, frequency, model_transfer
; SYNTAX: memory_plot, transfer_function, frequency, model_transfer
;
; Plots the processing results for the study of the memory effect.
;
; version: 21/09/2000
;
; for i=1,511 do model_transfer(i)=sin(!pi*frequency(i)/2544.5)$
; /(!pi*frequency(i)/2544.5)


set_plot, 'X'
;set_plot, 'PS'
;device,/inches, xsize=7.0, ysize=7.0
!p.position=[0.15,0.1,0.9,0.9]


window, 0, title='Temporal MTF compared to perfect integrator', xsize=800, ysize=600

;device, file='transfer_compare.ps'

plot, frequency, transfer_function(0:512), yrange=[0.5,1.2], xrange=[0,1300],$
       xtitle='Frequency (Hz)',$
       ytitle='LISA MTF (sampled by spikes) and perfect integrator (line)',$
       title='Temporal Modulation Transfer Function'
oplot, frequency, model_transfer
write_bmp, 'transfer_compare.bmp', tvrd()

wdelete, 0

;device, /close
;set_plot, 'X'
end
```

# 4. LdV Precision and Sensitivity

EUROPEAN SOUTHERN OBSERVATORY

Organisation Européenne pour des Recherches Astronomiques dans l'Hémisphère Austral
Europäische Organisation für astronomische Forschung in der südlichen Hemisphäre

# VERY LARGE TELESCOPE

## LEONARDO da VINCI

### LdV Precision and Sensitivity

Doc. No.: VLT-TRE-ESO-15810-2177

Issue: 1.0

Date: 12 July 2000

Prepared: P. Kervella
. . . . . .
Name Date Signature

Approved: A. Glindemann
. . . . . .
Name Date Signature

Released: M. Tarenghi
. . . . . .
Name Date Signature

CHANGE RECORD

| Issue | Date | Section/Page affected | Reason/ Initiation/Remarks |
|---|---|---|---|
| 1.0 | **Error! Reference source not found.** | All | first issue |

## TABLE OF CONTENTS

## Table of Contents

# 1. INTRODUCTION

## 1.1 SCOPE

This document gives estimates of the precision and sensitivity that will be achievable with VINCI in its stellar interferometer mode using the different VLTI light collectors. It gives the limiting magnitudes in each case, the statistical visibility precisions that will be achievable, and finally the calibrated visibilities accuracy. The impact of the use of a fringe tracker and adaptive optics is also described briefly.

## 1.2 REFERENCE DOCUMENTS

1. Interface control document between VLTI and its Instruments – VLT-ICD-ESO-15000-1826 v.1.0 – 16/11/1999

2. Functional description of the VLTI – VLT-ICD-ESO-15000-1918 v.1.0 – 16/11/1999

3. Test Siderostat Optical design, Pupil Shape and Sky Coverage – VLT-TRE-ESO-15000-1616 v.1.0 – 08/06/1998

4. Filtrage modal et recombinaison de grands telescopes. Contributions à l'instrument FLUOR – C. Ruilier – 1999

5. LdV Optical Definition – VLT-MEM-MEU-15810-1000 v.2.0 – 21/06/1999

6. LdV Sources and Guided Optics – VLT-SPE-MEU-15810-1001 v.1.0 – 10/07/1999

7. Transversal atmospheric dispersion in the VLTI – VLT-TRE-ESO-15000-1989 v.1.0 – 25/01/2000

8. Factors affecting the performance of stellar interferometers – B. Koehler

9. Specifications for the feasibility study of PRIMA – VLT-SPE-ESO-15800-1652 v.1.0 – 28/08/1998

10. PRIMA/FSU Final report – F. Cassaing et al., ONERA – 16/08/1999

11. LdV Optical Definition – VLT-SPE-MEU-15810-1000 v.2.0 – 21/06/1999

12. LISA Final Design Review – Hardware – R. Hofmann – 10/11/1999

# 2. PRECISION AND SENSITIVITY LIMITING FACTORS

VINCI is designed to be a test instrument. Though, because of its particular optical fiber beam combiner, it can achieve very high precisions in the measurement of visibilities. FLUOR has demonstrated remarkable capabilities using this combination principle.

Table 1 give the list of all known sensibility and precision limiting factors that will affect VINCI. Precision and sensitivity are the two sides of the same problem, and are considered simultaneously. Though, not all of the listed factors will cause both a precision and sensitivity degradation. The factors limiting mostly the precision, without affecting the sensitivity are in italic.

**Table 1. Precision and sensitivity limiting factors in VINCI**

| Optics | Detection | Atmosphere | Astrophysics |
|---|---|---|---|
| Area of the light collectors optics | Detector overall quantum efficiency | *Piston noise (direct sky or FSU residuals)* | *Uncertainty on the calibrator angular size* |
| Photometric transmissivity of the optical train | Detector read-out noise (Hawaii array RON) | Strehl ratio fluctuations (photometric noise) | *Knowledge of the target spectrum shape* |
| *Stability of the optical train (vibrations)* | Thermal background noise seen by the detector | Internal turbulence (non AO corrected) | *Statistical photon shot noise (photon noise)* |
| *Stability of the contrast loss (polarization)* | Sampling losses (non blocking sampler) | Atmospheric transmission in the K band | |
| Wavefront distortion due to the optical train | Possible additional detector noise (array defects) | *Differential longitudinal dispersion* | |
| Fiber injection losses (coupling efficiency < 0.8) | | *Transversal dispersion between visible and infrared* | |
| Photometric efficiency of the fibered triple coupler | | *Non stationarity of the atmospheric contrast loss* | |
| Interferometric efficiency of the fibered triple coupler | | *Correlation of the two channel visibilities* | |
| Bad imaging of the fibers on the detector pixels | | | |

# 3. OPTICS

## 3.1 AREA OF THE COLLECTORS OPTICS

The surfaces of the VLTI light collectors is given in Table 2. The siderostats have a limited aperture, equivalent to 355mm on the sky, that gives an area of 0.099m$^2$. It is also reduced by projection effects, and the effective area can be as small as 0.050m$^2$. The average effectie area for the 10 MIDI objects is 0.084m$^2$.

The pupil shape of the siderostats is never circular, but elliptic with an axis length ratio of 4/3 (at best) to 2/1 (at worst). The longer axis is about 80mm in all cases. The resulting star image shape on the fiber heads will therefore not be circular, and the injection efficiency will be reduced.

In the unfavorable case of the operation of VINCI without beam compressors in the laboratory, the efective entrance pupil diameter is reduced to 10 cm (2cm x magnifying factor). This results in a very small collecting surface and should be avoided as much as possible.

**Table 2. Areas of the collectors primary optics**

| Telescope type | Effective area (m$^2$) |
|---|---|
| Siderostat | **0.084 (average)** |
| Siderostat without BC | **0.039** |
| Auxiliary Telescope | **2.545** |
| Unit Telescope | **50.265** |

## 3.2 TRANSMISSION OF THE OPTICAL TRAIN

### 3.2.1 Photometry

The overall light transmission efficiency of the VLTI optical train is given in Table 3 for the different light collectors, including all the mirrors up to (and including) the folding mirrors on the VINCI table. The transmissivity up to M16 is taken from RD1. A flat reflectivity for the 6 excess siderostats mirrors of 98% in the K band has been assumed.

**Table 3. Transmission of the collectors in the K band**

| Telescope type | # mirrors | Transmission |
|---|---|---|
| Siderostat | 18 | **40%** |
| Siderostat without BC | 15 | **42%** |
| Auxiliary Telescope | 24 | **35%** |
| Unit Telescope | 24 | **35%** |

### 3.2.2 Vibrations and polarization contrast losses

Due mainly to residual longitudinal vibrations, the contrast of the fringes measured on a point source in the laboratory will not be 100%. The VLTI optical train has been specified for a maximum loss in visibility of 1 percent, and on-site tests on the Unit Telescopes (Koehler&Leveque 1999) have shown that a maximum contrast loss of 5% can be expected due to vibrations in the telescopes only.

In addition, a polarization mismatch is introduced after each reflection. A maximum overall loss of 0.4% in K is expected, and is neglected in the computations.

The expected interferometric efficiency of the VLTI is therefore **0.95**.

### 3.2.3 Static wavefront distortion due to the optical train

The static planeity of the wavefront produced by the optical train of the VLTI will impact on the quantity of flux injected into the fibers. The quality of the wavefront will be evaluated using the end-to-end model developed at ESO. Detailed beam propagation simulations are currently produced by Rainer Wilhelm.

### 3.2.4 Pupil lateral jitter

The pupil lateral positioning effect on the injection in a fiber is given in RD4. For the VLTI, the stability of the pupil lateral position depends on the bases used. The worst case is for the station located the farthest from the laboratory (e.g. the J6 station). Table 4 lists the pupil lateral jitter as given in RD1.

**Table 4. VLTI Pupil lateral jitter (worst case, J6 station)**

| Time window | AT without beam expanders | Siderostats, UT and AT with beam expander |
|---|---|---|
| 0.1 s | 400 μm RMS | 90 μm RMS |
| 1 s | 600 μm RMS | 135 μm RMS |
| 10 s | 730 μm RMS | 165 μm RMS |
| 30 min | 790 μm RMS | 180 μm RMS |

The mean time to acquire a scan in VINCI on a faint star is about 0.2 seconds, but the time between two optimizations will be of the order of 5 minutes. The figure to take into account is here the latter, as the flux loss will not be checked afterwards. The resulting flux loss is computed using the following formula (taken from RD4):

$$\frac{\rho}{\rho_{max}} \approx e^{-22.561\delta p^2}$$

with $\delta p$ the lateral misalignment as a fraction of the pupil size. In any case, the pupil size is 18mm at the entrance of the instruments.

**Table 5. RMS flux loss due to lateral jitterof the pupil**

| Light collector | Lateral relative RMS jitter | Flux loss |
|---|---|---|
| AT without beam expander | 750/18000= 4.2% | **3.9%** |
| Siderostats, UT, AT with beam expander | 170/18000= 0.94% | **0.2%** |

## 3.3 FIBER INJECTION STATIC LOSSES

The maximum fraction of the light injected into the optical fibers is **78%**. This is due to the fact that the mode on which the telescope diffraction pattern is projected has a gaussian shape (and not an Airy pattern).

## 3.4 FRESNEL LOSSES

Fresnel losses happen at the surface of the fiber, both at the entrance and output of the fiber. The theoretical maximum eficiency is 96%. Four fiber interfaces are foreseen on VINCI between the fiber input

and the detector, resulting in a transmission of **85%**. Antireflective coatings may cancel this effect, but their implementation is not yet certain on VINCI.

## 3.5 FIBER INJECTION DYNAMIC LOSSES

**Table 6. Tip-tilt residuals and flux losses**

| Telescope | UTs without AO | AT | AT + Beam Expander | Siderostats |
|---|---|---|---|---|
| **Arcsec/sky RMS** | 0.025 | 0.032 | 0.103 | 0.58 |
| **% of K band diffraction limit** | 45 | 13 | 42 | 53 |
| **Fraction of flux transmitted** | **0.80** | **0.95** | **0.80** | **0.70** |

Due to residual turbulent motions of the star image on the fiber head, the mean fraction of flux injected is lower than the theoretical 80% value. The values of RMS tip-tilt errors projected on the sky are listed in Table 6 (taken from RD1, including STRAP for the ATs and UTs, but not for siderostats). The flux loss values are directly the values of the mode of the fiber at the corresponding lateral displacement of the star image (RD4, p.66). The UTs with AO tip-tilt residuals are included in the Strehl ratio budget (Section 5.2).

## 3.6 EFFICIENCY OF THE TRIPLE COUPLER

The MONA fibered triple coupler is specified to have the following characteristics:

- minimum photometric efficiency of **75%**
- interferometric efficiency normally above **95%**.

## 3.7 IMAGING OF THE FIBER HEADS ON THE DETECTOR

The reimaging system is designed to fit all the light coming from the MONA outputs into four pixels. The photometric efficiency of this system can be estimated at **30%**. Table 7 lists the contributions to this number from the different optical elements (values taken from RD11 and RD12).

**Table 7. Fibers output block transmission**

| | |
|---|---|
| Off-axis parabola | 0.98 |
| Flat mirror | 0.98 |
| Camera window (CaF2) | 0.92 |
| K band filter | 0.80 |
| Sapphire lens | 0.85 |
| ZnSe lens | 0.65 |
| Ensquared energy on the detector | 0.77 |
| **Total transmission** | **0.30** |

# 4. DETECTION

## 4.1 DETECTOR QUANTUM EFFICIENCY

This curve is taken from the Rockwell web site, for the 1024x1024 HAWAII detector. The mean quantum efficiency in the K band is **62%**.

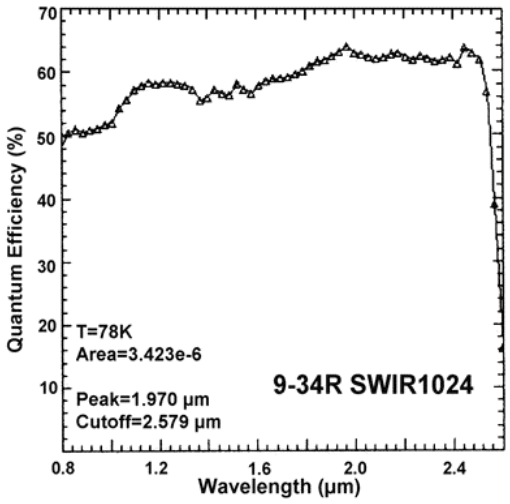


## 4.2 READOUT NOISE

The value given by Rockwell for the Hawaii chip minimum readout noise is <10 e-. However, the RON depends on the frequency and the readout electronics, and the detector of LdV is read relatively quickly. Therefore, it seems realistic to take the **10 e-** value as a basis.

## 4.3 THERMAL BACKGROUND NOISE

### 4.3.1 Temperature

This noise contribution is normally minor compared to the other noise sources in the K band. A photon shot noise is introduced on the detector by the infrared light emmited by the instrument. The temperature taken into account is the  of the warm optics. We adopt the mean value of the temperature in the laboratory of **15.5°C**.

### 4.3.2 Emissivity

The worst possible case is an emissivity of **1**. This means that the instrument is assumed to be a perfect blackbody. The thermal noise is negligible in the K band at the temperature considered here (15.5 Celsius degrees), and therefore the influence of this parameter is also negligible.

### 4.3.3 Beam etendue

The beam etendue is the product of the angle seen by the detector by its illuminated surface. It is 1 when the detector is seeing all the thermal light emitted by the instrument (this is not the case in reality, thanks to the cold stop in the detector dewar). For the same reason as for the emissivity (low thermal noise), this factor has a negligible influence on the results. As it is in addition relatively difficult to model, we take into account the worst possible case, i.e. a beam etendue of **1**.

### 4.4 SAMPLING LOSSES

The HAWAII detector is used as a non blocking sampler. The maximum efficiency in the transmission of the fringe contrast is reached for a sampling of 5 points per fringe, corresponding to an efficiency of **80%**.

### 4.5 DETECTOR DEFECTS

The HAWAII array of VINCI is an engineering grade detector. This means that the possibility exists that the detector presents some discrepancies from the mentioned characteristics, either in readout noise, frequency response, or other parameters. **No defect** has been taken into account here.

# 5. ATMOSPHERE

## 5.1 PISTON NOISE

### 5.1.1 Theoretical aspects

Fringe motion caused by the atmosphere is the most important precision limiting factor for VINCI. The differential piston between the two beams blurs the fringes, and therefore affects their visibility. Figure 1 shows the instrumental visibility as a function of the standard deviation of the piston over one scan duration (see RD8 for details). For small phase difference fluctuation:

$$V_{inst} = e^{-\frac{\sigma_\phi^2(T)}{2}}$$

with T the duration of the scanning of the fringes, and σ(T) the standard deviation of the piston in radians. $V_{inst}$ decreases from 100% when no piston is present to 10% for a standard deviation of λ/3 (at 2.2 microns). In the following, the uncertainty on the visibility estimate is assumed to be the same as the instrumental visibility degradation. A qualitative reason for this is that the energy in the interferometric fringes can be affected randomly, both positively and negatively, by the atmospheric OPD variations. The visibility degradation computed here corresponds to the "typical negative energy case", and therefore can be taken as a standard deviationvalue.

For further analysis of the behavior of the fringes when affected by piston, it is necessary to produce simulated interferograms affected by a typical atmospheric piston and then to compute the visibility using the standard pipeline. The dispersion on the final visibilities, as a function of the standard deviation of the OPD would give more realistic piston noise effects estimates.

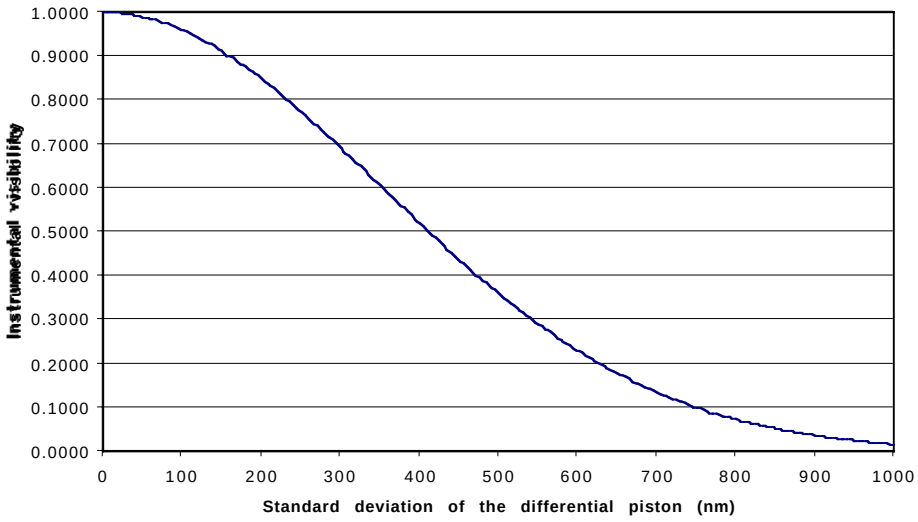


**Figure 1. Differential piston effect on the instrumental visibility in the K band**

An aproximate formula for the high frequency power spectrum (above 0.2 *v/B* with *v* the wind speed and *B* the baseline) of the OPD variation is (RD9):

$$\phi(f) = 0.0039 \frac{\lambda^2}{r_0^{5/3}} \frac{v^{5/3}}{f^{8/3}} \quad [m^2 / Hz]$$

*v* is the effective wind speed, $r_0$ the Fried parameter and *f* the frequency. As $r_0$ is proportional to $\lambda^{6/5}$ the power spectrum does not depend on the wavelength explicitely, but only on the seeing conditions, e.g. an $r_0$ of 15 cm at 0.5 μm (considered in the following as typical for Paranal) corresponds to a value of $r_0$ = 5.7 m at =10 μm ($r_0$ = 1371.9 $\lambda^{6/5}$ *[mJ]*). A value of 15 m/s for the wind speed is assumed in the following formula:

$$\sigma_\phi^2(T) = \int_{F_0=1/T}^{\infty} \phi(f)\,df = 4.29\,10^{-3}\,\frac{\lambda^2}{r_0^{5/3}}(Tv)^{5/3} \quad [m^2]$$

which gives

$$V_{inst}(T) = e^{-1.5\,T[s]^{5/3}}$$

$$\sigma(V_{star}) = 1 - e^{-1.5\,T[s]^{5/3}}$$

The resulting instrumental visibility as a function of the exposure time is plotted on Figure 2. The fastest integration time for the whole interferogram in VINCI will be 7 milliseconds (effective fringes length 70 microns, 10000 microns/s fringe speed). This gives a maximum visibility measurement precision per scan of **0.04%**.

The length taken into account is not the total scan length, but only the length of the fringes packet only (~70 microns including the secondary lobes). The piston has no effect on the flat part of the interferograms.

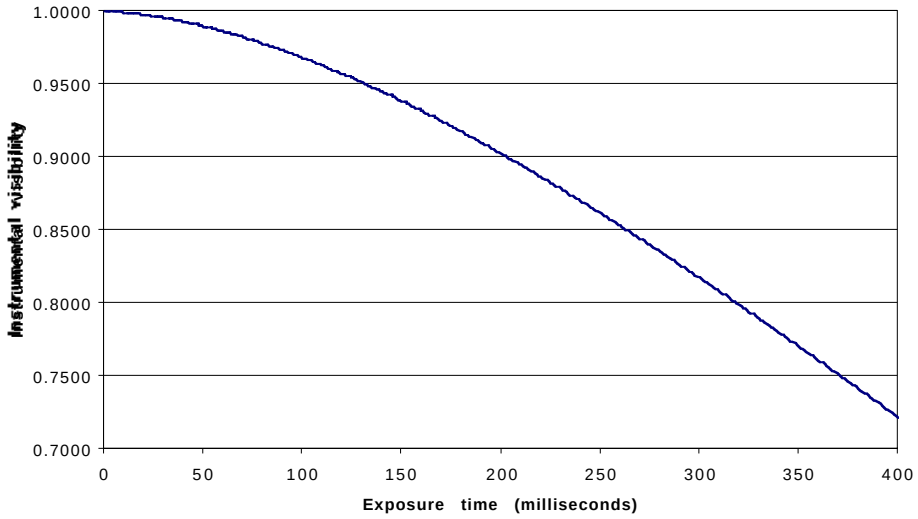


**Figure 2. Instrumental visibility as a function of scan duration**

### 5.1.2 FLUOR / IOTA experimental results

A piston noise value of 0.2 (multiplicative noise) is what is generally observed on IOTA, on the 40 meters baseline and for bright stars.Typically the signal to noise ratio of the squared instrumental visibility $\Delta\mu^2/\mu^2$=0.2 on the bright sources, with a fringe speed of ~500μm/s, and a 114 microns scan length.

This means that the piston noise equivalent power is one fifth of the star signal. Therefore, the precision obtained on the individual measurements of $\mu^2$ is assymptotically 20% (assuming no other source of noise). This translates into a ±1% precision limit on the visibility measurements in 100 scans.

This value is of the same order of magnitude as the 12% precision of the theoretical computations (for the same scan duration, i.e. with a fringe speed of 500µm/s) presented in Section 5.1.1, which is lower because the seeing conditions considered are for Paranal (hence with a better seeing than Mount Hopkins).

### 5.1.3 Fringe Sensor Unit

The role of the FSU is to reduce the piston sufficiently to have a maximum OPD error of 30 nm up to magH=13 (UTs) or 10 (ATs) as specified in RD9. When used with the FSU, the theoretical minimum precision with VINCI considering this residual piston only is **0.37%** (up to the limiting magnitude of the FSU, H~ 4 with the siderostats). For the brightest stars (K~ -2 on the siderostats), the theoretical OPD residual is about 1nm (taken from RD10), which translates into a theoretical visibility loss of **0.0004%** (4e-6). Such a number should not be considered reliable, as no experiment has ever demonstrated this kind of capabilities. Moreover, this is *not* the final precision, as it only takes into account the piston noise.

The PFSU can theoretically provide the same accuracy, but for stars about 2 magnitudes brighter (i.e. up to H~ 2). The parameters for the upgraded version FINITO should be close to the FSU values.

## 5.2 STREHL RATIO

The mean values of the Strehl ratios (apart from the quasi-static wavefront errors introduced by the optical train, see Section 3.2.3) expected for the different light collectors are listed in Table 8. The values without AO assume an $r_0$ of 1 meter in the K band at Paranal, and do not take into account the residual tip-tilt errors (see Section 3.5), except fo the UTs with AO.

**Table 8. Strehl ratios for different telescope configurations**

| Telescope type | Strehl without AO in K | Strehl with AO |
|---|---|---|
| Siderostat wihout BC | **~100%** | **-** |
| Siderostat with BC | **~100%** | **-** |
| AT | **30.8%** | **-** |
| UT | **1.56%** | **48% (K=12)** |

Shaklan (Applied Optics, 27, 2334, 1988) has shown that the optimal injection is obtained for a value of $D/r_0$ of 4 (with D the telescope diameter and r0 the Fried parameter). It could therefore be interesting to foresee pupil stops for the first observations with the UTs not equipped with AO systems.

## 5.3 PHOTOMETRIC NOISE

The adaptive optics and/or tip-tilt correction systems will leave some residual star motion on the fiber head. This will cause a degradation in the quantity of light coupled into the fibers, and random variations of the flux measured on the detector. From time to time, the flux injected in the fibers can drop to zero (or small values). As the interferometric signals are divided by the photometric signals, this causes a decrease in the SNR of the photometrically corrected fringes.

In the case of VINCI, this effect is equivalent to a random photometric loss. The single-mode fibers filter out completely the tip-tilt and high order wavefront errors, and the output wavefront is only affected by flux variations. These variations inject some power in the frequency range of the fringes, and therefore can affect the fringe visibility. To reduce this effect, the photometric signals are used to calibrate the interferometric outputs during the data reduction.

**Further simulations are required to estimate the impact of this kind of noise on the measurements.**

## 5.4 INTERNAL TURBULENCE

As stated in RD1 (p.20), the equivalent $r_0$ for the internal seeing is 125m at 2.2 microns. Therefore, the effect of internal seeing is **neglected** in the rest of this study.

## 5.5 ATMOSPHERIC TRANSMISSION IN THE K BAND

The following curves are taken from the www site: http://www.eso.org/gen-fac/pubs/astclim/paranal/h2o/

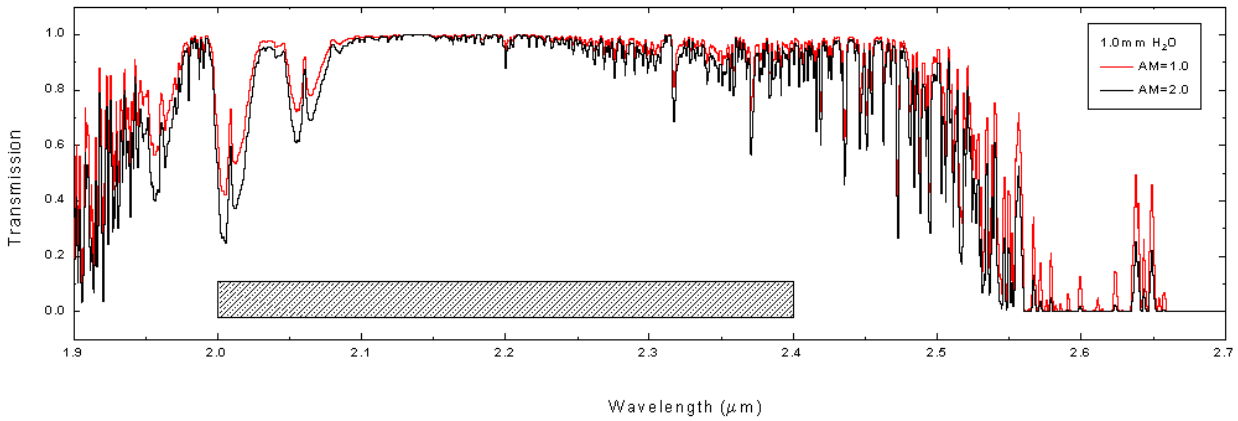


**Figure 3. Atmospheric transmission above Paranal in the K band for two airmasses (AM) and 1 mm precipitable water vapor. Typical values on Paranal are 1.5 (winter) to 2mm (summer).**

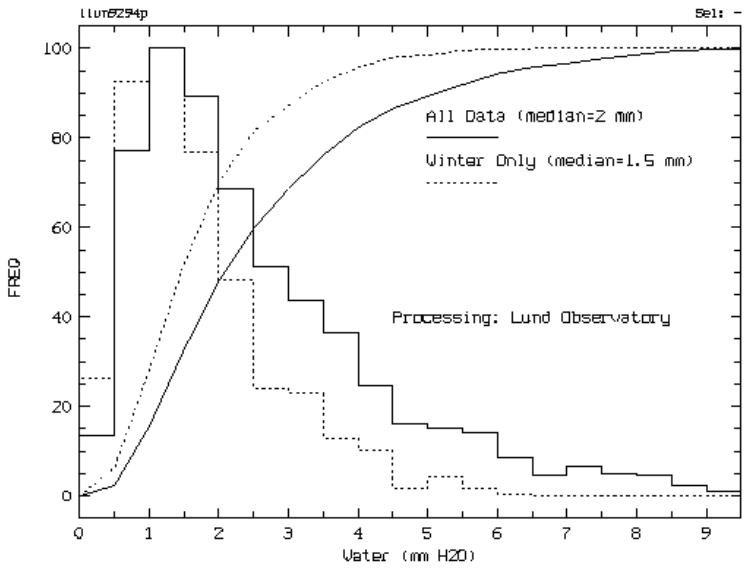


**Figure 4. Precipitable water vapor above Paranal.**

A typical value of **90%** for the overall transmission (assuming 2mm precipitable water vapor) in the K band is assumed in the following.

**Table 9. Atmospheric transmissions inside the K band.**

| **Wavelength range** | 2-2.1μm | 2.1-2.2μm | 2.2-2.3μm | 2.3-2.4μm |
|---|---|---|---|---|
| **Transmission (2mm water vapor)** | 0.72 | 1 | 0.96 | 0.93 |

## 5.6 TRANSVERSAL ATMOSPHERIC DISPERSION

Between different wavelengths, the vector pointing to the star from the telescopes is not exactly the same when the star is not at zenith. This results in a loss on the total flux injected into the optical fibers, as described in details in RD7. Two kinds of effects will happen on LdV:

### 5.6.1 Between the K band and the visible:

The guiding of the telescopes is achieved in the visible, therefore the lateral shift of the star image due to transversal dispersion. The difference between the apparent position of the star in the K band and in the visible will cause some flux loss, as the star will move slightly on the fiber head during the exposures (typically a few minutes long for LdV).

At 60 degrees of zenith angle (maximum value), the differential tilt between the R band (visible) and the K band can reach 1.41 arcsec. In this particular case, a correction has to be applied every 10 seconds, in order to limit the shift to a maximum of $\lambda/8D$.

Under normal conditions, and assuming that the relevant corrections are applied, this effect will not cause any flux loss, and is **neglected** in the following computations.

### 5.6.2 Inside the K band:

The K band spans from 2 to 2.4 microns. Between the two extreme wavelengths of the band, the atmospheric transversal dispersion will not be the same. For a star far from zenith, this results in a slightly elongated star image on the fibre head, and therefore in a degraded injection.

The modeling done by Francoise Delplancke (RD7) give a maximum flux loss of 4.6% for the UTs at 60 degrees of zenith angle, and negligible values for smaller zenith angles and other telescopes (< 0.5%).

The following flux loss values are assumed in the following (half of the maximum values):

- **0%** for the siderostats
- **0.2%** for the ATs
- **2.3%** for the UTs

## 5.7 NON STATIONARITY OF THE ATMOSPHERIC CONTRAST LOSS

Once the photometric corrections have been applied to the interferometric signals, the visibility measured by the instrument should always be the same (is no piston was present). In reality, the contrast loss due to the atmosphere itself (not to fast turbulence) and its large scale evolutions is still to be studied, but it is certainly at a very low level below the current foreseen precisions without fringe tracker. This effect was therefore not considered in the rest of this study.

## 5.8 CORRELATION OF THE TWO INTERFEROMETRIC CHANNELS

The reduction of the statistical uncertainty brought by the combination of the two visibility measurements coming from the two interferometric channels of VINCI is justified theoretically only if the two values are not correlated. In reality, this is not really the case but the approximation is usually good. The uncorrelated approximation is assumed in this study, but further investigations will be necessary once VINCI is working.

### 5.9 STATISTICAL PHOTON SHOT NOISE

Due to the statistics of the individual photons arriving on the detector, a noise proportional to the square root of the number of photons (or power) is introduced in the measurements. The contribution of this noise depends on the integration time. RElated formulae are given in the Appendix.

# 6. GLOBAL PARAMETERS

## 6.1 OVERALL PHOTOMETRIC EFFICIENCY

**Table 10. Photometric transmission coefficients**

| **Telescopes** | Siderostats without BC | Siderostats with BC | ATs + BE | UTs without AO | UTs with AO |
|---|---|---|---|---|---|
| Atmospheric transmission | 0.90 | 0.90 | 0.90 | 0.90 | 0.90 |
| Strehl ratio | 1.00 | 1.00 | 0.31 | 0.016 | 0.48 |
| Transversal dispersion | 1.00 | 1.00 | 1.00 | 0.98 | 0.98 |
| Optical train | 0.42 | 0.40 | 0.35 | 0.35 | 0.35 |
| Pupil lateral jitter | 1.00 | 1.00 | 0.96 | 1.00 | 1.00 |
| Fiber injection | 0.78 | 0.78 | 0.78 | 0.78 | 0.78 |
| Fresnel losses | 0.85 | 0.85 | 0.85 | 0.85 | 0.85 |
| Fiber injection tip-tilt residuals | 0.70 | 0.70 | 0.80 | 0.80 | 1.00 |
| Triple coupler | 0.75 | 0.75 | 0.75 | 0.75 | 0.75 |
| Outputs imaging | 0.30 | 0.30 | 0.30 | 0.30 | 0.30 |
| Signal splitting | 0.25 | 0.25 | 0.25 | 0.25 | 0.25 |
| Quantum efficiency | 0.62 | 0.62 | 0.62 | 0.62 | 0.62 |
| **TOTAL** | **0.00612** | **0.00582** | **0.00173** | **0.0000914** | **0.00342** |

## 6.2 OVERALL INTERFEROMETRIC EFFICIENCY

**Table 11. Interferometric transmission coefficients**

| **Telescopes** | Siderostats | ATs | UTs without AO | UTs with AO |
|---|---|---|---|---|
| Sampling losses | 0.80 | 0.80 | 0.80 | 0.80 |
| Telescopes and optical train | 0.95 | 0.95 | 0.95 | 0.95 |
| Triple coupler | 0.95 | 0.95 | 0.95 | 0.95 |
| **TOTAL** | **0.722** | **0.722** | **0.722** | **0.722** |

# 7. STATISTICAL VISIBILITY PRECISION CURVES

## 7.1 SIGNAL TO NOISE RATIO

The signal to noise ratio Ω is given by the following formula:

$$\Omega = \frac{S}{\sqrt{\varpi_{thermal}^4 + \varpi_{detector}^4 + \varpi_{piston}^4 + \varpi_{photon}^4}}$$

the fourth power on the NEP come from the fact that the signal is the squared visibility of the fringes.

## 7.2 OPTIMAL OPD SCAN SPEED

The effective precision attainable with VINCI will depend on the exposure time used on each star. The optimized parameter is the **OPD scan speed *v*** (in optical path difference, which is twice the piezo mirror motion speed). As a general rule, VINCI will sample the fringes at a fixed $n$ = 5 points per fringe (optimal value), gives directly the readout frequency of the detector through the formula : $f = n.v/\lambda$. This means that the readout frequency of the detector (and therefore the exposure time) is completely defined by the fringe speed.

As the star is brighter, the exposure time can be shorter, and therefore the piston noise impact on the fringes can be reduced. It is important though to have a sufficient number of photons in each OPD bin, so as not to be limited by the detector readout noise, but still not too large to avoid the photon shot noise. The determination of the optimal exposure time is therefore a trade-off between the piston noise, the photon noise and the detector noise, in order to minimize the total noise on the flux measurement. For the faint stars, the problem is the same, but the photon shot noise will be negligible compared to the readout noise of the detector and the piston noise.

The formulae for the different noise sources are given in the Appendix (Section 10). The minimization is done on the total signal to noise ratio Ω (as given in Section 7.1), assuming that only the **OPD scan speed** is variable. The piston has an effect on ly on the fringes part of the acquired interferograms. This means that the time used to compute the fringes blurring is the the time necessary to scan the 70 microns of the fringe packet (see Section 5.1 for details).

## 7.3 CURVES WITH THE DIFFERENT LIGHT COLLECTORS, WITHOUT FSU

For 100 scans and combining the two interferometric outputs. From left to right:

- Siderostats without beam compressors
- Siderostats with beam compressors
- ATs and UTs without Adaptive Optics (same curve)
- UTs with Adaptive Optics

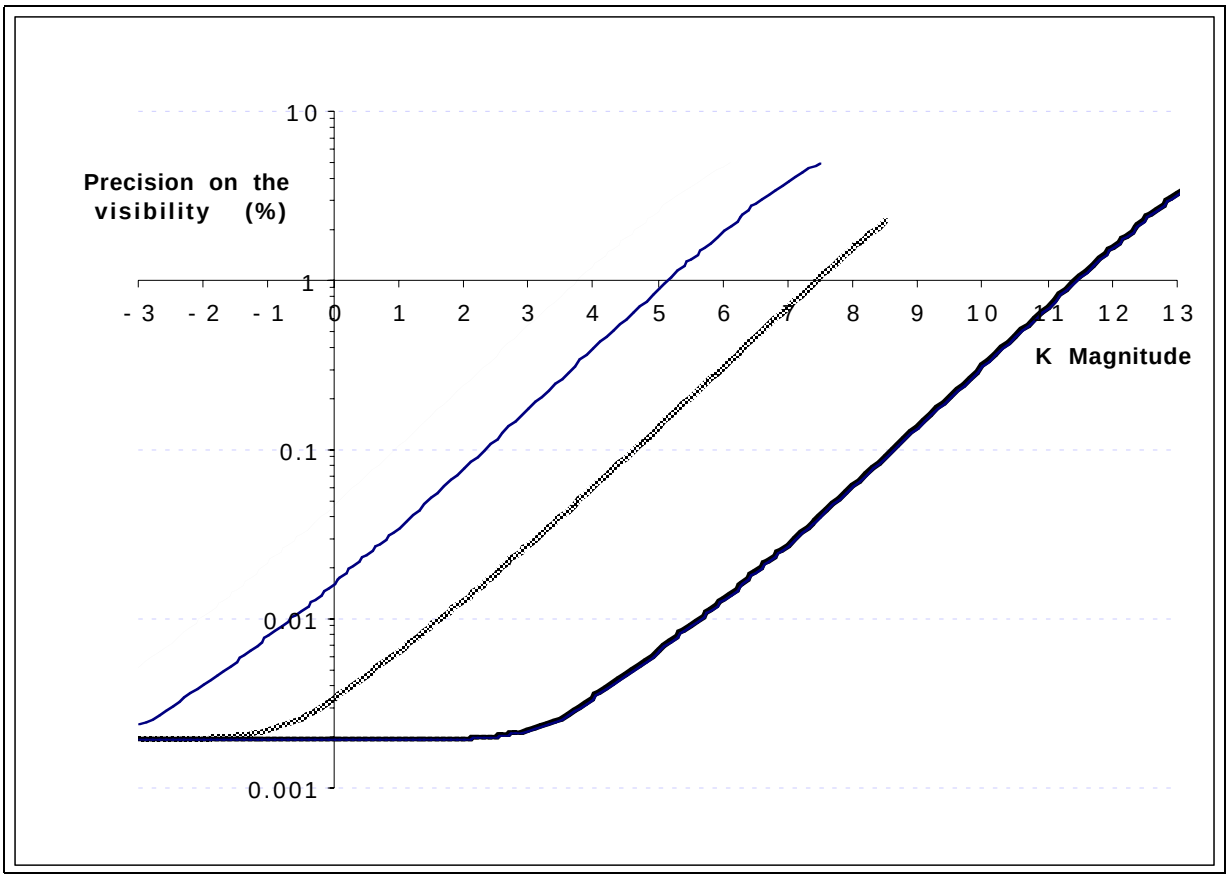


The maximum statistical precision theoretically attainable is about 0.002 % for the brightest stars. The limitation for the UTs comes from the photon noise, and is due to the limited maximum speed of the piezo mirror ($v_{max}$(OPD) = 1 cm/s). A practical limit for the observations can be set at 2% limiting precision (in 100 scans). After this limit, the calibration of the observation can be problematic, but the system can be usable up to a 5% precision. This gives the limiting magnitudes listed in Table 12. It should be stressed that the figures given in this table are for the statistical uncertainties only. They are useful to prepare an observation, as they give an estimate of the limiting magnitude of a single star observation, but the final calibrated visibilities will have a lower precision, due to the uncertainties on the calibrator angular size or other factors (see Section 9 for details).

**Table 12. VINCI *statistical* limiting magnitudes**

| Collector | Limiting magnitude 2% precision | Limiting magnitude 5% precision |
|---|---|---|
| Siderostats without beam compressors | 4.6 | 6.1 |
| Siderostats with beam compressors | 6.0 | 7.5 |
| Auxiliary Telescopes | 8.3 | 9.8 |
| Unit Telescopes without Adaptive Optics | 8.3 | 9.8 |
| Unit Telescopes with Adaptive Optics | 12.3 | 13.8 |

# 8. ASTROPHYSICS

## 8.1 UNCERTAINTY ON THE CALIBRATOR ANGULAR SIZE

### 8.1.1 Precision of the transfer function estimation

The precision of our *a priori* estimations of the angular sizes of the calibrators will directly impact the final precision of the science targets visibilities. In this section, the level of precision expectable from the calibrators is evaluated.

As a basis, we will consider the catalogue of infrared calibrators from Cohen et al. (AJ, **117**, 1864-1889, 1999). Other angular size sources are also accessible, but the Cohen catalogue has the advantage of providing a uniform coverage over the whole sky. It was created for the calibration of the space observatories in the infrared wavelengths. The level of uncertainty of this catalogue is typically $\sigma$ **= +/- 1.5%** of the limb darkened angular diameter of the selected calibrators.

The conversion of the limb darkened (LD) values to uniform disk (UD) angular diameters is relatively easy, as the Cohen stars are selected in well-known K5 giants region of the HR diagram. Therefore, it is possible to compute a high precision conversion factor between the LD and UD diameters, and to keep approximately the same error bar on the UD value.

The angular diameters range covered by the Cohen is typically 2.0 to 2.5 mas (+/- 0.03 to 0.04 mas). The extreme values of the catalogue are 1.6 and 10 mas. The following figure shows the precision on the interferometric transfer function estimate assuming a typical **2.3 +/- 0.035 mas** calibrator (bold curve) and a very favorable 1.0 +/- 0.015 mas calibrator (thin curve), for different baseline lengths in the K band (2.2 microns).

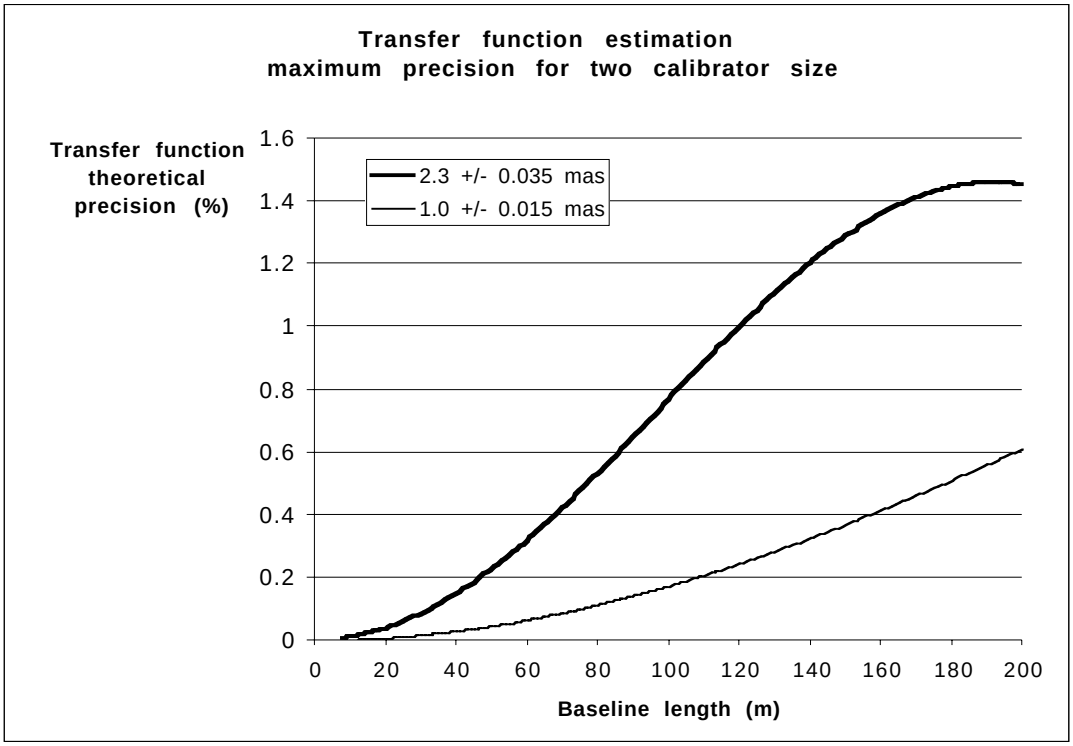

On the brightest stars, VINCI is able to reach a statistical precision of 0.002 %. This means that the final visibility estimation will be limited mainly by the calibrator size knowledge for baselines larger than a few tens of meters meters. It is important to realize that it will *not* be possible to increase this precision by observing the calibrator for a longer time, as it is a fundamental uncertainty (not of statistical origin).

One should also mention that the error on the transfer function measurement impacts the final calibrated precision in a way that is not multiplicative, but by division. This means that usually, if the observations on the target are very good and the calibrator is bad, then the final precision on the target will be substancially better than for the calibrator.

### 8.1.2 Multiple calibration

A way to solve this problem is to use several calibrators for the same science star. Assuming that the angular diameters are not biased, we can reduce the final uncertainty on the transfer function substantially.

If we consider the standard 2.3 +/- 0.035 mas calibrator case, observed with the 200 meters baseline, it is necessary to reduce the uncertainty from 1.45% to 0.04% to be limited only by the statistical uncertainty of VINCI (bright star). This means a factor 36, and more than 1300 calibrators to observe. Of course, this is impossible to achieve.

By using 10 calibrators (which is a reasonable maximum number for a single star), we can go to a transfer function precision of **0.43%** on the transfer function for the 200 meters baseline. This is still a factor 200 above the VINCI maximum precision, but this is probably the best we will be able to achieve on a single observation by using the “raw” Cohen calibrators catalogue.

### 8.1.3 Refinement of the calibrator catalogue

During the course of one night, and assuming that we observe a number of targets and calibrators together, it will be possible to cross calibrate the calibrators. The observations with the longest baselines are able to resolve almost completely the ~2 mas calibrators of Cohen. This means that we will have the possibility to measure all the angular diameter of each calibrator by comparing it to the other observed known stars. This comparison can only be done in a limited segment of time, as the transfer function of the whole VLTI+VINCI system must not evolve between the measurements.

As the catalogue of the observed sources will grow, so will the “cross-calibrated” calibrators catalogue. A first step could be to check the internal consistency of the whole southern sky Cohen catalogue (~ 300 stars). This would require to observe each star of the catalogue together with two other Cohen (or other external reference) stars (the number three is chosen to stay in a short time segment).

Each set of three stars will provide the calibrated diameters for two of them, while the third star can be used as a link to the rest of the catalogue. The total number of single star observations would therefore be:

$$(3 \text{ stars}) \times (2 \text{ observation per star}) \times (N_{total} / 2) = 900 \text{ observations.}$$

Assuming 80 observations per night (~one every 6 minutes), this could be completed in 12 nights.

It will also be possible to extend the Cohen catalogue by observing stable stars down to smaller sizes, and calibrating them with Cohen stars.

## 8.2 KNOWLEDGE OF THE TARGET SPECTRUM SHAPE

The spectral distribution of the energy received from the star can be far from beeing perfectly flat over the K band. Depending on the spectral type of the star, the mean slope of the star spectrum can be either nearly flat (hot stars) or rising steeply with wavelength (cold stars). During the data reduction process, it is important to know the effective mean wavelength of the observations, in order to locate correctly the peak of the fringe power in the Fourier transform of the corrected interferomtetric signals.

If no *shape factor* correction is applied on the data, the error on the visibility estimation can be as large as +/- 1% for extreme cases. This is especially important when the star and calibrator have significantly different spectral types.

It is possible to assemble a database of the shape factor corrections based on the spectral type, and therefore to cancel the difference between the science targets and calibrators. Though, for peculiar targets, for which the spectral type is not comparable to a standard type, is will be necessary to acquire a low resolution K band spectrum to compute the proper correction.

Eventually, the coupling of a low resolution spectrograph to the VLTI would be interesting to have a full calibration capability.

# 9. CALIBRATED VISIBILITIES

## 9.1 LIGHT COLLECTORS

The first fringes will be obtained with VINCI using the siderostats. It is still unclear whether the beam compressors will be present or not. There is a 1.4 limiting magnitude difference between the two configurations, but the limiting precision will not be reached for both types of collectors on the brightest stars (the photon noise will never be dominating).

In the present section all the light collector cases (including the siderostats with and without beam compressors) are examined.

## 9.2 PRECISION CURVES AND EXPOSURE TIME CALCULATOR TOOL

An Excel sheet (the graphical user interface is presented Figure 5) was created in order to estimate the impact of the variations of the numerous observational parameters on the precision obtainable with VINCI.

It takes as input parameters:
- the baseline length,
- all the statistical errors tables computed with Matlab as listed in Section 7,
- the magnitude of the calibrator,
- the angular diameter (uniform disk) of the calibrator,
- the uncertainty on the a priori angular diameter of the calibrator.

and specifically for the exposure time calculator:
- science target magnitude,
- science target estimated angular diameter,
- requested precision.

A short macro is used to adjust the observation duration to match the requested precision. It always considers the optimal scan as the actual acquisition rate. The precisions curves are plotted in real time as the user enters the parameters values.

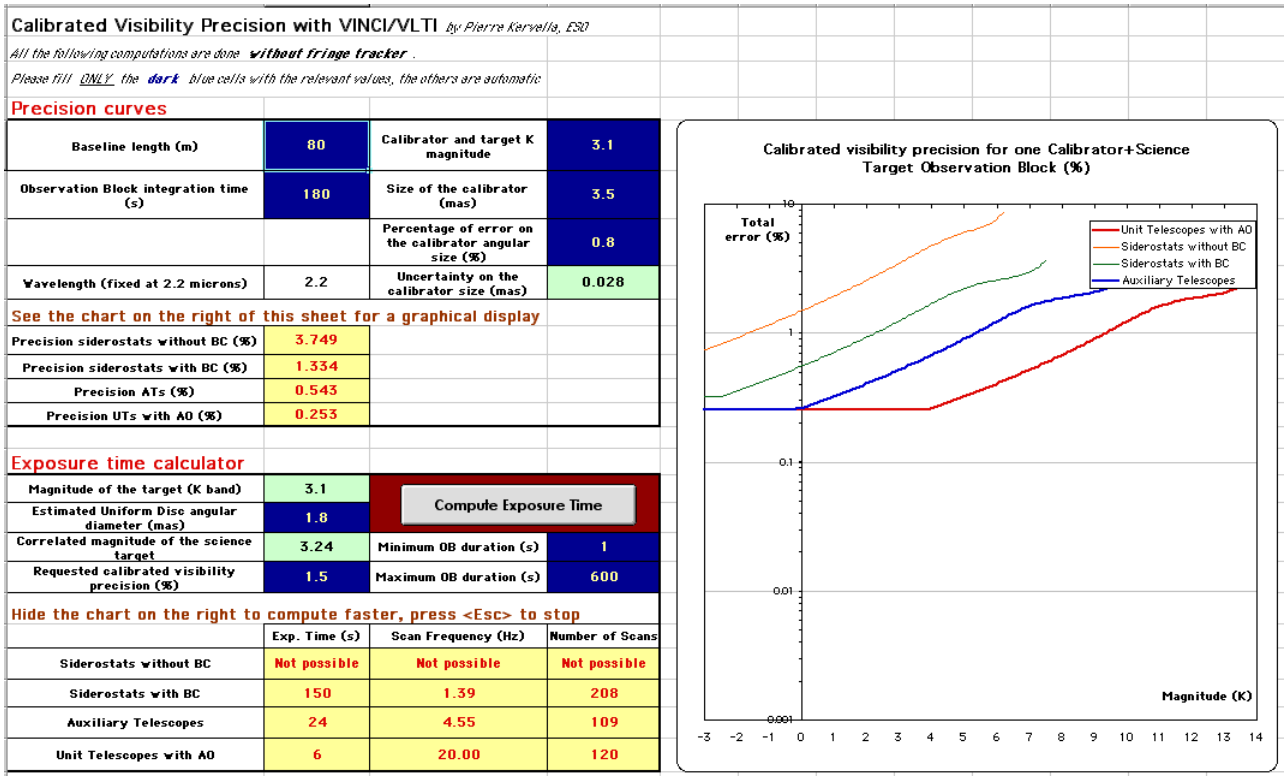


**Figure 5. Exposure time calculator graphical user interface**

## 9.3 CALIBRATORS, BASELINE AND SHAPE FACTOR

The calibrators available in the first weeks will not benefit from the accuracy improvement procedure proposed in Section 8.1.3. Therefore, the transfer function measurement accuracy will be limited for the longest baselines to about 1%. For the short baselines (up to 20 meters), the uncertainty will be less than 0.05%.

The shape factor will be derived from the catalogued spectral types, and is not expected to be a limiting parameter for the final precision, as no very peculiar sources are foreseen during this first period.

## 9.4 EXAMPLE: THE CASE OF ZETA GEMINORUM

In order to have a realistic case for the observation simulations, the case of the Cepheid Zeta Gem with the calibrator star HD 49968 is considered. Zeta Gem is a 1.98 magnitude star in K (angular diameter of aproximately 1.8 mas). HD 49968 is a 2.2 magnitude calibrator from the Cohen list, with a uniform disk angular diameter of 1.87 +/- 0.030 mas.

Considering the longest baseline of 195 meters, it will be necessary to observe for about 1300 seconds on each Zeta Gem and HD 49968 with the siderostats to get to a 2% accuracy on the visibilities. This results from the fact that the correlated visibility of this star is high (as it is resolved), but the uncertainty on the calibrator also adds to the difficulty of the observation.

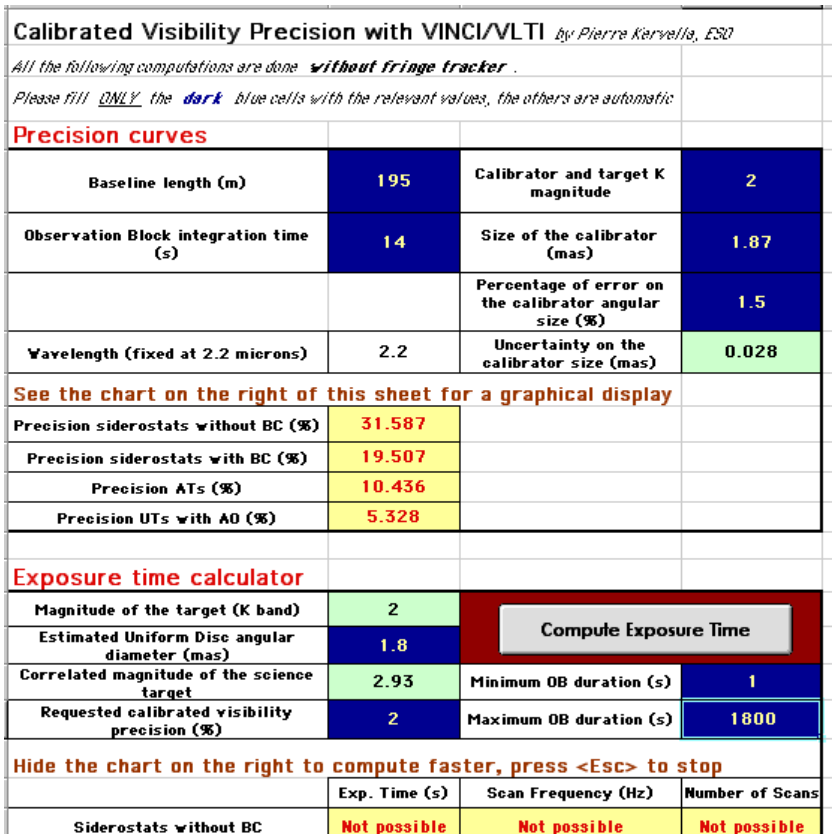

Calibrated Visibility Precision with VINCI/VLTI *by Pierre Kervella, ESO*

*All the following computations are done* ***without fringe tracker*** .

*Please fill ONLY the* ***dark*** *blue cells with the relevant values, the others are automatic*

Precision curves

| | | | |
|---|---|---|---|
| Baseline length (m) | 195 | Calibrator and target K magnitude | 2 |
| Observation Block integration time (s) | 14 | Size of the calibrator (mas) | 1.87 |
| | | Percentage of error on the calibrator angular size (%) | 1.5 |
| Wavelength (fixed at 2.2 microns) | 2.2 | Uncertainty on the calibrator size (mas) | 0.028 |

See the chart on the right of this sheet for a graphical display

| | |
|---|---|
| Precision siderostats without BC (%) | 31.587 |
| Precision siderostats with BC (%) | 19.507 |
| Precision ATs (%) | 10.436 |
| Precision UTs with AO (%) | 5.328 |

Exposure time calculator

| | | | |
|---|---|---|---|
| Magnitude of the target (K band) | 2 | Compute Exposure Time | |
| Estimated Uniform Disc angular diameter (mas) | 1.8 | | |
| Correlated magnitude of the science target | 2.93 | Minimum OB duration (s) | 1 |
| Requested calibrated visibility precision (%) | 2 | Maximum OB duration (s) | 1800 |

Hide the chart on the right to compute faster, press <Esc> to stop

| | Exp. Time (s) | Scan Frequency (Hz) | Number of Scans |
|---|---|---|---|
| Siderostats without BC | Not possible | Not possible | Not possible |

**Figure 6. Zeta Geminorum observations**

## 9.5 CALIBRATED VISIBILITY PRECISION CURVES FOR 40 M AND 195 M BASELINES

A typical 2.3 mas +/- 0.035 mas, K magnitude = 2 calibrator star is assumed, with an observation time of 180 seconds. The vertical scale is different between the two plots.

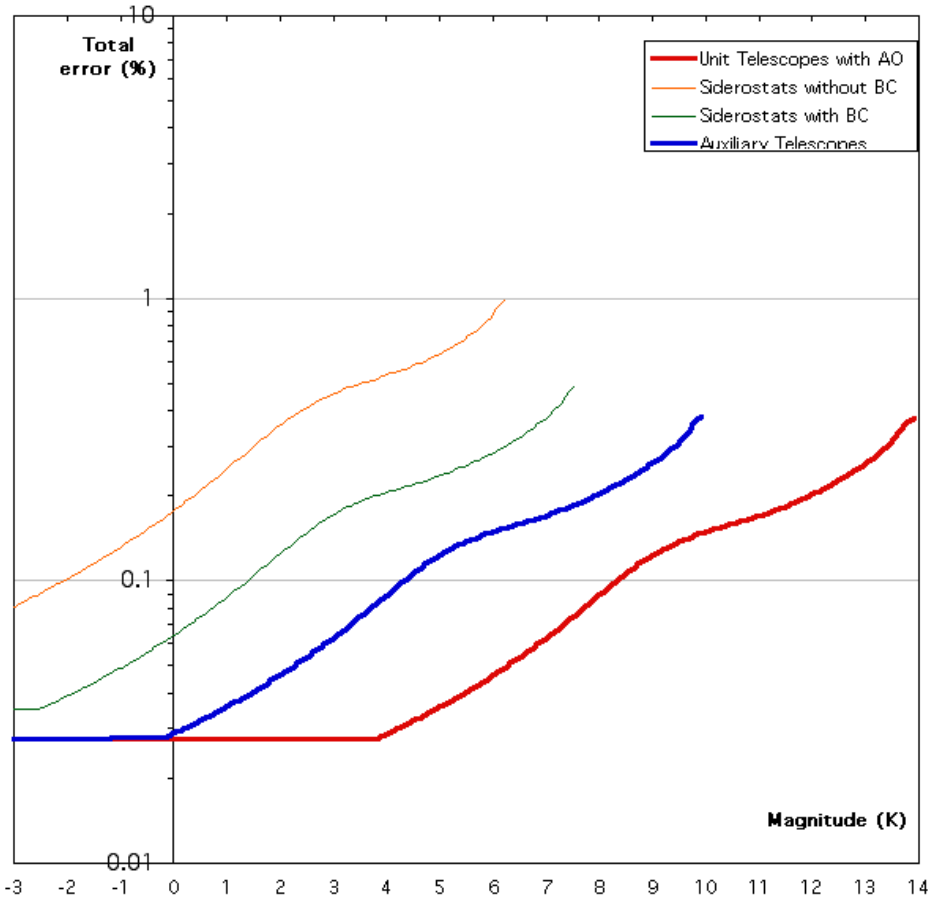


**Figure 7. Precision on the calibrated visibility for a 40 m baseline**

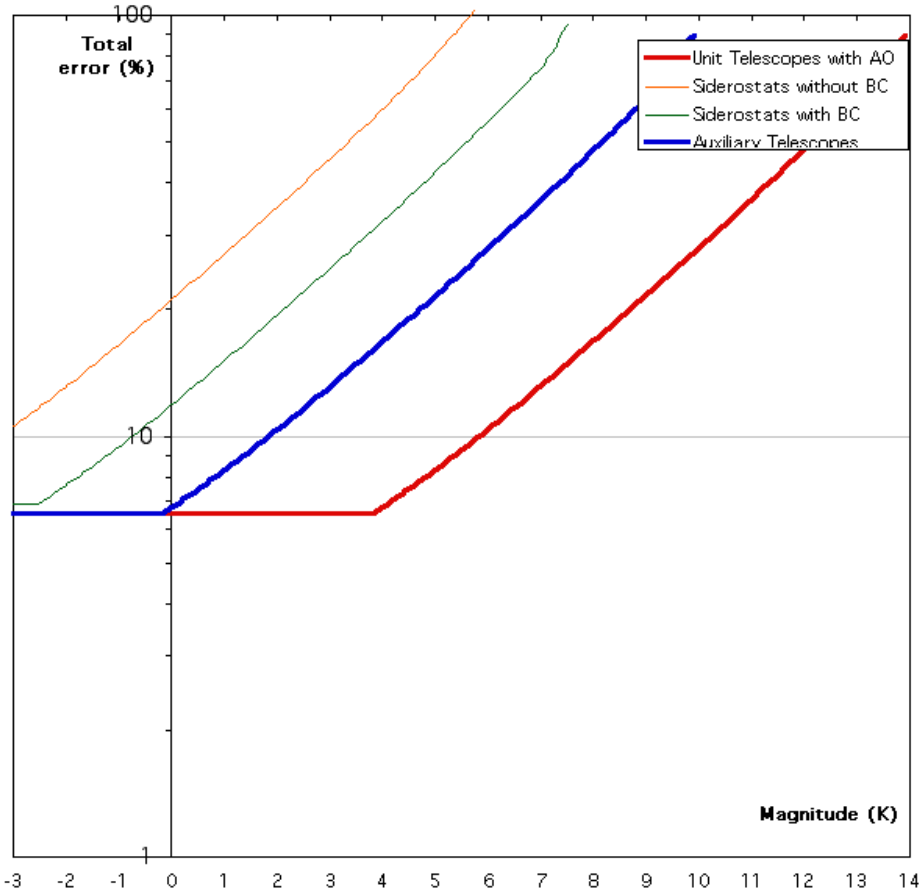


**Figure 8. Precision on the calibrated visibility for a 195 m baseline**

## 9.6 ATMOSPHERIC TURBULENCE AND FRINGE SENSOR IMPORTANCE

The atmospheric turbulence introduces random corrugation of the incoming wavefront, both in shape (perpendicular to the propagation direction) and longitudinal delay (along the direction of propagation, also called differential piston effect). The adaptive optics allows the flattening of the wavefront in the perpendicular direction. Once corrected, the wavefront can be injected much more efficiently in single-mode optical fibers. This results in a higher flux used for beam combination, and increased sensitivity.

The role of the fringe sensor unit (FSU) is to stabilize the fringes longitudinally, to allow for longer integration times with the science instrument. Normally, the piston effect limits the scan time to a few tens of milliseconds. The FSU removes it by quickly adjusting the internal OPD by means of a delay line. The FSU could become available for the testing period with the siderostats. The effect of the FSU is important on the precision of the visibility measurements (reduced or canceled piston noise), but *not primarily on the limiting magnitude of the instrument*. With a FSU, the maximum measurement accuracy can be reached on all reachable stars, but the observable targets number will not be significantly larger than without FSU. As VINCI and the FSU will supposedly have the same limiting magnitude, fainter stars will not be accessible before the arrival of PRIMA and its dual-beam capability. With PRIMA though, the limiting magnitude will become much higher (Mag K ~ 19).

The Fringe Sensor Unit is absolutely essential for the most demanding observation programs, such as the exoplanets, and the efforts should be concentrated on having it available on Paranal as soon as possible. The limiting precision reachable with the FSU is not yet certain, but could be as low as 0.001 % (10^-5) for all observable stars.

# 10. APPENDIX: SIGNAL AND NOISE FORMULAE

## 10.1 USEFUL VALUES

$$f_{fringes} = \frac{f_{acq}}{n}$$

$$\Delta t = \frac{l}{V_{fringes}} = \frac{l.n}{f_{acq}\,\lambda}$$

$$\sigma_{min} = \frac{1}{\lambda_{max\ integration}} \qquad \sigma_{max} = \frac{1}{\lambda_{min\ integration}}$$

$$\Delta F = f_{fringes}\lambda\left(\sigma_{max} - \sigma_{min}\right)$$

## 10.2 SIGNAL

| | |
|---|---|
| $\Delta\lambda$ | Wavelength range (micron) |
| A | Effective single telescope collecting area ($m^2$) |
| T | Overall photometric efficiency of the optical train |
| I | Overall interferometric efficiency of VINCI/VLTI |
| *m* | K magnitude of the star |
| $F_0$ | Reference flux for $mag_K$=0 ($3.9.10^{-10}$ W/$m^2$/micron) |
| $\Delta t$ | Duration of one scan (s) |
| *S* | Signal in each of the four channels (photometry and interferences) |

$$S = \left(2A\,\Delta\lambda\,T\,I\,F_0.10^{\frac{m}{-2.5}}\right)^2 \frac{\Delta t}{4}$$

This can also be written as:

| | |
|---|---|
| l | Scan length (μm) |
| n | Number of samples per fringe |
| $n_{channels}$ | Number of channels onto which the signal is detected |
| $\lambda$ | Effective central wavelength (μm) |
| $\Delta\lambda$ | Wavelength range (μm) |
| A | Effective single telescope collecting area ($m^2$) |
| T | Overall photometric efficiency of the optical train |
| I | Overall interferometric efficiency of VINCI/VLTI |
| *m* | K magnitude of the star |
| $F_0$ | Reference flux for $mag_K$=0 ($3.9.10^{-10}$ W/$m^2$/micron) |
| *S* | Signal in each of the four channels (photometry and interferences) |
| $f_{acq}$ | Acquisition frequency (Hz) |

$$S = \left( 2A\,\Delta\lambda\,T\,I\,F_0.10^{\frac{m}{-2.5}} \right)^2 \frac{\Delta t}{n_{channels}}$$

### 10.3 THERMAL NOISE

| | |
|---|---|
| $T_K$ | Temperature (K) |
| l | Scan length (m) |
| n | Number of samples per fringe |
| $\lambda$ | Effective central wavelength (m) |
| $\Delta\lambda$ | Wavelength range (m) |
| $E$ | Beam etendue |
| $\varepsilon$ | Emissivity |
| $B$ | Blackbody function (W/m$^2$/sr/m) |
| $\Delta t$ | Scan duration (s) |
| $\varpi_{thermal}$ | Thermal noise equivalent power (W/Hz$^{0.5}$) |

$$B(T,\lambda) = \frac{2h\frac{c}{\lambda^3}}{e^{\frac{hc}{\lambda k T_K}} - 1}$$

$$\varpi^4_{thermal} = \left[ \frac{2hc}{\lambda} \Delta\lambda . B(T,\lambda) E \lambda^2 . \varepsilon \right]^2 . \Delta t . \Delta F$$

### 10.4 PISTON NOISE

| | |
|---|---|
| S | Signal in each of the four channels |
| $\chi$ | Fraction of the star signal equivalent to piston noise |
| $\varpi_{piston}$ | Piston noise equivalent power (W/Hz$^{0.5}$) |

$$\varpi^2_{piston} = (S.\chi)$$

Another expression is the following (see Section 5.1 for details):

| | |
|---|---|
| l | Scan length (µm) |
| n | Number of samples per fringe |
| $\lambda$ | Effective central wavelength (m) |
| $f_{acq}$ | Acquisition frequency (Hz) |
| $V_{fringes}$ | Fringe speed (m/s) |
| $\varpi_{piston}$ | Piston noise equivalent power (W/Hz$^{0.5}$) |

$$V_{fringes} = \frac{\lambda f}{n}$$

$$\varpi^4_{piston} = \left[ S\left( 1 - e^{-1.5\left( \frac{l.n}{\lambda f_{acq}} \right)^{5/3}} \right) \right]^2$$

## 10.5 DETECTOR NOISE

| | |
|---|---|
| $f_{acq}$ | Acquisition frequency (Hz) |
| $f_{fringes}$ | Fringe frequency (Hz) |
| n | Number of samples per fringe |
| $\phi$ | Read out noise (e-) |
| $\eta$ | Quantum efficiency |
| $\varpi_{detector}$ | Detector noise equivalent power (W/Hz$^{0.5}$) |

$$\varpi_{detector}^4 = \left[ 2\left( \frac{\phi}{\eta} . \frac{hc}{\lambda} . \sqrt{n_{pixels}} \right)^2 f_{acq} \right]^2 \Delta t \, \Delta F$$

## 10.6 PHOTON NOISE

| | |
|---|---|
| $\lambda$ | Effective central wavelength (m) |
| $\Delta\lambda$ | Wavelength range (μm) |
| A | Effective single telescope collecting area (m$^2$) |
| T | Photometric transmission of the optical train |
| $m$ | K magnitude of the star |
| $F_0$ | Reference flux for mag$_K$=0 (3.9.10$^{-10}$ W/m$^2$/μm) |
| $\varpi_{photon}$ | Photon noise equivalent power (W/Hz$^{0.5}$) |

$$\varpi_{photon}^4 = \left[ \frac{2hc}{\lambda} \left( 2A \, \Delta\lambda \, T \, F_0 . 10^{\frac{m}{-2.5}} \right) \right]^2 \Delta t \, \Delta F$$

## 10.7 UNCERTAINTY ON THE VISIBILITY

By combining the visibilities of the two interferometric channels, and assuming that they are not correlated, the resulting uncertainty $\vartheta$ on the visibility for one scan is (for N interferograms, with $\Omega$ the SNR):

$$\vartheta = \frac{2}{\sqrt{N} . \Omega}$$

# 11. APPENDIX: MATLAB ROUTINES

## 11.1 EXECUTION BATCH

The files are written in wk1 spreadsheet format for use in Excel.

```
table_siderostats_without_bc=abaque(0);
wk1write('table_sids_witout_bc',table_siderostats_without_bc);
table_siderostats=abaque(1);
wk1write('table_sids',table_siderostats);
table_ats=abaque(2);
wk1write('table_ats',table_ats);
table_uts_without_ao=abaque(3);
wk1write('table_uts_without_ao',table_uts_without_ao);
table_uts_with_ao=abaque(4);
wk1write('table_uts_with_ao',table_uts_with_ao);
```

## 11.2 MAIN PROGRAM (ABAQUE)

```
function table_results=abaque(telescope);

% table_results contains the following data:
% 1- magnitude of the star
% 2- resulting SNR per channel per scan
% 3- resulting precision for 1 scan and 1 channel
% 4- optimal frequency for acquisition
% 5- required piezo speed
% 6- precision for 100 scans and the two channels (supposed decorrelated)
% 7- fraction of noise due to the piston;
% 8- fraction of noise due to the detector;
% 9- fraction of noise due to the photon;

l = 51.2*2.2e-6;       % Total length of the scan in m
lambda = 2.2e-6;       % Wavelength in m
n = 5;                         % Points per fringe
max_speed = 0.01;      % Maximum scan speed in m/s

% Siderostat without Beam Compressors
if telescope==0,
        max_loop=85+31;
end
% Siderostat with BC
if telescope==1,
        max_loop=85+31;
end
% AT
if telescope==2,
        max_loop=110+31;
end
% UT without AO
if telescope==3,
        max_loop=110+31;
end
% UT with AO
if telescope==4,
        max_loop=150+31;
end

for i=1:max_loop,
        magnitude = (i-31)/10;
        scan_speed=fmins('snr_vinci',5e-4,foptions,[],magnitude,telescope);

        % If the scan speed is larger than the maximum speed of the piezo, then
        % take the maximum value.
        if scan_speed>0.01,
```

```
                scan_speed=max_speed;
                freq=max_speed*n/lambda;
        end
        % Maximum SNR
        snr_max = -snr_vinci(scan_speed,magnitude,telescope);
        % Maximum precision in percents per scan and per channel
        precision_max_percents = 100/snr_max;
        % Maximum precision in percents for 100 scans and two channels
        precision_max_percents_2_channels = 100/(20*snr_max);
        % Scan duration in seconds
        scan_duration = 1/(scan_speed);
        % Noises contributions
        [fraction_piston,fraction_detector,fraction_photon]=noises_cont(scan_speed,magnitude,telesco
pe);
        % Storage of the results
        table_results(i,1)=magnitude;
        table_results(i,2)=snr_max;
        table_results(i,3)=precision_max_percents;
        table_results(i,4)=scan_speed*n/lambda;
        table_results(i,5)=scan_speed;
        table_results(i,6)=precision_max_percents_2_channels;
        table_results(i,7)=fraction_piston;
        table_results(i,8)=fraction_detector;
        table_results(i,9)=fraction_photon;
end

% For the plots:
% Precisions (all telescopes)
plot(table_siderostats_without_bc(1:100,1),table_siderostats_without_bc(1:100,6),...
table_siderostats(1:100,1),table_siderostats(1:100,6),table_ats(:,1),table_ats(:,6),table_uts_witho
ut_ao(:,1),table_uts_without_ao(:,6),table_uts_with_ao(:,1),table_uts_with_ao(:,6))
% Noise sources (sids)
%
plot(table_siderostats(:,1),table_siderostats(:,7),table_siderostats(:,1),table_siderostats(:,8),ta
ble_siderostats(:,1),table_siderostats(:,9))
```

## 11.3 SNR COMPUTATION (SNR_VINCI)

```
function snr=snr_vinci(scan_speed,magnitude,telescope)
% This function computes the signal to noise ratio as a function of the
% VINCI observations, for a given detector frequency.
% version 17/05/00

% These parameters change with the telescope:
% Siderostat without Beam Compressors
if telescope==0,
       A = 0.084;                       % Area of the telescope (m2)
       T = 0.00612;                     % Photometric transmission
       I = 0.722;                       % Interferometric efficiency
end
% Siderostat with BC
if telescope==1,
       A = 0.084;                       % Area of the telescope (m2)
       T = 0.00582;                     % Photometric transmission
       I = 0.722;                       % Interferometric efficiency
end
% AT
if telescope==2,
       A = 2.545;                       % Area of the telescope (m2)
       T = 0.00173;                     % Photometric transmission
       I = 0.722;                       % Interferometric efficiency
end
% UT without AO
if telescope==3,
       A = 50.265;                      % Area of the telescope (m2)
       T = 0.0000914;                         % Photometric transmission
       I = 0.722;                       % Interferometric efficiency
end
% UT with AO
if telescope==4,
```

```
      A = 50.265;                       % Area of the telescope (m2)
      T = 0.00342;                      % Photometric transmission
      I = 0.722;                        % Interferometric efficiency
end

% These parameters are not telescope dependant:
lambda = 2.2e-6;           % Effective central wavelength (m)
delta_lambda = 0.4e-6;     % Wavelength range (m)
m = magnitude;                   % K magnitude of the star
F0 = 3.9e-10;              % K magnitude 0 flux (W/m2/MICRON)
l = 51.2*2.2e-6;           % Effective total scan length (m)
l_fringes = 70e-6;         % Fringe packet length
n = 5;                     % Number of samples per fringe
Temp = 288;                % Temperature (K)
E = 1;                     % Beam etendue
epsilon = 1;               % Emissivity
QE = 0.62;                 % Quantum efficiency of the detector
RON = 10;                  % Read out noise of the detector (e-)
h = 6.6226e-34;            % Planck constant (J.s)
k = 1.38062e-23;           % Boltzmann constant (J/s)
c = 3e8;                   % Speed of light (m/s)
sigma_min_integ=3e5;       % Minimum integration wavenumber (m^-1) (fringe power)
sigma_max_integ=6e5;       % Maximum integration wavenumber (m^-1) (fringe power)

% ==============

% Acquisition frequency of the camera (Hz)
frequency=n*scan_speed/lambda;

if frequency<1e-6,
       frequency = 1e-6;
end

% Scan duration
dt = l*n/(frequency*lambda);
% Frequency bandwidth
df = (lambda*frequency/n)*(sigma_max_integ-sigma_min_integ);

% Signal
S = (2*A*delta_lambda*1e6*T*I*F0*10^(m/-2.5))^2*dt/4;
% The 1e6 factor is to account for the W/m2/MICRON reference flux

% Thermal noise equivalent power squared ****
nu = c/lambda;
delta_nu = c/(lambda-delta_lambda/2)-c/(lambda+delta_lambda/2);
B = ((2*h*nu^3)/c^2) * 1/(exp((h*nu)/(k*Temp)) -1);
etendue=E*lambda^2*epsilon;
n_thermal = ((2*h*c/lambda)*delta_nu*B*etendue)^2;

% Piston noise equivalent power squared ****
piston = 1-exp(-1.5*((l_fringes*n)/(lambda*frequency))^(5/3));
n_piston = S*piston;

% Detector noise equivalent power squared ****
n_detector = 2*frequency*(RON*h*c/(QE*lambda))^2;

% Photon noise equivalent power squared ****
n_photon = ((2*h*c/lambda)*(2*A*delta_lambda*1e6*T*F0*10^(m/-2.5)));
% The 1e6 factor is to account for the W/m2/MICRON reference flux

% Returns MINUS the SNR
total_noise = n_thermal^2*dt*df + n_piston^2 + n_detector^2*dt*df + n_photon^2*dt*df;
snr = -S/sqrt(total_noise);
```

## 11.4 NOISES CONTRIBUTIONS (NOISES_CONT)

```
function
[fraction_piston,fraction_detector,fraction_photon]=noises_cont(scan_speed,magnitude,tel
escope)
% This function computes the contributions of each source
% of noise
% version 17/05/00

% These parameters change with the telescope:
% Siderostat without Beam Compressors
if telescope==0,
       A = 0.084;                       % Area of the telescope (m2)
       T = 0.00612;                     % Photometric transmission
       I = 0.722;                       % Interferometric efficiency
end
% Siderostat with BC
if telescope==1,
       A = 0.084;                       % Area of the telescope (m2)
       T = 0.00582;                     % Photometric transmission
       I = 0.722;                       % Interferometric efficiency
end
% AT
if telescope==2,
       A = 2.545;                       % Area of the telescope (m2)
       T = 0.00173;                     % Photometric transmission
       I = 0.722;                       % Interferometric efficiency
end
% UT without AO
if telescope==3,
       A = 50.265;                      % Area of the telescope (m2)
       T = 0.0000914;                         % Photometric transmission
       I = 0.722;                       % Interferometric efficiency
end
% UT with AO
if telescope==4,
       A = 50.265;                      % Area of the telescope (m2)
       T = 0.00342;                     % Photometric transmission
       I = 0.722;                       % Interferometric efficiency
end

% These parameters are not telescope dependant:
lambda = 2.2e-6;            % Effective central wavelength (m)
delta_lambda = 0.4e-6;      % Wavelength range (m)
m = magnitude;                    % K magnitude of the star
F0 = 3.9e-10;               % K magnitude 0 flux (W/m2/MICRON)
l = 51.2*2.2e-6;            % Effective total scan length (m)
l_fringes = 70e-6;          % Fringe packet length
n = 5;                      % Number of samples per fringe
Temp = 288;                 % Temperature (K)
E = 1;                      % Beam etendue
epsilon = 1;                % Emissivity
QE = 0.62;                  % Quantum efficiency of the detector
RON = 10;                   % Read out noise of the detector (e-)
h = 6.6226e-34;             % Planck constant (J.s)
k = 1.38062e-23;            % Boltzmann constant (J/s)
c = 3e8;                    % Speed of light (m/s)
sigma_min_integ=3e5;        % Minimum integration wavenumber (m^-1) (fringe power)
sigma_max_integ=6e5;        % Maximum integration wavenumber (m^-1) (fringe power)

% ==============

% Acquisition frequency of the camera (Hz)
frequency=n*scan_speed/lambda;
```

```
if frequency<1e-6,
       frequency = 1e-6;
end

% Scan duration
dt = l*n/(frequency*lambda);
% Frequency bandwidth
df = (lambda*frequency/n)*(sigma_max_integ-sigma_min_integ);

% Signal
S = (2*A*delta_lambda*1e6*T*I*F0*10^(m/-2.5))^2*dt/4;
% The 1e6 factor is to account for the W/m2/MICRON reference flux

% Thermal noise equivalent power squared ****
nu = c/lambda;
delta_nu = c/(lambda-delta_lambda/2)-c/(lambda+delta_lambda/2);
B = ((2*h*nu^3)/c^2) * 1/(exp((h*nu)/(k*Temp)) -1);
etendue=E*lambda^2*epsilon;
n_thermal = ((2*h*c/lambda)*delta_nu*B*etendue)^2;

% Piston noise equivalent power squared ****
piston = 1-exp(-1.5*((l_fringes*n)/(lambda*frequency))^(5/3));
n_piston = S*piston;

% Detector noise equivalent power squared ****
n_detector = 2*frequency*(RON*h*c/(QE*lambda))^2;

% Photon noise equivalent power squared ****
n_photon = ((2*h*c/lambda)*(2*A*delta_lambda*1e6*T*F0*10^(m/-2.5)));
% The 1e6 factor is to account for the W/m2/MICRON reference flux

% Returns the SNR
total_noise = n_thermal^2*dt*df + n_piston^2 + n_detector^2*dt*df + n_photon^2*dt*df;
snr = S/sqrt(total_noise);

fraction_thermal = n_thermal^2*dt*df/total_noise;
fraction_piston = n_piston^2/total_noise;
fraction_detector = n_detector^2*dt*df/total_noise;
fraction_photon = n_photon^2*dt*df/total_noise;
```